F79-08

NASA CR- 166680

PERFORMANCE, OPERATIONAL LIMITS, OF AN ELECTRONIC SWITCHING SPHERICAL ARRAY (ESSA) ANTENNA

Microprocessor controller provides multi-mode operation for TDRSS User antenna system.

Final Report For Period August 1977-June 1979

Ron Stockton

Ball Aerospace Systems Division
P.O. Box 1062
Boulder, Colorado 80306

JULY 1979

Prepared for
GODDARD SPACE FLIGHT CENTER
Microwave Instrument and RF Technology Branch
Greenbelt, Maryland 20771

Richard P. Hockensmith , Technical Officer

Ball Aerospace Systems Division

TECHNICAL REPORT STANDARD TITLE PAGE

1. Report No.	2. Government Accession No.	3. Recipient's Catalog No.
F79-08		

4. Title and Subtitle
PERFORMANCE, OPERATIONAL LIMITS, OF AN ELECTRONIC SWITCHING SPHERICAL ARRAY (ESSA) ANTENNA

5. Report Date
2 July 1979

6. Performing Organization Code

7. Author(s)
Ron Stockton

8. Performing Organization Report No.
F79-08

9. Performing Organization Name and Address
Ball Aerospace Systems Division
P.O. Box 1062
Boulder, CO 80306

10. Work Unit No.

11. Contract or Grant No.
NAS 5-24268

12. Sponsoring Agency Name and Address
Goddard Space Flight Center
Greenbelt, MD 20771
Technical Monitor: Richard P. Hockensmith

13. Type of Report and Period Covered
Final
August 1977 - June 1979

14. Sponsoring Agency Code

15. Supplementary Notes

16. Abstract

This report describes the development of a microprocessor controller which provides multi-mode operational capability for the Electronic Switching Spherical Array (ESSA) Antenna previously developed on NASA Contract NAS5-23518. The purpose was first to determine the best set of operating conditions and then to demonstrate the performance of an ESSA Antenna in the following modes: 1) Omni, 2) 2) Acquisition/Track, 3) Directive, and 4) Multibeam. The program was conducted in two phases. The control algorithms, software flow diagrams and electronic circuitry were developed during an initial study phase. The microprocessor and control electronics were then built and interfaced with the antenna to carry out performance testing. Throughout, emphasis was placed on the acquisition/track mode for Users in the Tracking and Data Relay Satellite System (TDRSS).

17. Key Words (Selected by Author(s))	18. Distribution Statement
Electronic Switching Spherical Array; TDRSS User Antenna; Microprocessor Controller	

19. Security Classif. (of this report)	20. Security Classif. (of this page)	21. No. of Pages	22. Price*
UNCLASSIFIED	UNCLASSIFIED	100	Unknown

*For sale by the Clearinghouse for Federal Scientific and Technical Information, Springfield, Virginia 22151.

PERFORMANCE, OPERATIONAL LIMITS, OF AN ELECTRONIC SWITCHING SPHERICAL ARRAY (ESSA) ANTENNA

FINAL REPORT

F79-08

Period

August 1977 - June 1979

Prepared for

National Aeronautics & Space Administration
Goddard Space Flight Center
Greenbelt Road
Greenbelt, Maryland 20771

Richard P. Hockensmith, Technical Officer

Prepared by:

Ron Stockton

Ron Stockton,
Program Manager

Approved by:

R. E. Munson

R. E. Munson, Manager
Antenna Systems

Ball Aerospace Systems Division

BOULDER, COLORADO 80306

PREFACE

This report describes the development of a microprocessor controller which provides multi-mode operational capability for the Electronic Switching Spherical Array (ESSA) Antenna previously developed on NASA Contract NAS5-23518. This work was conducted by Ball Aerospace Systems Division (BASD), Boulder, Colorado, between August 1977 and September 1978, for Goddard Space Flight Center, Greenbelt, Maryland, under NASA Contract NAS5-24268.

The purpose of this work was first to determine the best set of operating conditions and then to demonstrate the performance of an ESSA Antenna in the following modes: 1) Omni, 2) Acquisition/Track, 3) Directive, and 4) Multi-beam. The program was conducted in two phases. The control algorithms, software flow diagrams and electronic circuitry were developed during an initial study phase. The microprocessor and control electronics were then built and interfaced with the antenna to carry out performance testing. Throughout, emphasis was placed on the acquisition/track mode for Users in the Tracking and Data Relay Satellite System (TDRSS).

The engineering model system consisting of the ESSA antenna and the microprocessor controller developed on this contract performed exceptionally well in all four modes of operation. Using a converging algorithm sequence in a closed loop mode, the ESSA antenna system will independently perform the TDRSS acqusition and auto-track functions for either a 3-axis stabilized or spinning User spacecraft. The system size, weight and power are compatible with small scientific satellites. Typical ESSA antenna gains are 8-25 dB with 90% spherical coverage.[1]

Recommendations for future development work are primarily related to ESSA system checkout using the NASA standard TDRSS transponder. Specific areas which need to be investigated include the following: 1) specify and design the AGC or equivalent analog feedback signal interface, 2) specify and design the command detector digital interface, 3) determine the effect of acquisition sequence phase errors on transponder lock, 4) verify total system performance with antenna range tests.

TABLE OF CONTENTS

ILLUSTRATIONS

TABLES

1.0 INTRODUCTION

With the advent of the Tracking and Data Relay Satellite System (TDRSS), user satellite antennas must provide directed gain in order to transmit even moderate data rates through the multiple access return link. Omnidirectional and low gain antennas are inadequate for data rates over 500 b/s, hence the need for high gain.

This new requirement for higher gain over large coverage angles prompted the development of the Electronic Switching Spherical Array (ESSA) Antenna, which is expected to be the forerunner of a standard integrated antenna system for scientific satellites. This antenna will satisfy gain requirements between 8 and 25 dB with 90% spherical coverage depending on type and size.

The initial engineering model developed on NASA Contract NAS5-23518 was a 76 cm diameter hemispherical configuration with a measured coverage gain of 13 dB. A manual control box provided a directive mode only capability since all 551 beam positions were preprogrammed in memory.

The objective of this follow-on work was to extend the capabilities of the ESSA antenna and make it a comprehensive system solution to the TDRSS user spacecraft antenna problem. To do so, a dedicated microprocessor controller was selected to take advantage of the electronic beam steering agility inherent with the ESSA antenna.

An initial six week analysis phase determined the optimum set of operating conditions for the omni, multi-beam and acquisition/track modes. The functional software required to implement each of these modes was specified by flow charts. The microprocessor and control electronics were defined to the schematic level and test procedures designed to verify performance in each mode were outlined. The remainder of the program was dedicated to hardware implementation, software programming, system debugging and antenna range performance verification tests.

The following sections of this report describe the software, hardware and test results for a multimode ESSA antenna system. A technical summary is provided in Section 2.0. Section 3.0 describes the control logic, algorithms and software

for each mode, while Section 4.0 is a description of the microprocessor and antenna interface control circuitry. Section 5.0 contains a summary of the test data with typical examples.

2.0 SUMMARY AND RECOMMENDATIONS

2.1 Summary

A software study and system design were conducted to determine the best set of operating conditions for a GFE ESSA antenna in the following modes of operation: 1) Directive, 2) Omni, 3) Multi-beam, 4) Acquisition/Track. At the conclusion of this effort the microprocessor controller was fabricated and programmed to operate the antenna in all four modes. A series of tests were carried out to characterize the operational performance in each mode. The system consisting of the engineering model ESSA antenna and microprocessor controller during test is shown in Figure 2-1. A close-up of the controller with its display dome is shown in Figure 2-2.

The directive mode was implemented by means of a beam forming algorithm which selects the twelve subarray elements as a function of pointing direction. The algorithm was designed and programmed for minimum execution time since it is a major component in the Acquisition/Track function. Test results indicated that the mean pointing error was 3.6^{0} which is comparable to the $\pm 3^{0}$ beam pointing granularity. The peak gain was typically 13.74 dBi which corresponds to a 13.04 dBi coverage gain.

In the omni mode the goal was -7 dBi gain throughout the upper hemisphere. Since analysis and experiments showed that this was not possible with a single twelve element configuration, toggling between two arrays was required. The controller samples the received signal level for each array and selects the optimum beam. The interval between samples is a software variable. By employing this toggling technique hemispherical coverage at -7 dBi gain level was improved from 82% (for either beam separately) to 98%.

Figure 2-1 Engineering Model ESSA Antenna and Microprocessor Controller Under Test

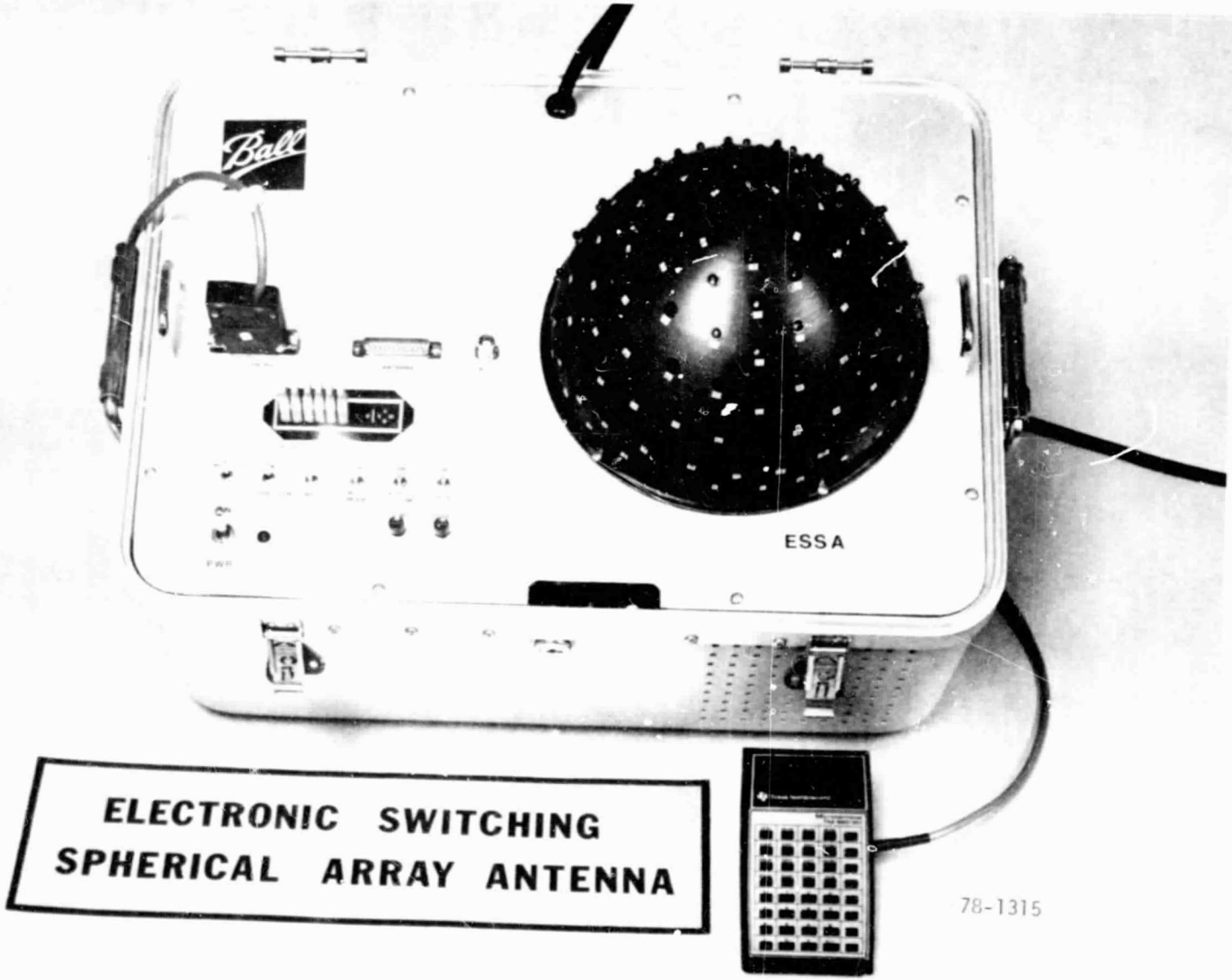

Figure 2-2 Microprocessor Controller

The multi-beam mode is merely a special case of the directive mode. The same algorithm is used but the number of elements per subarray is either 6, 4 or 3 for 2, 3 and 4 beams respectively. The peak gain for each beam is approximately 10 log 1/n below the directive mode gain, where n is the number of beams. The test results verified that the gain, beamwidths and pointing directions are very close to the nominal values as long as the solid angle separation between pointing directions is greater than the half power beamwidth. When this condition is not met an interferometer effect distorts the radiation pattern and substantially degrades performance.

The Acquisition/Track mode was implemented for both 3-axis stabilized and spinning spacecraft, although emphasis was on the former. A closed-loop converging algorithm sequence is used to determine the real time direction of arrival of the received signal. For a 3-axis stabilized spacecraft, once this is accomplished, a 40-minute open-loop track function begins immediately. In the case of a spinning spacecraft, however, an additional data collection period and spin rate calculation is required prior to the 40-minute open-loop track function.

Mean pointing error for the stabilized case was 5.2^{0}. Although this value exceeds the $\pm 3^{0}$ beam steering increment, it is acceptable because the coverage gain is unaffected. Beam to beam phase variations were below the 20^{0} specification limit throughout the acquisition phase. Performance testing for the spinning case was limited to determining spin rate accuracy as a function of the data collection period. Based on this limited data, acquisition periods of 108 and 80 seconds are required for 5 and 10 rpm spin rates respectively in order to despin the beam accurately for 40 minutes.

The control theory, algorithms and logic for each operational mode are presented in detail in Section 3.0. An analysis and description of the performance test data is included in Section 5.0.

An important feature of the overall system design is the use of standard, off-the-shelf electronic components in the microprocessor controller. The operational versatility is strictly a function of the software programming.

As a result a basic operational format can be included as part of the system design with mission unique parameters incorporated on an as required basis. Size, weight and prime power consumption estimates for a flight qualified controller compatible with 150 - 200 element ESSA antenna are given below:

Controller Size:	18 cm x 11 cm x 5 cm
Weight:	0.8 kg
Power:	11.5 watts

A more detailed description of the controller hardware is contained in Section 4.0.

The contract also included several related study efforts in the following special interest areas: 1) low gain ESSA configurations for spinning spacecraft applications, 2) thermal model descriptions and analysis results, and 3) gain improvement feasibility study and test results. Although this subject material is outside the scope of this report, the objective and conclusion for each of these efforts is summarized in Section 6.0. Separate study reports were delivered as contract items.

2.2 Future Development Recommendations

Although performance in each of the operational modes was successfully demonstrated, additional development work must be performed before the ESSA antenna system becomes a standard for scientific spacecraft. The primary development items are described in the following paragraphs.

2.2.1 Develop Integrated Communications Subsystem

In the Omni and Acquisition/Track modes, logic decisions are based on amplitude comparisons between pre-programmed beam positions. During the performance tests a dc signal level proportional to the received signal strength was derived from the antenna range receiver. However, in an actual spacecraft application this detection function can be performed by the TDRSS transponder. It

is logical, therefore, to interface these two systems to create an integrated communication subsystem compatible with scientific spacecraft. This task would include an interface requirement analysis, hardware and/or software modification, physical interconnections and performance demonstration tests.

2.2.2 Verify Subsystem Performance

An extensive test program is required to demonstrate performance of this communication subsystem in each of the operational modes. The purpose of these tests is to ensure operational compatibility with the Tracking and Data Relay Satellite System requirements. A complete simulation of the return link including a bit error rate measurement capability is preferred for final testing.

3.0 CONTROL LOGIC, ALGORITHMS AND SOFTWARE

This section describes the control logic and specific algorithms developed for the ESSA antenna system for each mode of operation. Software descriptions are limited to a general flow chart sequence, however, supplementary detailed flow charts are provided in Appendix A.

3.1 OMNI Mode

The design goal for omni mode performance was -7 dBi gain throughout a hemisphere. This gain level is significant since it represents the minimum antenna gain for normal TDRSS transponder operation.

In order to maintain the proper input and output impedance levels for the switching power divider, only 12-element combinations were considered for omni coverage.[2] The three configurations evaluated during the study phase are shown in Figure 3-1. The belt antenna (Figure 3-1A) provided 74% hemispherical coverage at the -7 dB gain level. The four clusters of three elements each (Figure 3-1B) and the double belt (Figure 3-1C) had 72% and 65% coverage respectively at -7 dB. This information was obtained from computer analysis of measured radiation distribution patterns (RDPs).

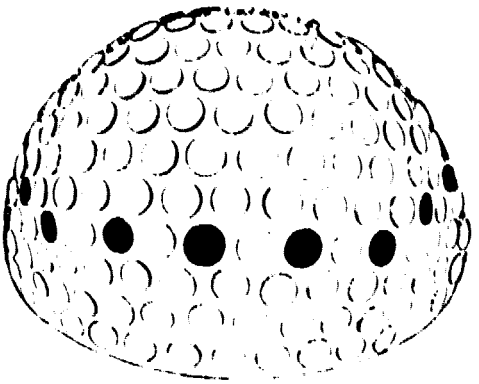

(A) Single Belt

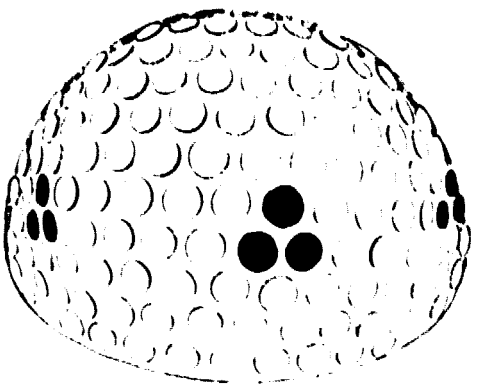

(B) Clusters

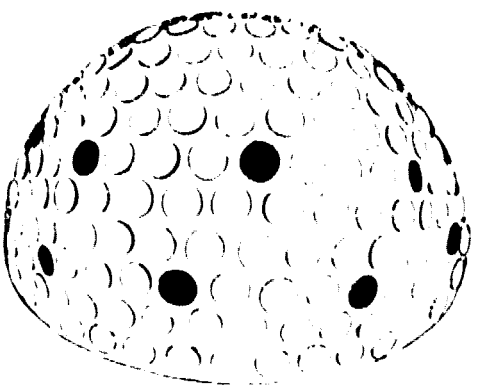

(C) Double Belt

Figure 3-1 Omni Configurations

Since hemispherical coverage at the specified level did not appear possible for a single 12-element array, a second array was used to fill in the nulls of the cloverleaf pattern and to improve coverage. Computer analysis indicated that two arrays identical to Figure 3-1B offset by 45^{0} in azimuth would provide 93% coverage at the -7 dB level. This combination was realized by toggling between the two 12-element arrays.

The control sequence developed for this mode is intended to provide a gain of -7 dB or greater for receive applications. Initially each array is turned on and the transponder AGC (which provides an analog signal level proportional to the received signal strength) is sampled to determine relative amplitudes. The beam with the highest received signal level is selected and maintained until the AGC drops below a pre-set minimum which indicates that the received signal is entering an antenna pattern null. When this occurs the alternate beam is turned on. If the AGC from this beam exceeds the threshold, it is selected and maintained until the AGC again reaches the threshold level at which time the cycle is repeated. The total beam interrogation and selection process is less than 1 millisecond.

For a 3-axis stabilized spacecraft the beams may only switch several times per orbit. However, for a spin stabilized spacecraft the toggling rate will be proportional to the spin rate. For example, at a spin rate of 3 rpm or 1 revolution per 20 seconds, beam switching will occur at least every 2.5 seconds at each of the eight crossover points illustrated in Figure 3-2. This beam switching is apparent when the control box is operated in the simulator mode (without an external AGC input). As the simulated target rotates, beam selection will alternate between the two candidates.

The measured gain and coverage data using this control sequence is presented in Section 5.1.

3.2 Directive Mode

In the GFE manual control box the element groups for each of the 551 beam positions were defined and stored in pre-programmed PROMs. During the study

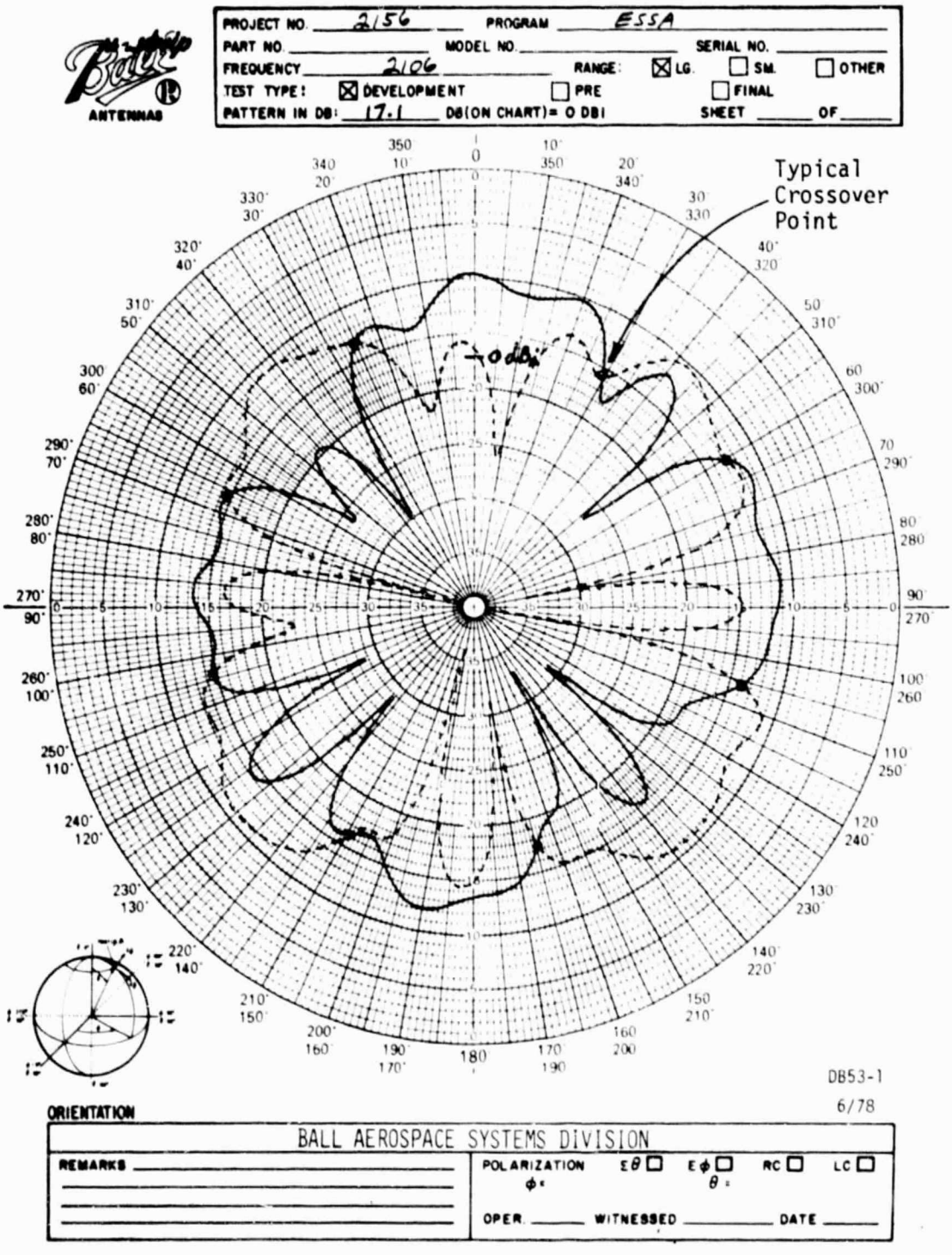

Figure 3-2 Omni Mode Beams and Crossover Points

a beam forming algorithm was developed to replace this stored information for two reasons. First, microprocessor implementation of the directive mode was an essential step in the development of an effective Acquisition/Track function, and second, the amount of hardware is substantially reduced which results in decreased dc power consumption, weight and volume.

The algorithm selects the appropriate element group or subarray when given a θ, ϕ direction. Since this algorithm is a critical subroutine in ary beam control program, it was programmed and evaluated for accuracy and execution time. The initial evaluation was done in Fortran on a Xerox 530. Accuracy was evaluated by comparing 30 beams selected at random to the same beams from the manual control box. The agreement was excellent.

A flow diagram for the beam forming algorithm is shown in Appendix A. The basic theory of operation is as follows: A range of θ and ϕ are established with respect to the input values. All element locations are examined and those that fall within the range of θ (first) and ϕ (second) become potential elements. The subarray is made up of the twelve elements closest to the input θ, ϕ location. Both the logic and programming techniques used in this algorithm were selected for minimum execution time. The measured execution time for this subroutine as programmed in the TI990 microprocessor is 850 microseconds.

With respect to the software structure, the beam forming algorithm called "beams" is a subroutine used by the acquisition/track program. To implement the directive mode the entry point into the acquisition/track program is altered by the panel switch. The coordinates for the directive beam are manually inserted into the appropriate memory locations and the beam is formed by executing "beams".

3.3 Multi-Beam Mode

The objective of the multi-beam mode is to form n independent beams with $1 \leq n \leq 4$. The gain of each beam will decrease from the directive mode gain by approximately 10 log 1/n. The objective gain is, therefore, 10.7, 8.9 and 7.7 dB for 2, 3 and 4 beams respectively.

Implementation of the multi-beam mode is a simple modification of the directive mode algorithm. When the panel switch is set the "beams" subroutine is modified to check specific memory locations for the number of beams to be formed and their coordinates. Since the total number of active elements is fixed at twelve due to the switching power divider design, the number of elements per beam is 12/n. This limitation is one modification to the algorithm. A second, related change reduces the range of θ, ϕ in proportion to the number of elements per beam. The result is a fewer number of candidate elements and improved processing efficiency.

Although this approach is easy to implement, it imposes certain constraints on the proximity of adjacent beams. The pointing directions must differ by at least one beam steering increment or seven solid angle degrees to avoid sharing of elements between beams. Since the element set for each beam is determined independently by the modified algorithm, the total number of active elements will be less than twelve if elements are shared. That is, the same element may be turned on more than once. To avoid this problem a specialized multi-beam algorithm must be developed to handle the general case.

3.4 Acquisition/Track Mode

The objective of this mode was to develop a sequence of control algorithms to determine the direction of arrival for a received signal and to maintain a directive mode beam on the source. Although emphasis was placed on the 3-axis stabilized spacecraft, additional algorithms were developed to provide the same capability for a spin stabilized spacecraft.

The control sequence is comprised of four distinct functions; a search routine, data collection, data processing and a tracking routine. This sequence was specifically developed for a User in the Tracking and Data Relay Satellite System and uses several assumptions as ground rules to demonstrate ESSA performance. The assumptions which were made to simulate this practical application are listed below:

- A S-band forward link transmission is available from a TDRS during the acquisition phase.

- The NASA standard TDRSS transponder will provide a suitable AGC or analog signal proportional to the received signal strength.

Additional assumptions related to spinning spacecraft are:

- The antenna is spinning about its axis of symmetry.
- Spin rates are on the order of 10 rpm or less.

NOTE: Total ESSA capability is not limited to the above ground rules.

Control of the antenna in this mode uses a specific combination of software and hardware. The software contains the algorithms for each function in the sequence while the hardware provides a real-time feedback loop by sampling the AGC and returning the data in digital form to the microprocessor controller. This real-time adaptive approach enables the ESSA antenna to acquire and track a desired target independent of any ground or spacecraft inputs.

3.4.1 3-Axis Stabilized Spacecraft

A typical scenario which may be repeated thousands of times during the life of a mission will proceed as follows: As a TDRS comes into view of the User spacecraft, a forward link transmission begins. Concurrently the ESSA Antenna on the User leaves the quiesent omnidirectional mode and initiates the acquisition sequence. The objective is to determine the correct pointing direction toward the TDRS.

Upon entering the sequence the ESSA antenna has no knowledge of the TDRS location. The search subroutine which has three phases is designed to educate the antenna so it knows the direction of arrival of the received signal in real-time. Phase I provides a coarse θ, ϕ location by determining the general area with maximum received signal. The microprocessor activates each of the 120-elements one at a time and samples the AGC voltage from the transponder. Since the switching power divider was designed to feed 12-element subarrays, a single active element creates a significant mismatch which reduces the

element gain from 7 dB to 1 dB. (It should be noted, however, that alternate Phase I techniques with higher gain levels are practical and that this single element approach was selected for demonstration purposes). Since small variations in system losses between elements and a 60^{o} element beamwidth make it impractical to select a single element, the five elements with the highest AGC values are stored in memory. The coarse direction of arrival for the received signal is then the mean θ, ϕ location from these five elements. More precise information is needed however, so the microprocessor continues to Phase II.

The objective of Phase II is to determine the most probable direction in which to continue the search for the received signal starting from the θ, ϕ coordinates of Phase I. A substantial amount of information can be obtained by forming three directive (12-element subarray) beams around the point θ, ϕ as shown in Figure 3-3. The beams are formed one at a time so that the HPBWs intersect at θ, ϕ. By comparing the AGC levels for these three beams, the great circle direction to the received signal relative to the point θ, ϕ can be resolved to within $\pm 15^{o}$. For example, designate the AGC values for beams 1, 2 and 3 as A1, A2, A3 respectively. Then, if A1 > A2 > A3 the received signal has a high probability of coming from a point on or near the 30^{o} great circle direction. Similarly if A2 = A3, and both A2 and A3 are greater than A1, the received signal is probably coming from a point on or near the 180^{o} great circle direction.

In the Study Report [3] a digital filter was specified as the process by which the microprocessor compares A1, A2 and A3 and selects one of the twelve great circle directions. This procedure, however, was replaced with a less complex and more accurate method involving the equations given below.

For $A2 \geq A3$ use:

$$\frac{(A1-Am) + 5(A2-Am) + 9(A3-Am)}{(A1-Am) + (A2-Am) + (A3-Am)} \qquad (1)$$

For $A2 < A3$ use:

$$\frac{12(A1-Am) + 5(A2-Am) + 9(A3-Am)}{(A1-Am) + (A2-Am) + (A3-Am)} \qquad (2)$$

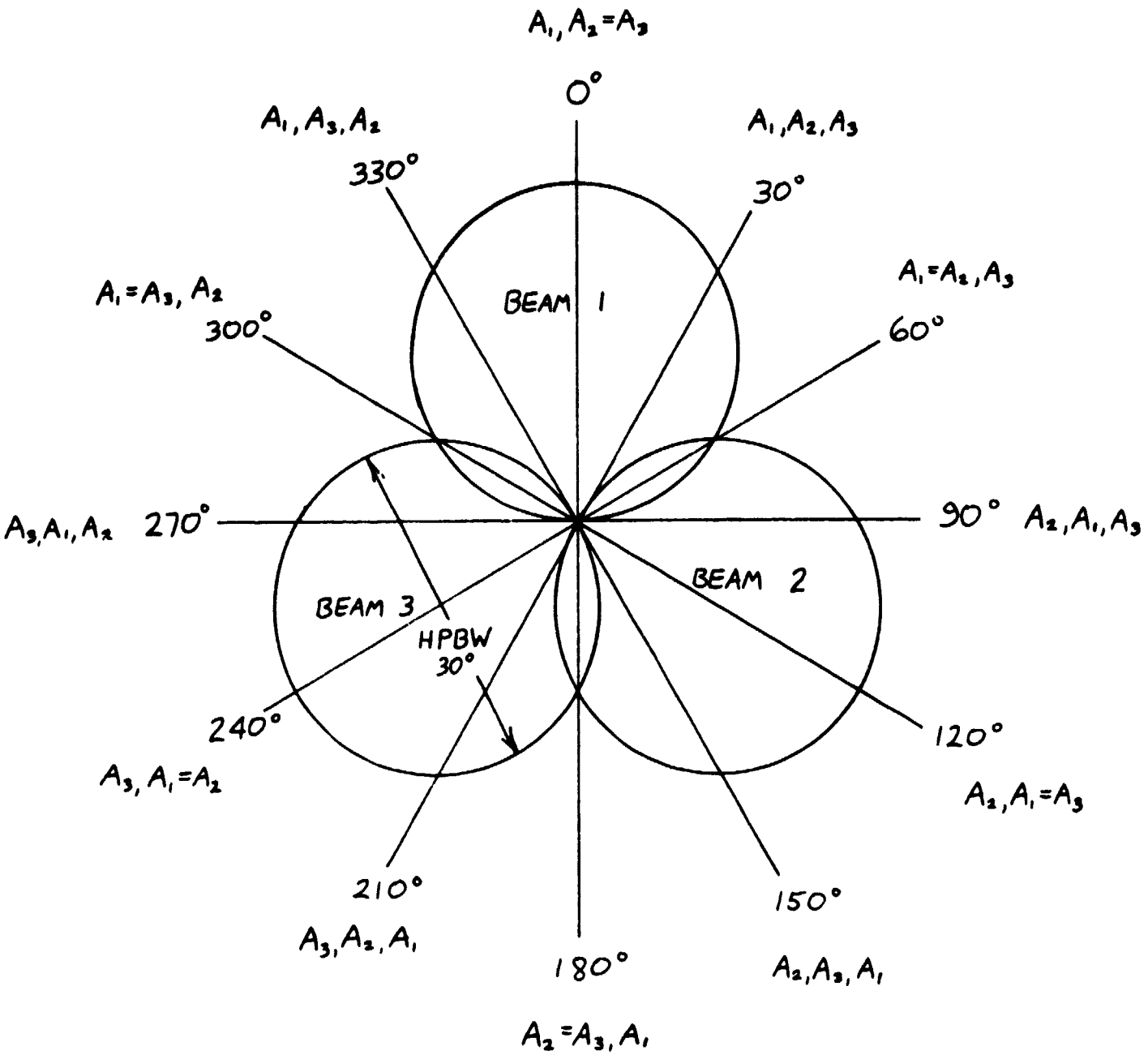

Figure 3-3 Beam Tests for Determining most Probable Direction for Search

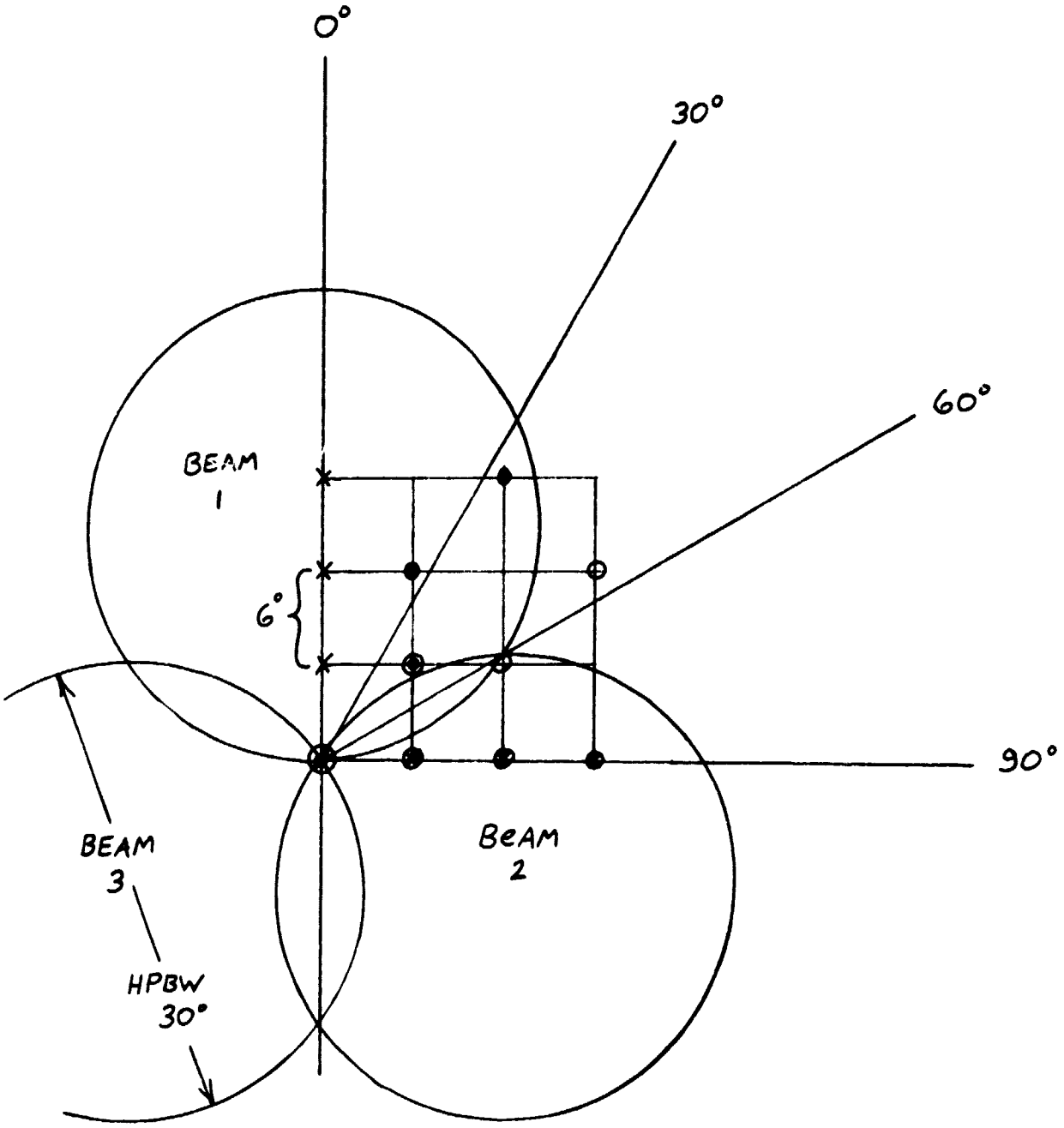

Figure 3-4 Four Beam Search Sequence

In a spacecraft application the controller and antenna driver electronics will be connected in parallel to achieve a 75% reduction in acquisition time. The effect of this improvement is probably negligible for the 3-axis stabilized spacecraft, but it is quite significant for a spinner. A typical acquisition time for Phases I, II and III will be 99 msec.

A general case track mode for a 3-axis stabilized spacecraft was not attempted due its dependence on mission unique parameters.

The acquisition phase provides an accurate pointing direction to the TDRS for a particular instant of time. As time progresses, however, the orbital dynamics tend to alter this initial vector. The direction and rate of change are mission unique parameters which must be included in the track mode software.

In general, pointing corrections will be small, requiring only a few beam changes per TDRS view period. They can be determined prior to launch and incorporated as time dependent software functions.

3.4.2 Spinning Spacecraft

Phases I, II and III described in the previous paragraph also provide initial, real-time acquisition information for the spin stabilized spacecraft. Acquisition time is much more important, however, since the antenna must appear stationary during the computational process. This condition is met even with the serial data transmission from the microprocessor and antenna driver board. During the present 396 msec acquisition time, an antenna rotating at 10 rpm will only traverse 24 degrees of arc. With the projected acquisition time of 99 msec, spin rates up to 30 rpm will present no problem.

From Phase III, the direction of the received signal has been resolved to the nearest directive beam at a particular instant in time. The microprocessor now has sufficient information to anticipate the approximate direction for the received signal as time progresses, and begins to collect data which will lead to an accurate spin rate computation.

In phase IV the microprocessor anticipates the direction of the received signal for future time. It jumps ahead of the received signal and forms three beams on a constant ϕ line. It loops through these beams testing the AGC values and waits for the antenna to rotate through the direction of arrival.

A typical three beam set formed in Phase IV is shown in Figure 3-5. The location of beam #2 is adjacent to the nearest directive beam found in Phase III. The θ position is the same but ϕ is advanced one beam steering increment or approximately 6^{o} in the direction of rotation. Beams #1 and #3 are one beam steering increment above and below Beam #2 respectively. The microprocessor forms the beam and samples the AGC value. This cycle is repeated until the AGC value for one of the new beams is within 0.5 dB of the AGC value from Phase III. AGC values are considered equal when they are within 0.5 dB of each other since non-uniform system losses may cause the subarray gains to vary slightly. Since the software processing time is extremely short compared to the rotational rate of the antenna, the three beams are formed and the AGC values are tested many times before this AGC equality condition is met. However, as time progresses the peak of the beam is rotating toward the true direction of arrival for the received signal and the AGC value is increasing. When the equality condition is met, the θ, ϕ location of the beam is stored in a table. Having found a valid data point, the microprocessor continues by advancing ϕ one beam steering increment in the direction of rotation and repeats the same steps. The three beams are again formed on a new constant ϕ line with the same values. When an AGC value for one of the three beams comes within 0.5 dB of the AGC value from Phase III, the location is stored as the second entry in the table. This process continues for 90^{o} of rotation and then the average θ value from these 15 beams is computed. This θ direction remains constant since the antenna is spinning about its axis of symmetry.

The basic data collection process of Phase IV is repeated in Phase V with two changes. First, a single beam is formed ahead of the target at the average value from Phase IV. The AGC is continuously sampled until the equality condition is met. Second, when the equality condition is met, both the location and a relative time are logged. Time is provided by a 32-bit counter which is set to zero at the beginning of Phase V.

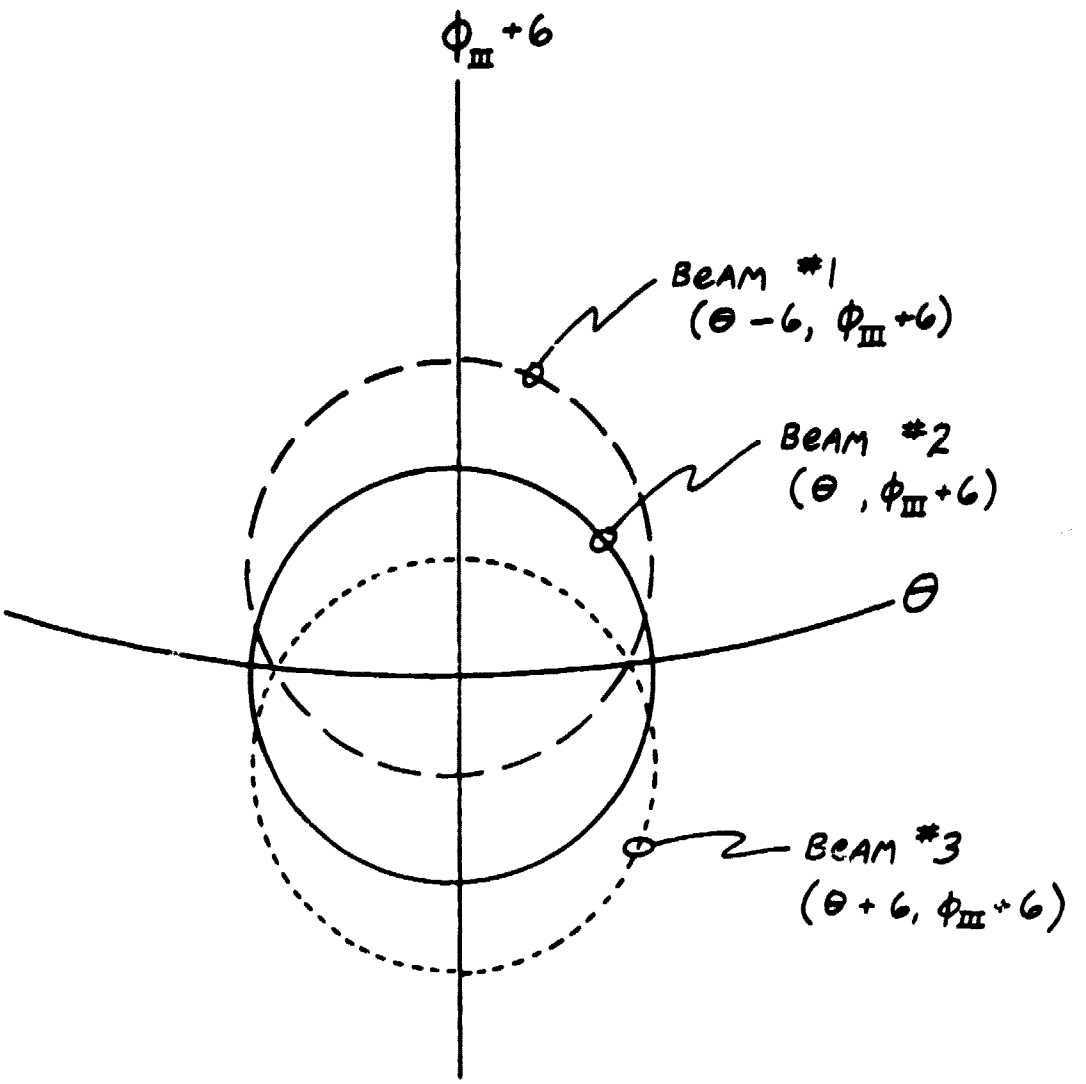

ϕ_{III} = ϕ value from Phase III

Figure 3-5 Three Beam Set - Phase IV

This single beam data collection process continues for three revolutions (i.e. ϕ is advanced 1080^0 from its initial Phase IV value).

The data table has approximately 180 entries at the completion of Phase V. The data is correlated because the AGC equality condition is generally satisfied on the "leading edge" of the beam or before the peak of the beam is coincident with the direction of arrival for the received signal.

The data collected in Phase V provides adequate information to compute the spin rate $\dot{\phi}$ ($d\phi/dt$).

$\dot{\phi}$ is the change in angle ϕ divided by the time it takes to traverse this angle. This computation is performed between adjacent entries in the data table. The average of all these values is taken to reduce systematic errors.

Since the beam steering increment is a known constant, the time between beam changes is also a constant inversely proportional to $\dot{\phi}$. The inverse of $\dot{\phi}$ is the beam switching time between adjacent beams and is a function of the actual spin rate.

During the 400 msec it takes to perform these calculations the ESSA antenna has rotated a small amount and the exact direction of the received signal is no longer known. The final task in the acquisition sequence then is to re-establish this direction in real-time before the track mode is initiated. This is a straightforward procedure using the equation below since all the data is known:

$$\phi_{now} = \phi_{initial} + \dot{\phi}(T_{now} - T_{initial})$$

The initial values of ϕ and T can refer to any entry in the data table. The time T_{now} can be read from the internal counter which is still keeping time relative to the start of Phase V. (This is the same counter which provided the time for each data entry). The spin rate $\dot{\phi}$ is known from an earlier

calculation. The microprocessor controller will form a beam at the predicted location and test the AGC level to verify the direction upon entering the track mode.

Track Mode: The controller enters the track mode with a calculated position ϕ_{now} for time T_{now}. This is not a valid position, however, since ϕ_{now} lags the real-time position by an amount equal to the computational time. To overcome this intrinsic delay the first beam is formed ahead of the current position for a time T_{first} which is calculated and stored in memory. The microprocessor continuously compares the time from the real-time clock to the time stored in memory and when the two are equal the despin or track mode is in sync with the actual position. The AGC is sampled and compared to a predetermined level for final verification before the track mode is initiated. This entire procedure requires 7 msec.

In the track mode the next beam position and time are computed in advance. When the time on the real-time clock equals the calculated value, the new beam is formed in less than 1 microsecond. This process is repeated throughout the 40 minute TDRS view period. At the end of that time the controller enters the acquisition sequence again in anticipation of the second TDRS. The tracking function developed for a spinning spacecraft provides an accurate spin rate and elevation angle determination, and performs electronic beam despinning without any ground or spacecraft inputs. However, it is still incomplete because the mission unique orbit aspects mentioned in Section 3.4.1 must be included to update the pointing direction several times during each TDRS view period.

4.0 HARDWARE DESCRIPTION AND FUNCTION

An important feature of the overall system design is the use of standard circuitry and off-the-shelf components in the microprocessor controller. The operational versatility is strictly a function of the software programming. As a result only a basic functional description is provided in the following sections. A complete set of controller schematics are provided in Appendix B.

4.1 Antenna Control System

A block diagram of the ESSA antenna control electronics is shown in Figure 4-1. Hardware implementation consists of four main boards; the Texas Instruments TM990/100M microcomputer, the input/output board, the LED dome driver, and the PIN diode driver. All boards and the commercial power supplies are located in the ESSA control box except the PIN diode driver board which is attached to the antenna structure and connected to the console via a serial interface. The serial interface was selected only to facilitate antenna range testing. Reducing the number of wires between the controller and antenna driver board was imperative since the spinning tests required the use of slip rings. In an actual spacecraft application, however, a parallel interface will be used for improved performance and higher reliability.

The TM900/100M CPU board contains 4096 16-bit words of EPROM (Erasable Programmable Read Only Memory), the TMS 9900 microprocessor, terminal interfaces, and TIBUG. Four type 2716 (2K x 8) EPROMS are used and contain all of the operating software and TIBUG which is a comprehensive, interactive debug monitor written by Texas Instruments. The 512 words of RAM proved to be adequate for temporary storage and therefore no RAM expansion was required. The TMS9900 microprocessor utilizes a versatile direct command-driven I/O interface designated as the communications-register unit (CRU). The CRU provides up to 4096 directly addressable input bits and 4096 directly addressable output bits. Both input and output bits can be addressed individually or in fields of 1 to 16-bits. The TM990/100M also contains one TMS 9901 which provides the necessary address decoding and latches to implement 16 CRU I/O lines. These I/O lines are used as discretes (single bit) for controlling the analog to digital converter and not for parallel I/O. The TMS 9901 also contains the hardware for all interrupts used in ESSA. The CPU board provides the necessary hardware and software to communicate with either a ASR733 keyboard/printer terminal which was used during the development phase or the handheld TM990/301 microterminal which is used for normal operation of the ESSA console.

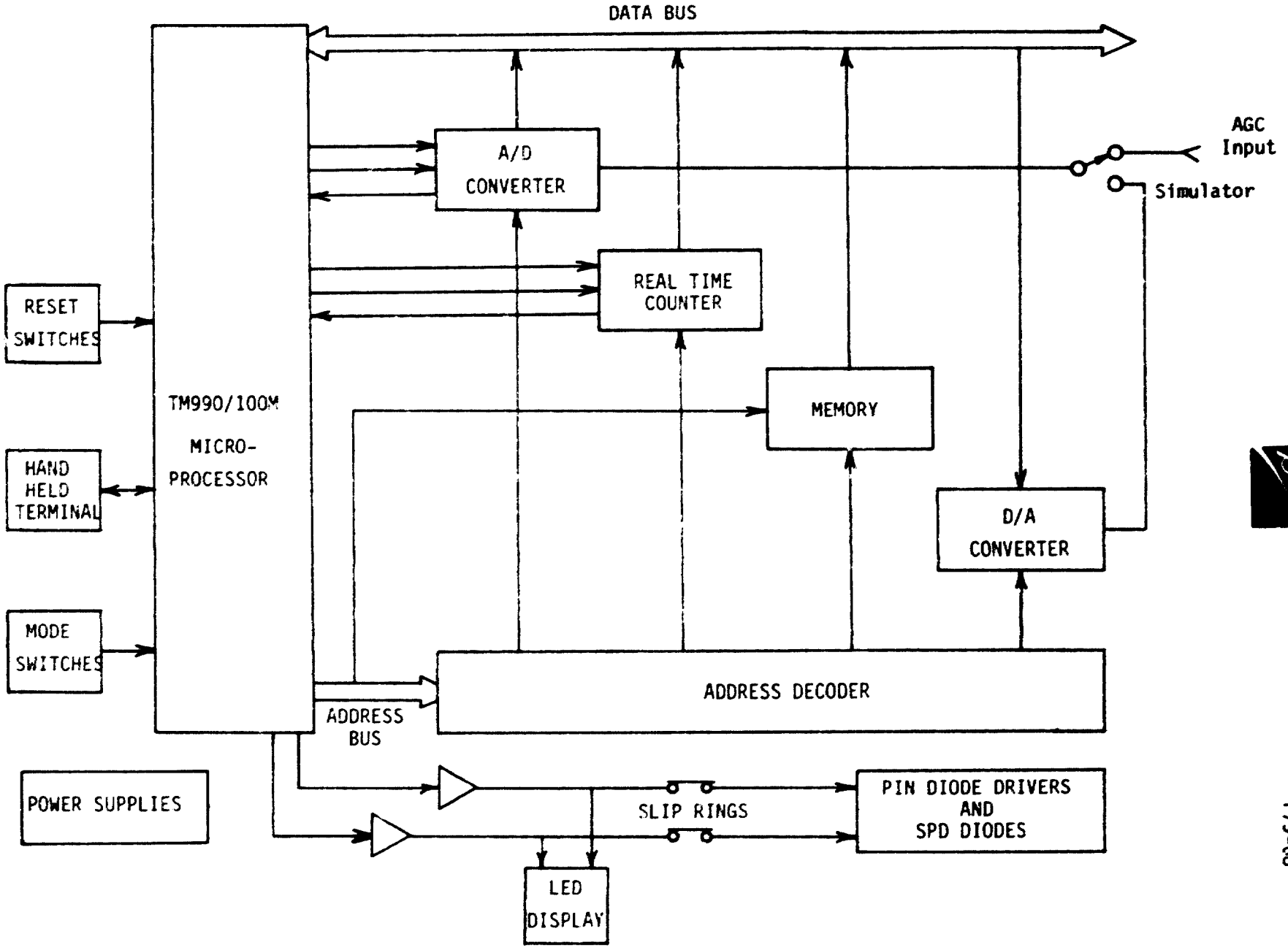

Figure 4-1 ESSA Controller Block Diagram

F79-08

The I/O (Input/Output) board which was designed by BASD contains the two converters, a real-time counter, and overhead circuits. A 12-bit analog to digital converter is used to convert the 0 to +6 VDC AGC analog signal to a digital word representing the signal level. The second converter is a digital to analog type that is used to generate the AGC signal from the simulator described in Section 4.2. The lower half of the real-time counter is implemented in hardware and interrupts the microprocessor every 10.9 msec while the upper half of the real-time counter is implemented in software. All of the above I/O devices are connected in parallel between the data bus and the address bus; and each has a unique address which the CPU board outputs on the address bus when transferring data to or from the I/O board on the data bus. (This technique is known as Memory Mapped I/O). The main overhead circuits are the address decoder which enables only one I/O device at a time and the bi-directional bus buffers which control the direction of data flow.

The LED dome and PIN diode driver boards are BASD designed and are essentially the same as those used in the manual ESSA control box from Contract NAS5-23518 except for two aspects. Both boards now communicate with the CPU board via several interfaces and the PIN diode driver board has an extra set of registers which allows all 120 elements to update in less than 1 μsec.

4.2 AGC Simulator

An AGC simulator was included to simplify software development and system check-out in the absence of an antenna range test facility. This capability was incorporated as a permanent feature in the engineering system to permit conference room type demonstrations.

The simulator is primarily a software package requiring only two toggle switches and digital to analog converter for implementation. Its function is the internal generation of an AGC voltage proportional to the received signal strength. The theory of operation is as follows. When the simulation switch is set, a target position is created by the simulation software. This target can be at a fixed position or rotating depending on the spin mode toggle switch. When an AGC voltage is called for the simulation software computes the solid angle between the calculated beam position and the target. This angle becomes the argument

in a second order polynomial which provides a mathematical model of the antenna pattern with accurate gain roll-off characteristics as a function of solid angle away from the beam peak. This gain level is converted into a dc voltage by the D/A converter and fed back into the AGC input port. A separate polynomial function is used to represent a single element pattern as well.

The disadvantage of the simulator is a substantial overhead burden on the microprocessor. The effect is to slow down the execution of the algorithm sequence due to the long pauses imposed by the AGC computations.

5.0 PERFORMANCE TEST RESULTS

Upon completion of the microprocessor controller and subsequent software debugging, the performance characteristics of the engineering model system were evaluated with antenna range tests. All tests were carried out per the requirements of Test Procedure 58826. The test results with typical data examples are described for each mode in the sections that follow.

5.1 Omnidirectional Mode

Separate Radiation Distribution Patterns (RDPs) were taken for each of the two beams described in Section 3.1. Computer analysis of this data is presented in Tables 5-1 and 5-2 in terms of gain level and percent of hemispherical coverage. Coverage at the -7 dB level is roughly 82% for both patterns.

A composite RDP was created in real-time allowing the microprocessor to select the beam having the maximum amplitude. Computer analysis of this pattern is summarized in Table 5-3. A significant coverage improvement over either of the individual patterns is apparent at the -7 dB gain level. The percent of hemispherical coverage increased from 82 to 97.6. Conical cuts of the far-field patterns are shown in Figures 5-1 through 5-4 for $\theta = 90^{0}$, 60^{0}, 30^{0} and 0^{0} respectively. The two independent beams are identified by the solid and dashed lines. The composite pattern is the circumference of the plot. Figure 5-5

Table 5-1

OMNI MODE PERFORMANCE - BEAM #1

LIMIT IN dB	% > OR = LIMIT
0.0 dB	39.0 %
-1.0 dB	46.9 %
-2.0 dB	53.4 %
-3.0 dB	60.3 %
-4.0 dB	66.4 %
-5.0 dB	72.3 %
-6.0 dB	76.9 %
-7.0 dB	81.0 %
-8.0 dB	84.5 %
-9.0 dB	87.8 %
-10.0 dB	90.5 %
-11.0 dB	92.7 %
-12.0 dB	94.4 %
-13.0 dB	95.9 %
-14.0 dB	96.8 %
-15.0 dB	97.5 %
-16.0 dB	98.0 %
-17.0 dB	98.5 %
-18.0 dB	98.9 %
-19.0 dB	99.1 %
-20.0 dB	99.3 %

Table 5-2

OMNI MODE PERFORMANCE - BEAM #2

LIMIT IN dB	% > OR = LIMIT
0.0 dB	35.0 %
-1.0 dB	44.4 %
-2.0 dB	51.9 %
-3.0 dB	59.9 %
-4.0 dB	66.8 %
-5.0 dB	73.8 %
-6.0 dB	78.7 %
-7.0 dB	82.7 %
-8.0 dB	85.7 %
-9.0 dB	88.5 %
-10.0 dB	91.1 %
-11.0 dB	93.0 %
-12.0 dB	94.5 %
-13.0 dB	95.6 %
-14.0 dB	96.4 %
-15.0 dB	97.2 %
-16.0 dB	97.7 %
-17.0 dB	98.2 %
-18.0 dB	98.5 %
-19.0 dB	98.8 %
-20.0 dB	99.0 %

Table 5-3

OMNI MODE PERFORMANCE WITH BEAM SWITCHING

LIMIT IN dB	% > OR = LIMIT
0.0 dB	72.0 %
-1.0 dB	79.1 %
-2.0 dB	85.2 %
-3.0 dB	89.4 %
-4.0 dB	92.5 %
-5.0 dB	94.7 %
-6.0 dB	96.6 %
-7.0 dB	97.6 %
-8.0 dB	98.2 %
-9.0 dB	98.8 %
-10.0 dB	99.2 %
-11.0 dB	99.5 %
-12.0 dB	99.7 %
-13.0 dB	99.8 %
-14.0 dB	99.9 %
-15.0 dB	99.9 %
-16.0 dB	100.0 %
-17.0 dB	100.0 %
-18.0 dB	100.0 %
-19.0 dB	100.0 %
-20.0 dB	100.0 %

shows a real-time composite amplitude pattern created by the microprocessor. The antenna was spinning on axis while receiving a signal from a fixed source. The "spikes" on the pattern indicate amplitude comparison during 5 revolutions or 1800° degrees of mechanical rotation.

Phase information related to the composite pattern is presented in Table 5-4. Instantaneous phase changes due to beam switching were recorded for a range of differential amplitudes. For example, a 0 dB amplitude differential corresponds to the beam crossover points. The measured phase increments refer to the difference in electrical path length from the phase center of each beam to the source.

The beam toggling concept was introduced to meet the hemispherical coverage requirement at the -7 dB gain level. The composite pattern successfully does this, however, the effect of the instantaneous phase and amplitude variations due to beam switching has not been determined. Therefore the phase information in Table 5-4 is included to support a future quantitative telemetry link analysis based on known modulation formats. Such an analysis is beyond the scope of this contract.

Table 5-4

OMNI MODE BEAM TO BEAM PHASE VARIATIONS

ELEVATION ANGLE	DIFFERENTIAL AMPLITUDE (dB)	PHASE VARIATION BEAM TO BEAM (deg.)
$\theta = 90^{o}$	0	-16.3^{o}
	2	+20
	4	+22
	6	-43
	8	+103
	10	-41
$\theta = 60^{o}$	0	+15.8
	2	+14.5
	4	-11.5
	6	+7.2
	8	+6.0
	10	-7.0
$\theta = 30^{o}$	0	+25
	2	-15
	4	+9.8
	6	-4.5
	8	-3.5
	10	+16.5
$\theta = 0^{o}$	No Crossovers	No Data Taken

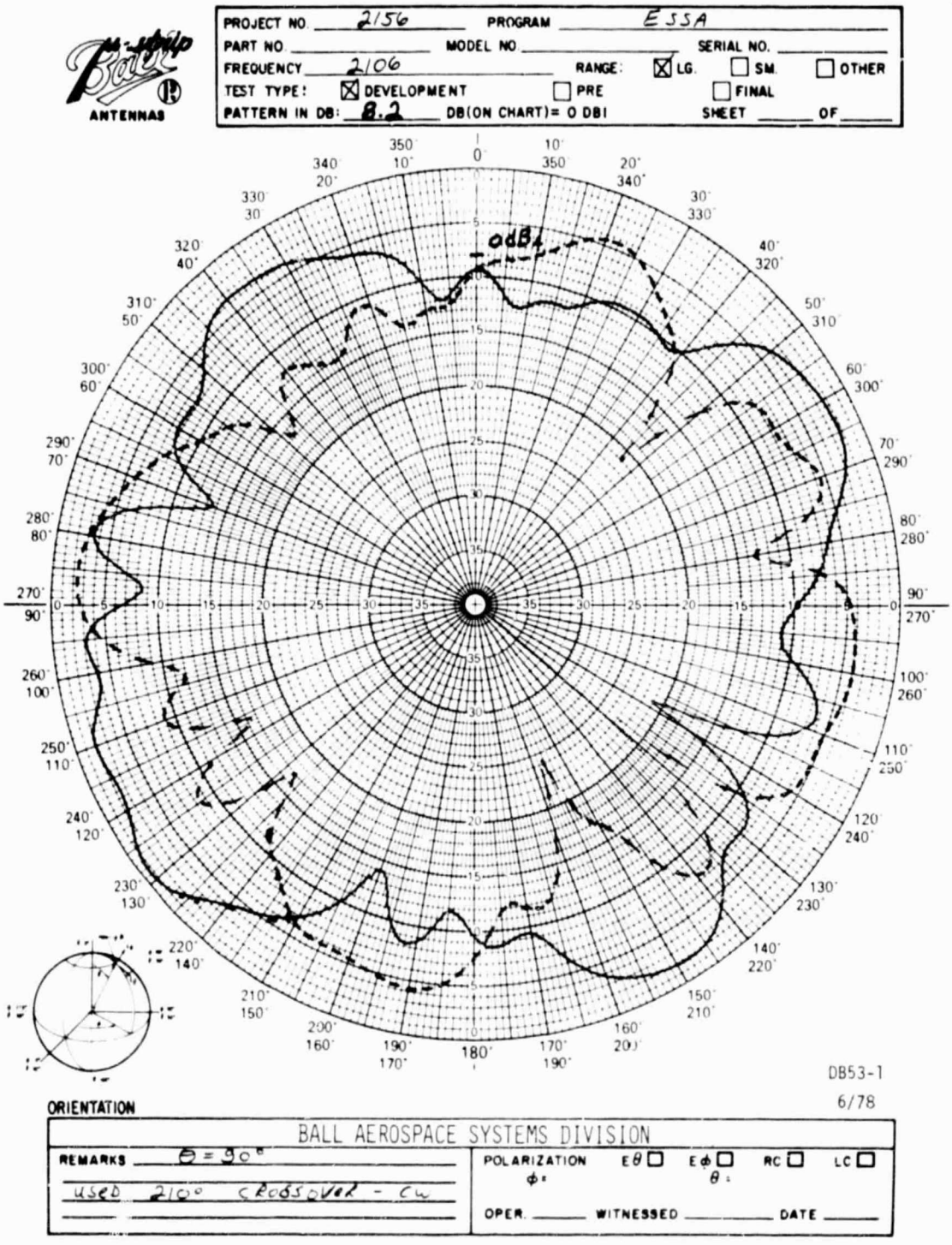

Figure 5-1 Omni Mode Pattern, $\theta=90^{0}$

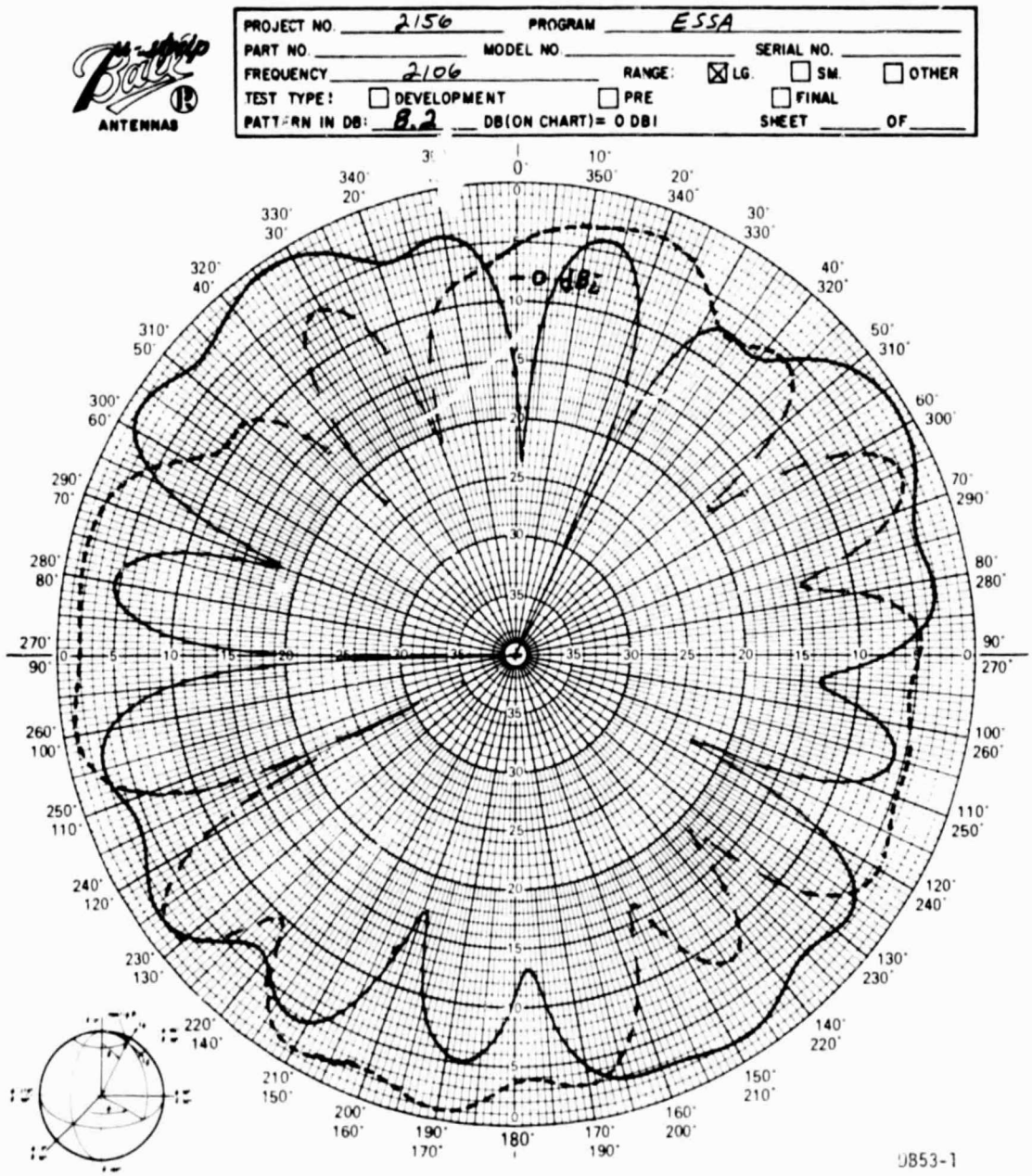

Figure 5-2 Omni Mode Pattern, $\theta=60^{0}$

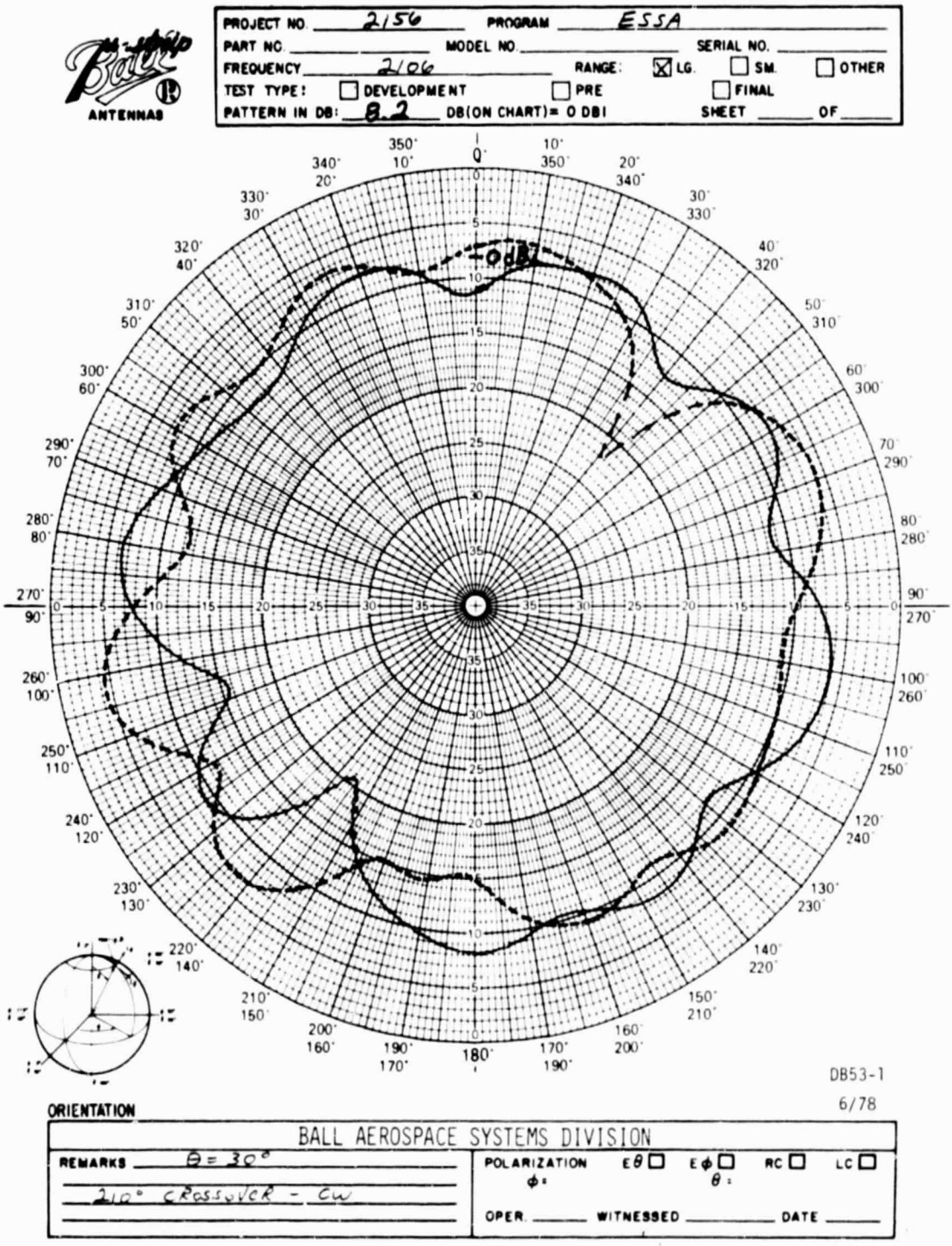

Figure 5-3 Omni-Mode Patterns, $\theta=30^{o}$

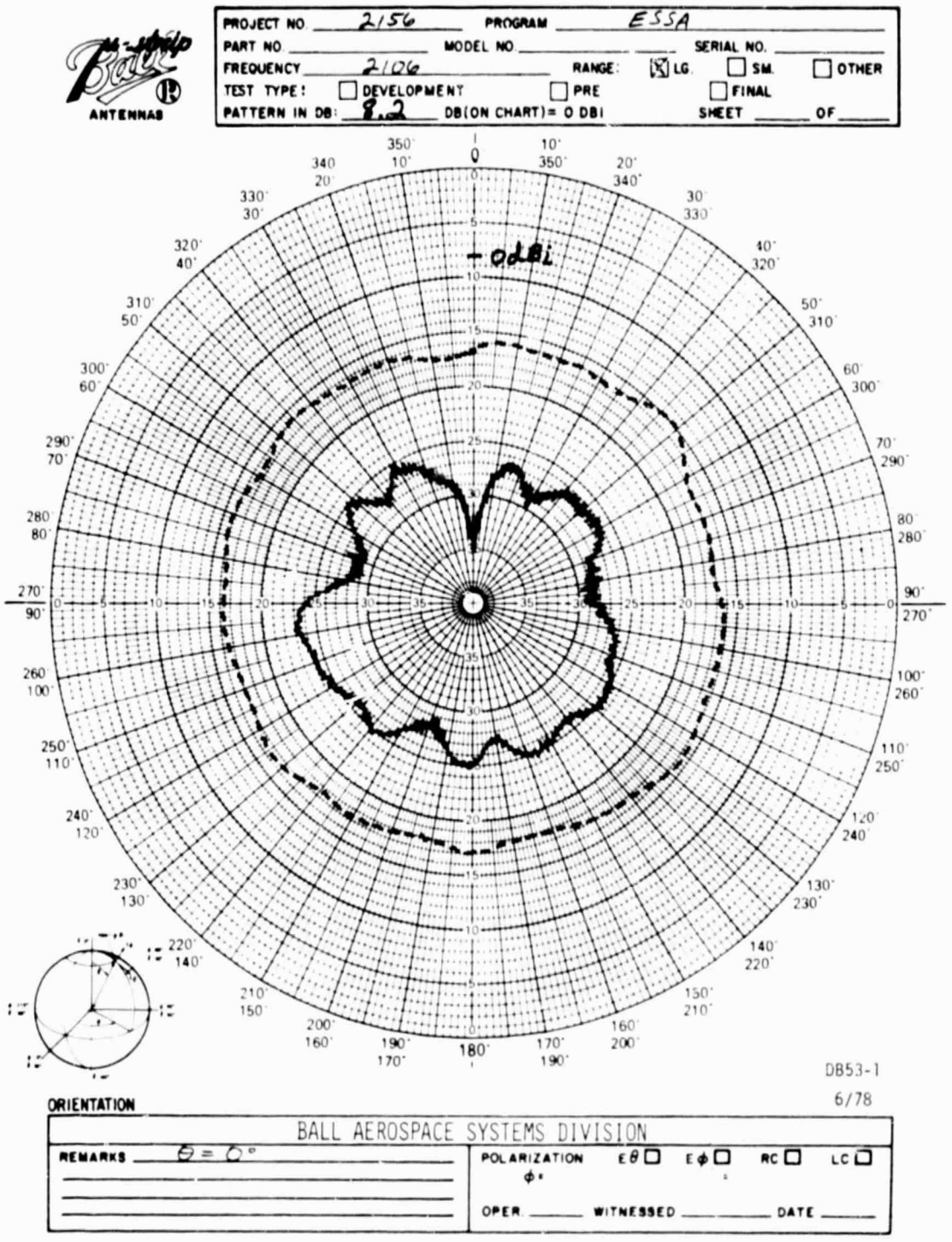

Figure 5-4 Omni-Mode Pattern, $\theta=0^{o}$

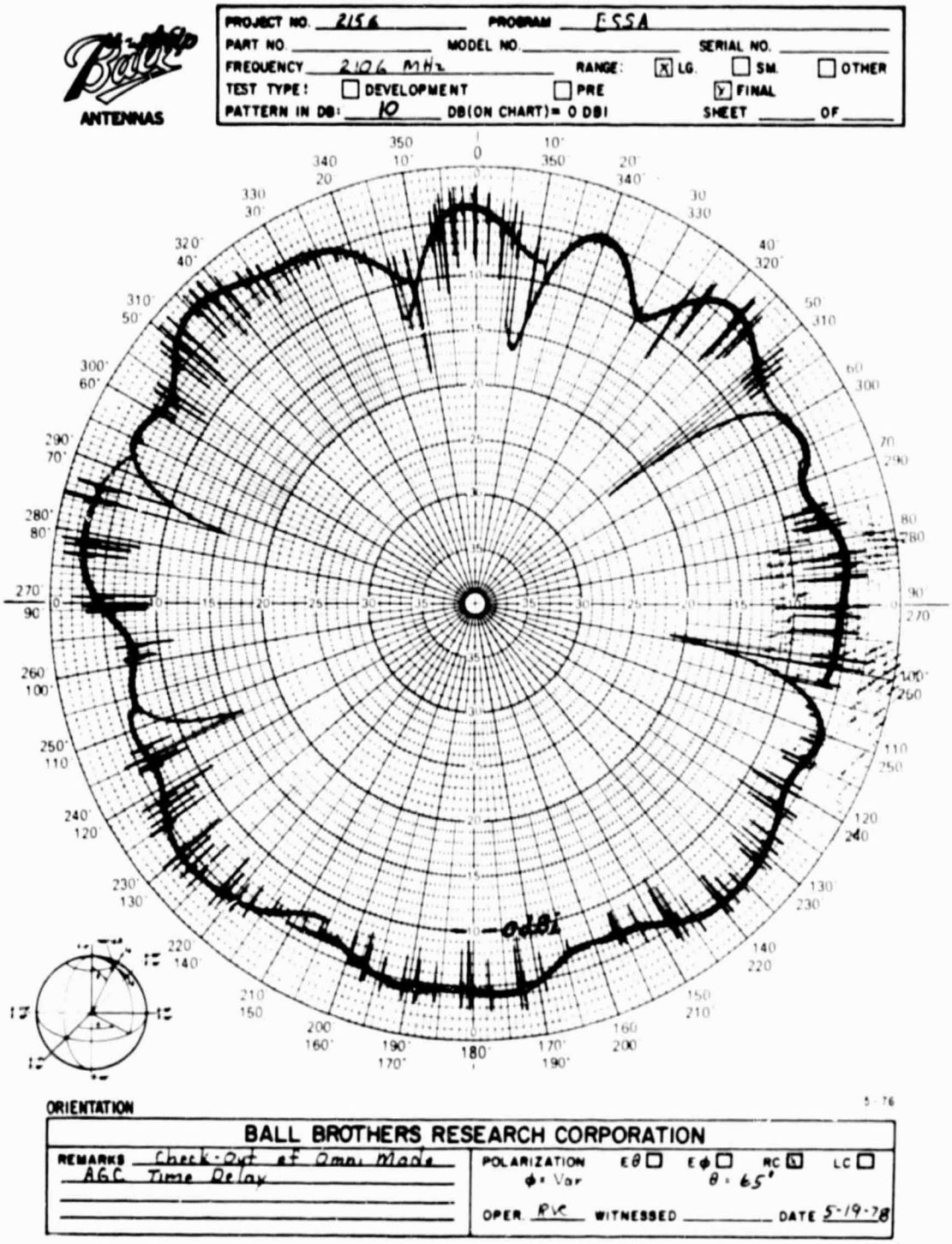

Figure 5-5 Omni Mode Pattern with Beam Switching

5.2 Directive Mode

Directive mode performance was characterized by measurements on fifty beams distributed within the hemispherical coverage region. Emphasis was placed on verification of the beam forming algorithm which selected the subarray elements. The purpose of the directive mode tests was to determine the pointing error between the desired and actual directions.

The test procedure was as follows:

- Both the ESSA antenna and antenna range coordinate systems were synchronized.
- The desired beam pointing direction was inputted to the controller and the antenna range was mechanically aligned in that direction.
- A gain measurement was taken.
- The peak of the beam was found by tweaking the mechanical alignment and the actual azimuth and elevation angles were recorded.
- The solid angle pointing error was calculated using the azimuth and elevation angle differences between the desired and actual pointing directions.

The test data is presented in Table 5-5. The mean angular pointing error is 3.6^{0} which is comparable to the $\pm 3^{0}$ beam pointing capability of the ESSA array. It is also interesting to note that the mean gain which includes all pointing errors is 13.74 dB. Subtracting the 0.7 dB allotted for beam crossover losses results in a coverage gain of 13.04 dB which is 0.2 dB greater than the previous 12.85 dB figure (4). The reason for this gain improvement can be explained as follows. The beam forming algorithm always selects the 12 closest elements to the desired pointing vector. The result is that every subarray consists of

Table 5-5

DIRECTIVE MODE PERFORMANCE

BEAM	DESIRED DIRECTION		ACTUAL DIRECTION		MEASURED GAIN (dB)	POINTING ERROR (DEG)
	θ	ϕ	θ	ϕ		
1	0	0	1	0	14.5	1.0
2	1.5	45	2	45	14.0	0.5
3	3.0	90	3	90	14.2	0
4	4.5	135	4.5	135	14.5	0
5	6.0	180	2	180	14.0	4.0
6	7.5	225	1	180	13.9	6.8
7	9.0	270	14	270	13.5	5.0
8	10.5	315	13	315	13.7	2.5
9	12.0	5	14	5	13.7	2.0
10	13.5	50	14	58	13.9	2.0
11	15.0	95	17	88	14.2	2.8
12	16.5	140	17.5	134	14.6	2.0
13	18.0	185	18.5	193	14.5	2.6
14	19.5	230	18.5	235	14.75	1.9
15	21.0	275	21	270	14.2	1.8
16	22.5	320	22.5	325	13.7	1.9
17	24.0	10	26	20	13.6	4.7
18	25.5	55	28.5	62	14.1	3.3
19	27.0	100	27.5	105	14.1	2.3
20	28.5	145	30	142	14.2	2.1
21	30.0	190	30	195	13.7	2.5
22	31.5	235	31	230	14.6	2.6
23	33.0	280	33	280	13.6	0
24	34.5	325	35.5	330	14.8	3.0
25	36.0	15	40	22	13.0	5.9
26	37.5	60	42.0	60	14.7	4.5
27	39.0	105	41.0	108	14.0	2.8
28	40.5	150	44.0	160	13.9	7.6
29	42.0	195	42.0	188	14.0	4.7
30	43.5	240	42.0	245	14.4	3.7
31	45.0	285	48.5	287	13.7	3.8
32	46.5	330	47.5	337	12.0	5.2
33	48.0	20	46.5	28	13.1	6.1
34	49.5	65	46.5	65	13.7	3.0
35	51.0	110	57.0	115	13.1	7.2

Table 5-5 (Cont'd)
DIRECTIVE MODE PERFORMANCE

BEAM	DESIRED DIRECTION θ	DESIRED DIRECTION φ	ACTUAL DIRECTION θ	ACTUAL DIRECTION φ	MEASURED GAIN (dB)	POINTING ERROR (DEG)
36	52.5	155	57.0	155	14.2	4.5
37	54.0	200	54.0	205	13.1	4.0
38	55.5	245	55.0	250	14.4	4.8
39	57.0	290	61.0	293	14.3	6.9
40	58.5	335	53.0	340	12.3	6.9
41	60.0	25	60.0	30	12.7	4.3
42	61.5	70	62.0	75	12.9	4.4
43	63.0	115	63.0	117	14.6	1.8
44	64.5	160	64.5	160	13.6	0.1
45	66.0	205	64.0	203	13.8	3.5
46	67.5	250	67.5	260	13.9	9.2
47	69.0	295	69.0	298	14.8	2.8
48	70.5	340	72.0	345	12.1	5.0
49	72.0	30	72.0	33	12.9	2.9
50	73.5	75	77.5	83	11.1	8.7

contiguous elements. This was not the case however, with the manual control box. The pre-programmed element combinations were derived to provide 6^{o} beam steering increments. Although the desirability of adjacent elements subarrays recognized for optimum gain, this was not a hard requirement imposed on subarray configurations.

This earlier design error was pointed out and corrected by means of micro-processor controller and the beam forming algorithm. The conclusion is that an overall improvement in coverage gain results when contiguous element subarrays are used exclusively. The additional gain provided by these optimum subarray configurations more than compensates for any losses due to irregular beam steering increments caused by the non-uniform element distribution.

5.3 Multi-Beam Mode

Four sample cases were evaluated in each of the 2, 3 and 4 beam configurations. The test results are summarized in Tables 5-6 and 5-7, and the supporting patterns are shown in Figures 5-6 through 5-17. Assuming a mean peak gain of 13.7 dB from section 5.2, the expected gains for 2, 3 and 4 beams are 10.7 dB, 8.9 dB and 7.7 dB respectively.

The results of the 2 beam tests, Table 5-6, are encouraging in terms of both measured gain and pointing direction. Two distinct beams failed to develop in case 4 because the 45^0 angular separation was small compared to the 53^0 beamwidths. Therefore the two subarrays merged into a single elongated aperture and a fan beam resulted.

Table 5-6
MULTI-BEAM PERFORMANCE - 2 BEAMS

CASE	θ	DESIRED DIRECTION		ACTUAL DIRECTION			
		ϕ_1	ϕ_2	ϕ_1	GAIN	ϕ_2	GAIN
1	27	0	180	5	10.1	179	8.8
2	40	90	225	90	9.4	226	10.3
3	50	45	135	53	10.9	129	11.2
4	60	270	315	301	13.3	---	----

Table 5-7
MULTI-BEAM PERFORMANCE - 3 BEAMS

CASE	θ	DESIRED DIRECTION			ACTUAL DIRECTION					
		ϕ_1	ϕ_2	ϕ_3	ϕ_1	GAIN	ϕ_2	GAIN	ϕ_3	GAIN
1	27	0	120	240	4	7.6	124	8.8	234	8.3
2	40	45	135	225	47	8.2	140	8.2	221	9.0
3	50	90	150	210	90	6.7	152	6.9	219	8.2
4	60	250	295	340	247	8.8	---	---	---	---

Cases 1 and 2 in the 3 beam test results, Table 5-7, are as expected. The beamwidths are broad approximately 70^0 and the gain figures are roughly equal. However, in cases 3 and 4 the solid angle pointing separations are small compared to the beamwidth and the overlapping beams create an interferometer type pattern. This is particularly evident in Figure 5-13 by the narrow beamwidths and deep nulls.

In all of the 4 beam cases the interferometer effect dominates, since the maximum angular separation of 90^0 is nearly equal to 82^0 half power beamwidth. This is evident by examining the patterns in Figures 5-14 through 5-17. This is the same phenomena which limited the performance of a single array in the omni mode. In fact, if case 1, Figure 5-14, had a θ value of 60^0 instead of 27^0, the pattern would be identical to either one of the single beams which is used in the omni mode.

In addition to the multi-beam tests described above a two beam crossing test was also performed. A six element subarray remained fixed as a second six-element subarray was steered closer and closer until a single 12-element subarray resulted. This sequence is presented in Figures 5-18 through 5-21. In view of the 2 beam test results there are no surprises. At a separation of 45^0, Figure 5-18, two distinct beams are present. As the separation is decreased to 34^0 and then to 23^0, Figures 5-19 and 5-20 respectively, a fan beam results from the single elongated aperture. Finally at a separation of 12^0 a single circular aperture is created with a gain of 13.8 dB. (Note the 0 dBi reference level change in Figure 5-21). The pattern for 0^0 separation was identical to that of Figure 5-21 since the subarray elements remained unchanged.

In summary these test results indicate that multiple beams are practical using the ESSA array as long as the interferometer effect is avoided. This is accomplished by paying careful attention to the angular pointing direction and beamwidth combinations. When this is done both the gain and pointing direction are very close to the predicted values.

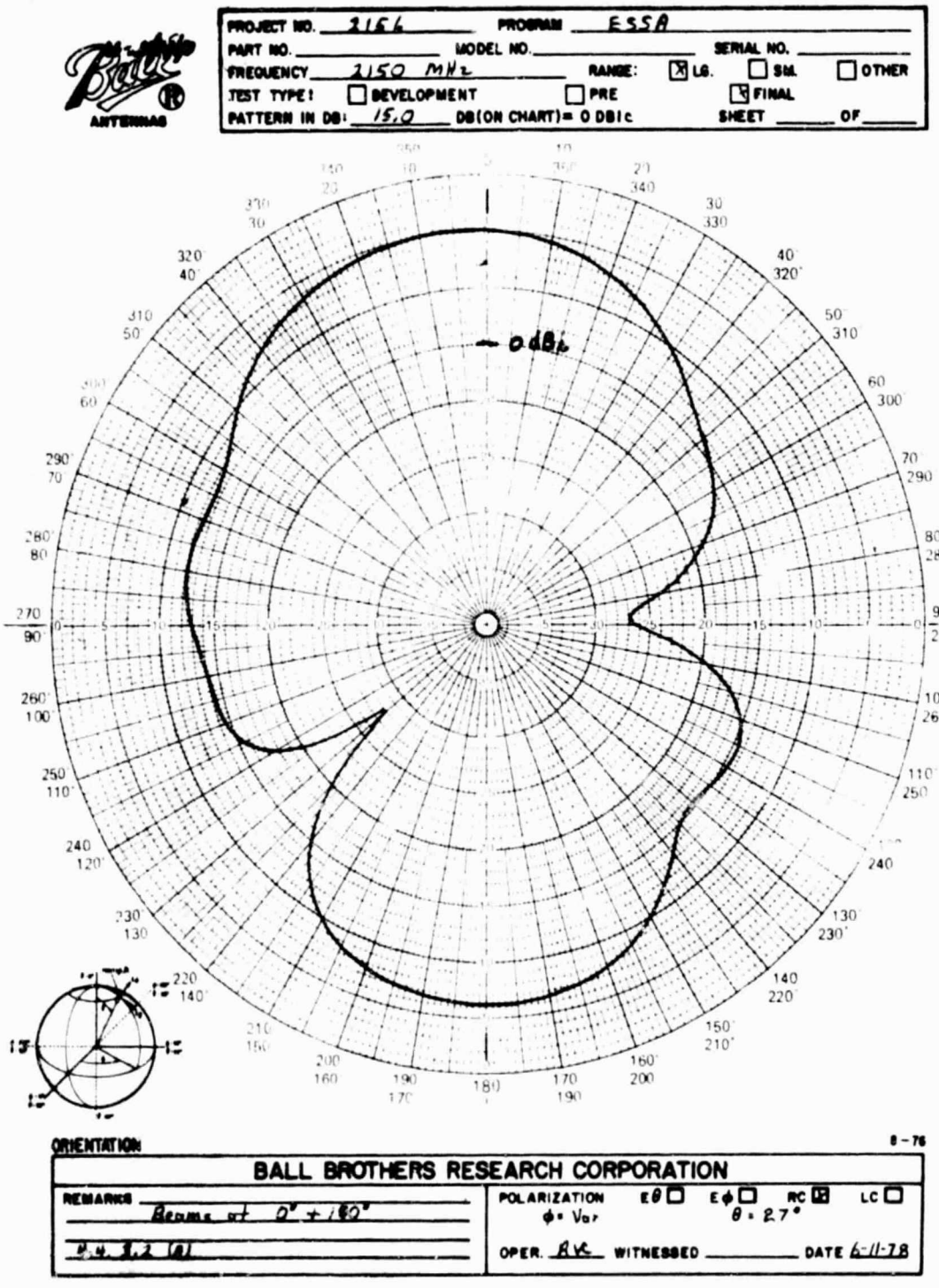

Figure 5-6 Two Beam Pattern - 0^{o} & 180^{o}

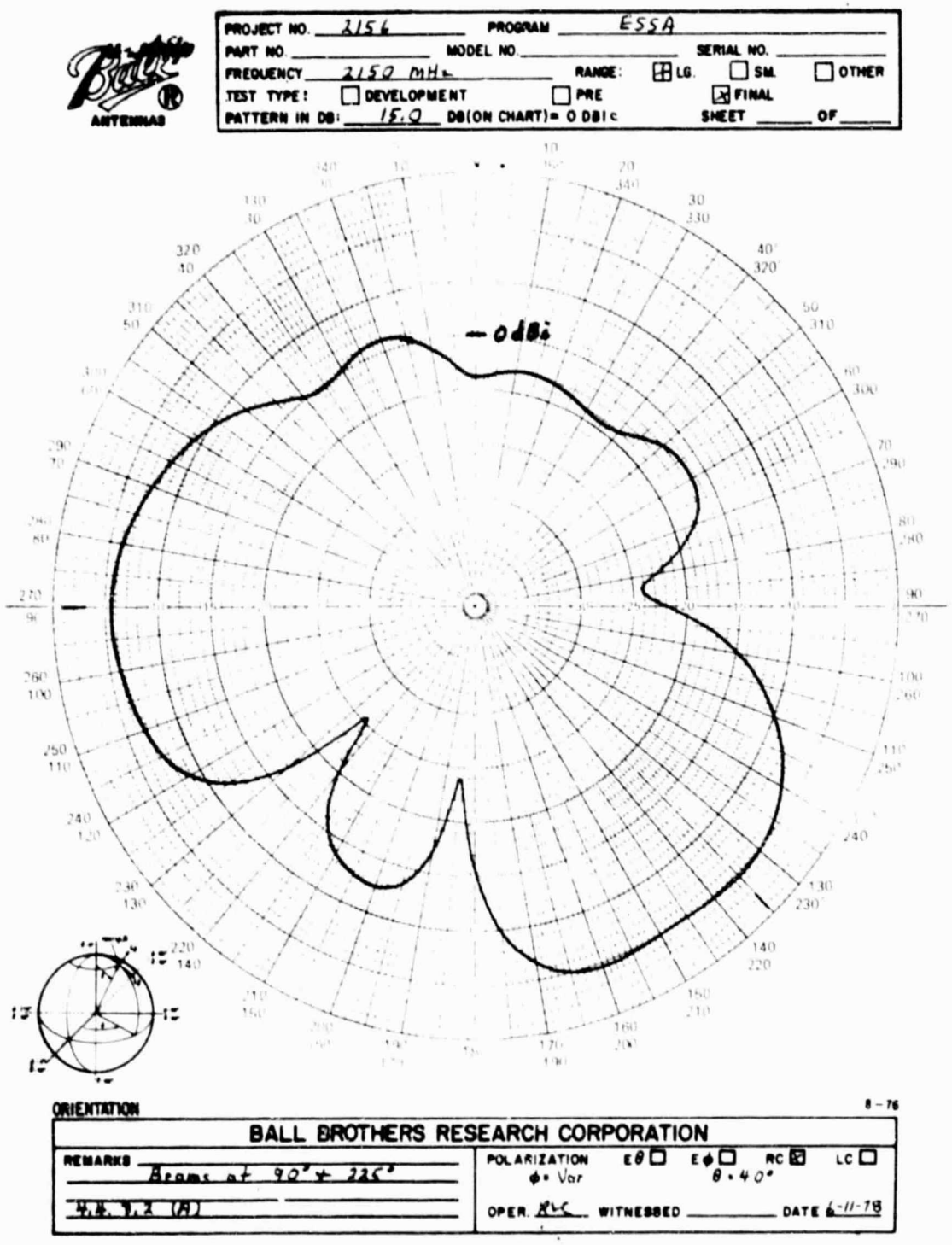

Figure 5-7 Two Beam Pattern - 90° & 225°

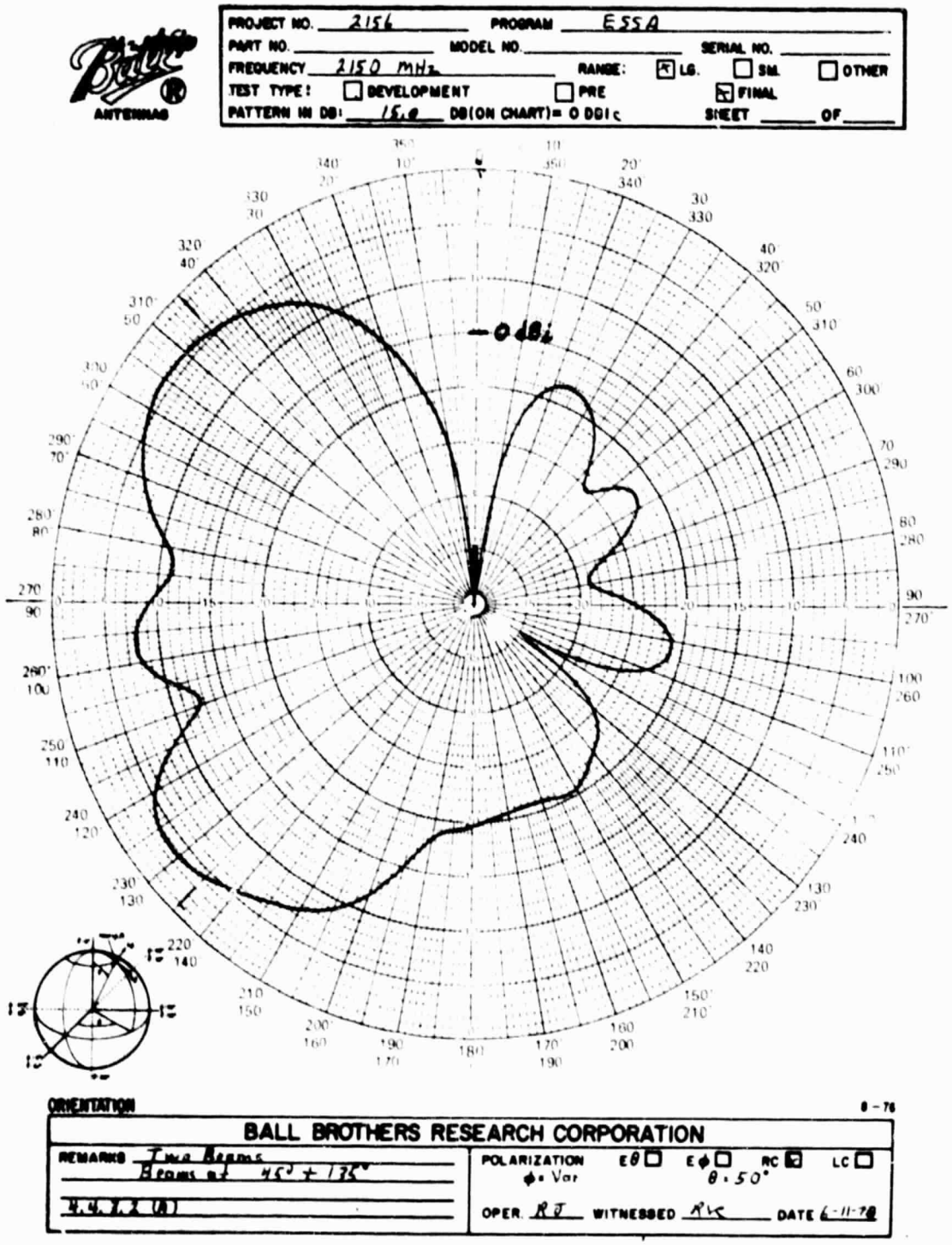

Figure 5-8 Two Beam Pattern - 45° & 135°

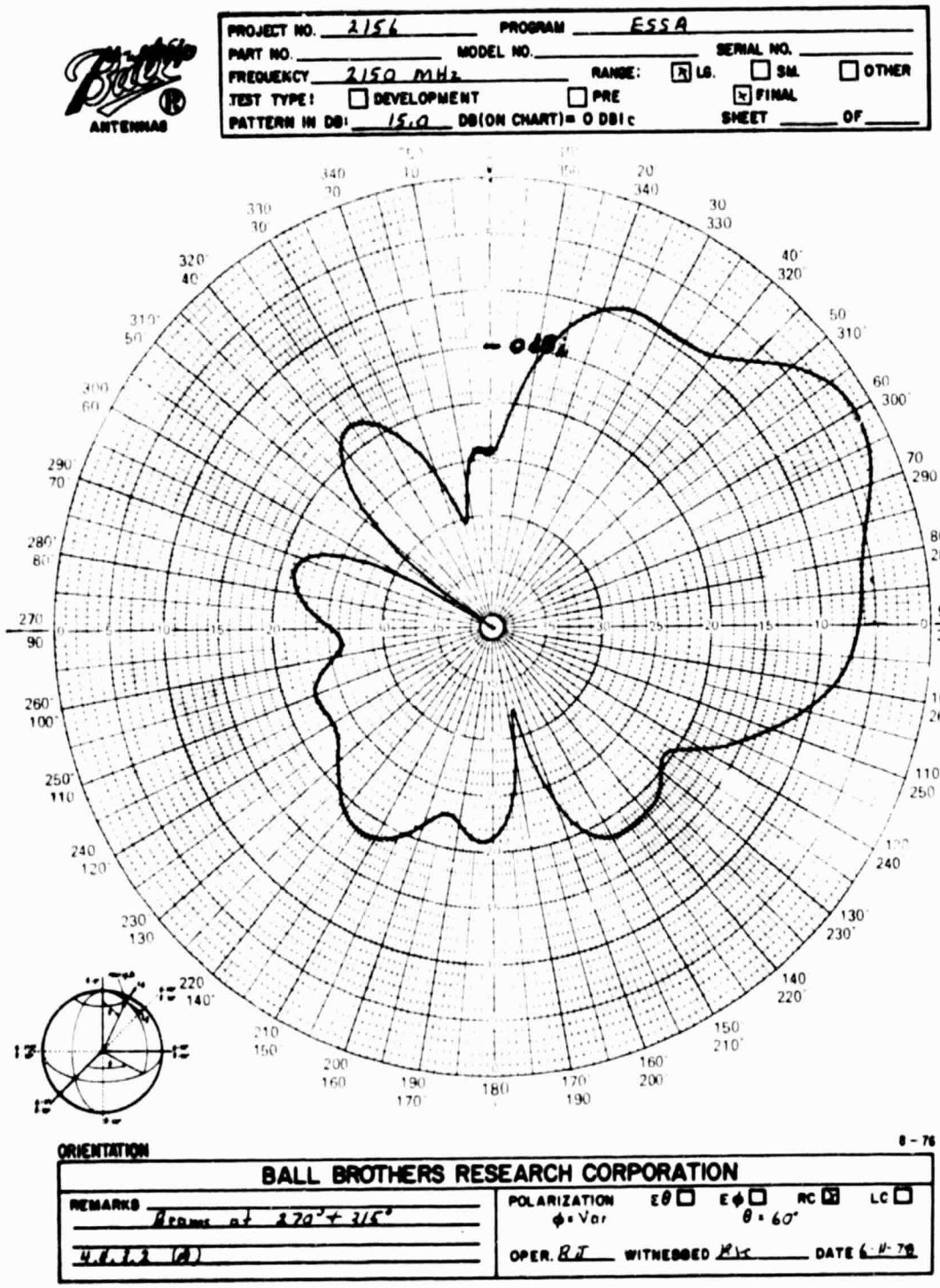

Figure 5-9 Two Beam Pattern - 270° & 315°

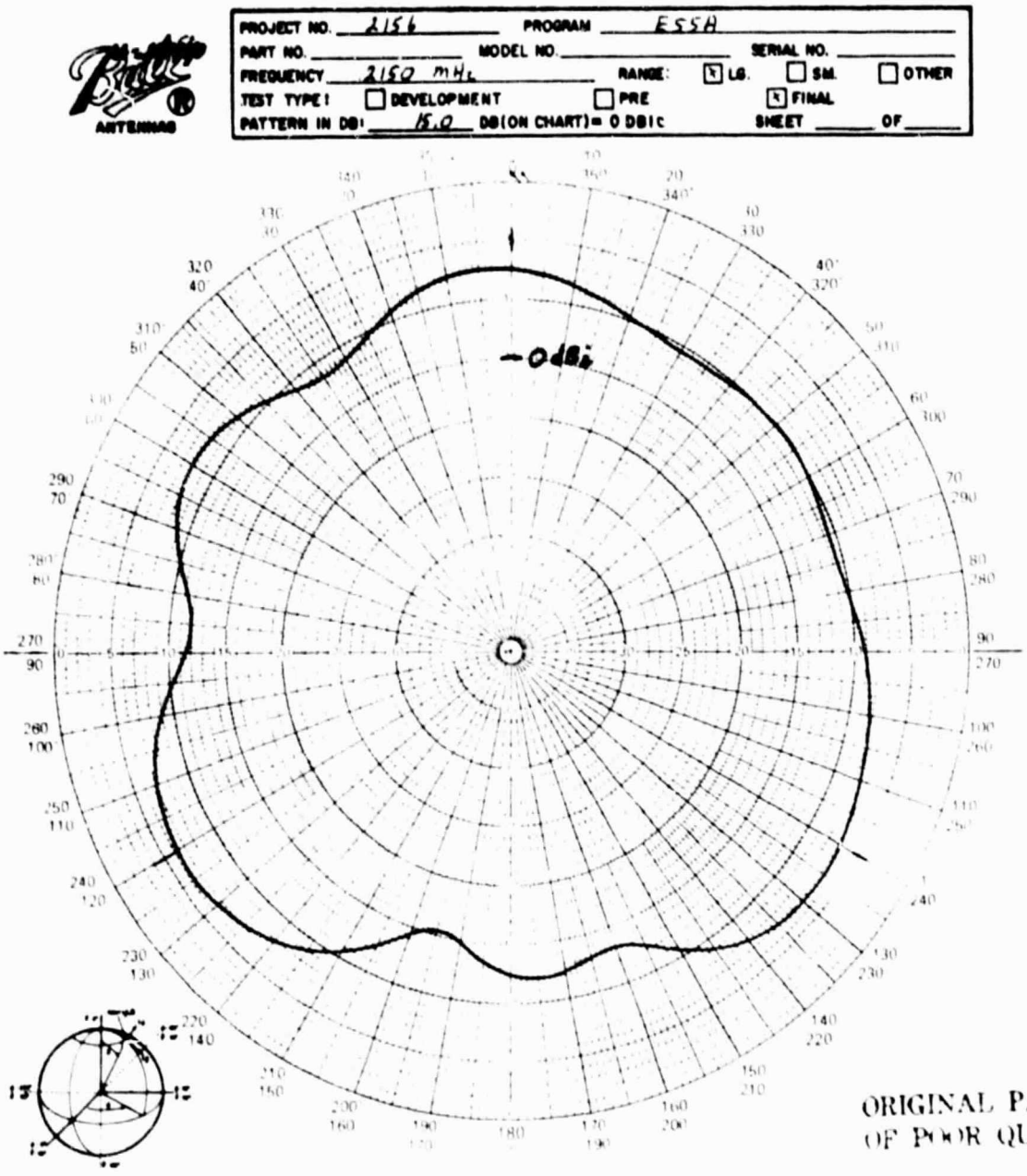

ORIGINAL PAGE IS
OF POOR QUALITY

Figure 5-10 Three Beam Pattern - 0^{0}, 120^{0} & 240^{0}

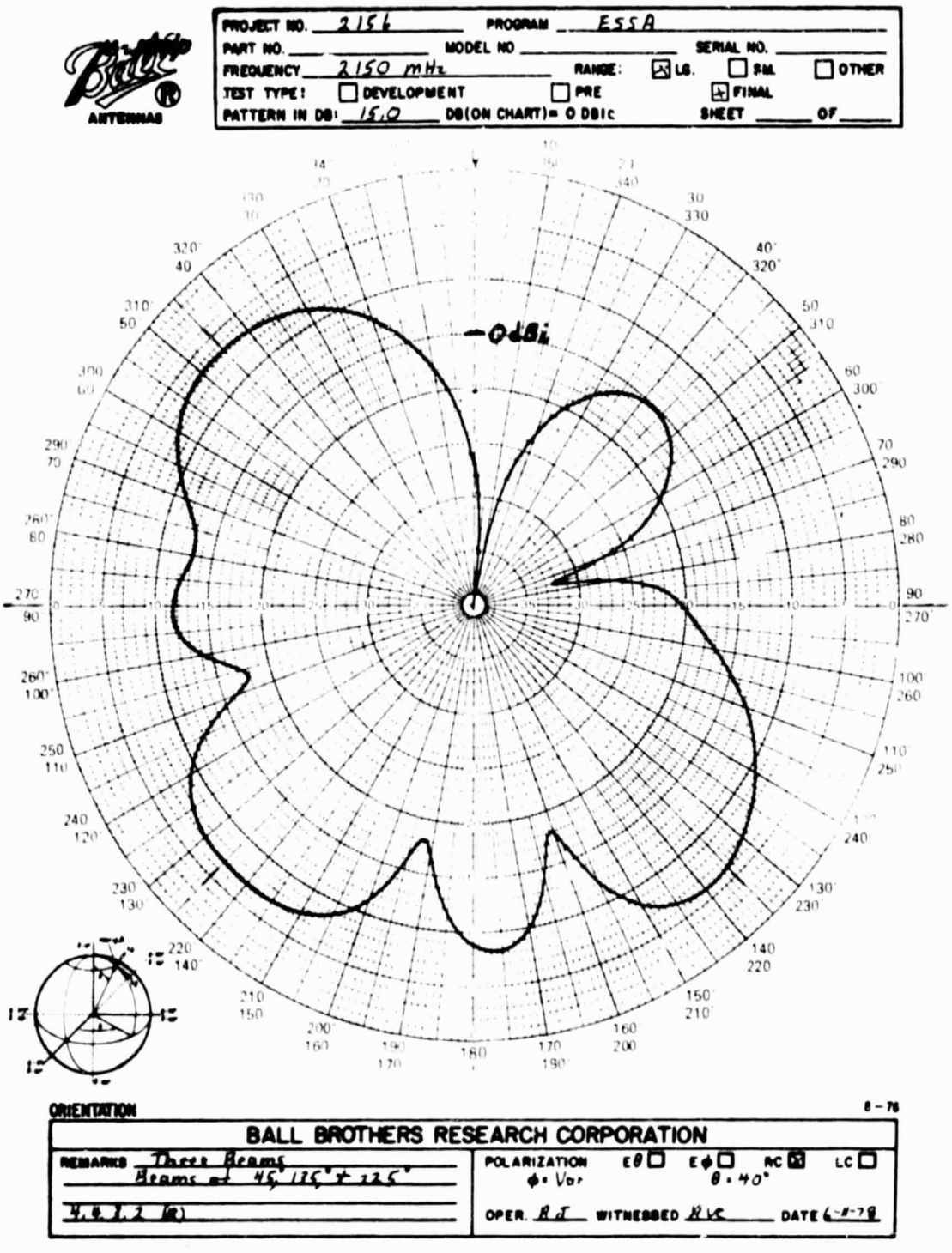

Figure 5-11 Three Beam Pattern - 45°, 135° & 225°

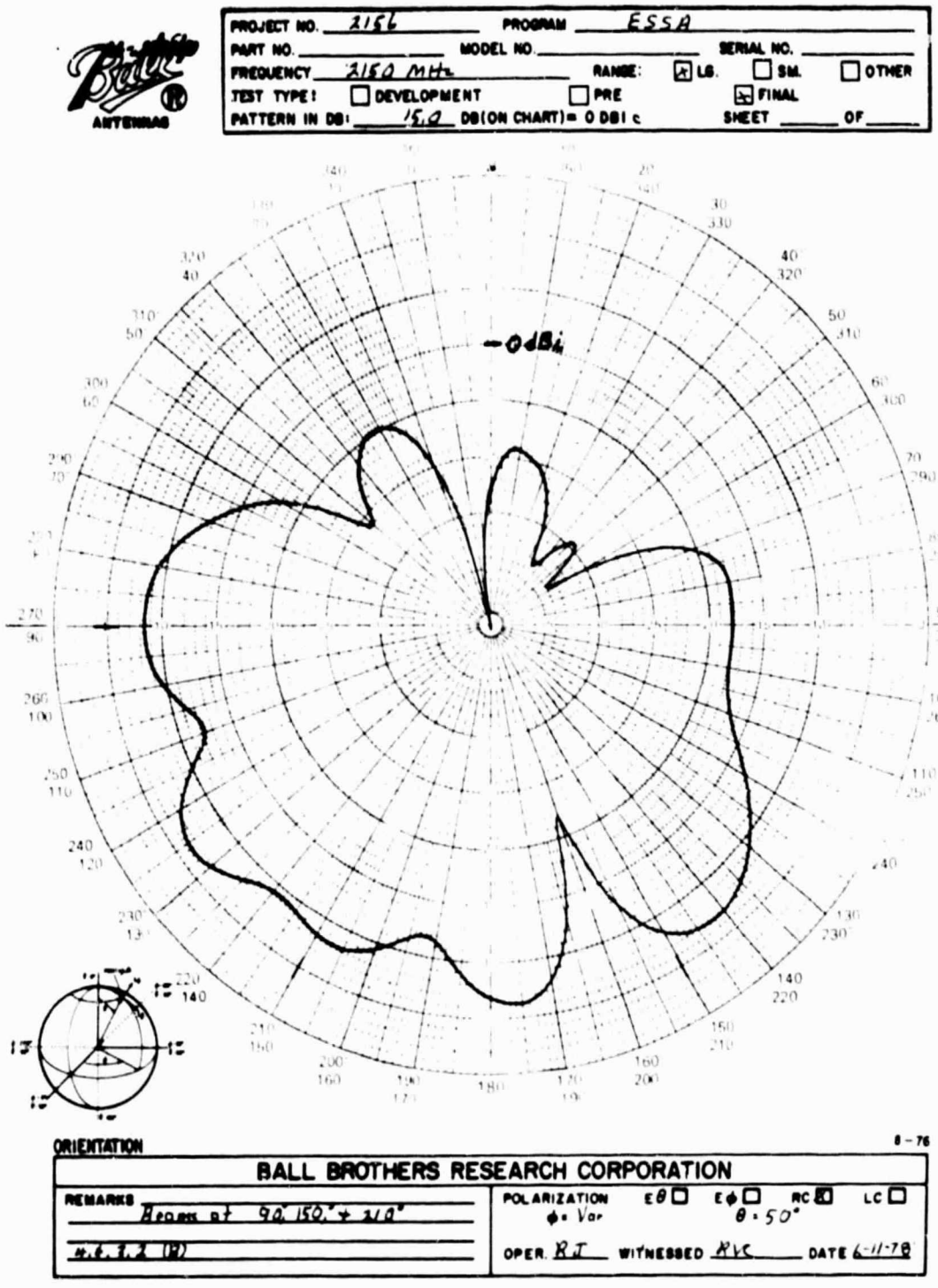

Figure 5-12 Three Beam Pattern - 90°, 150° & 210°

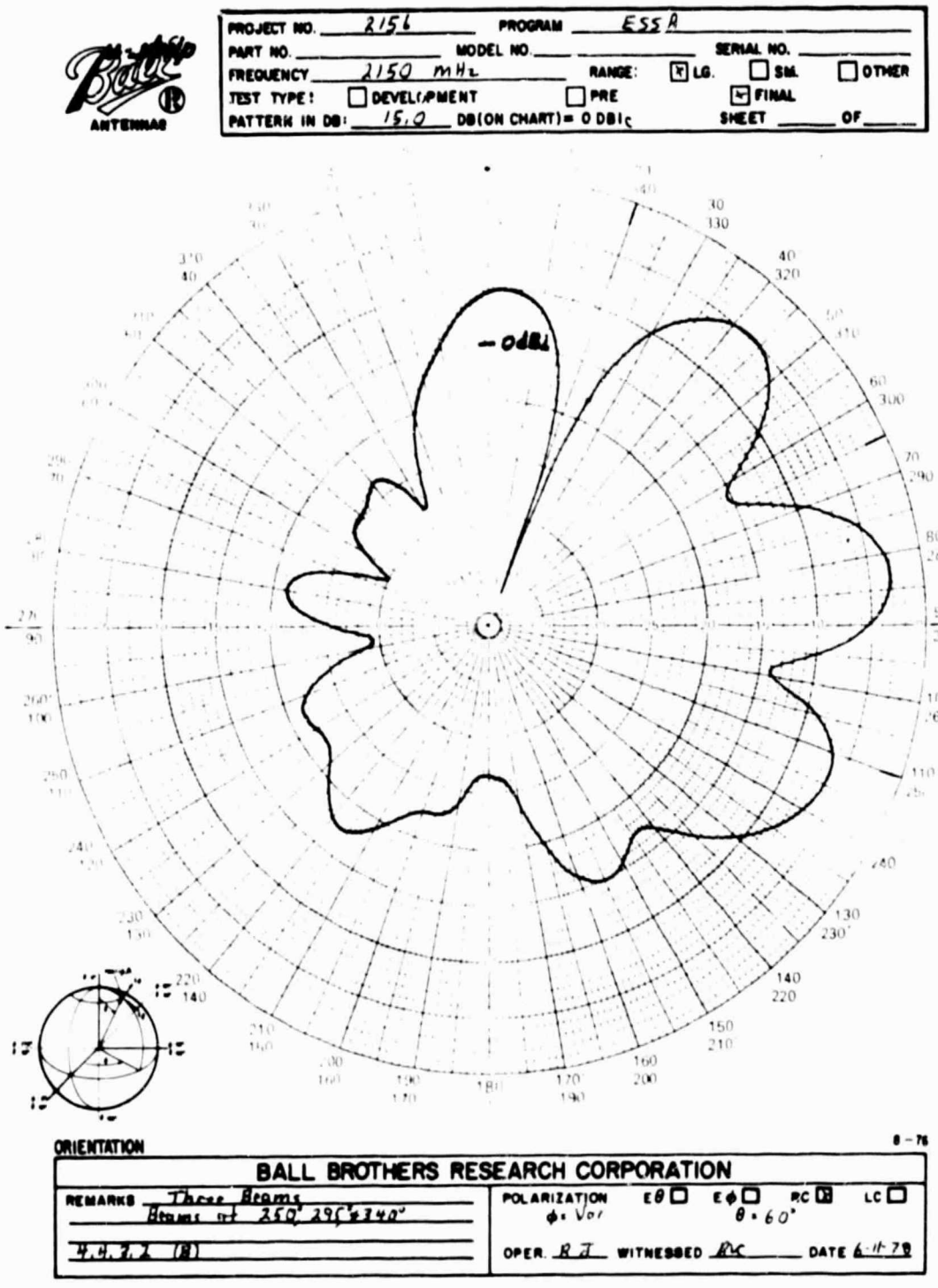

Figure 5-13 Three Beam Pattern - 250°, 295° & 340°

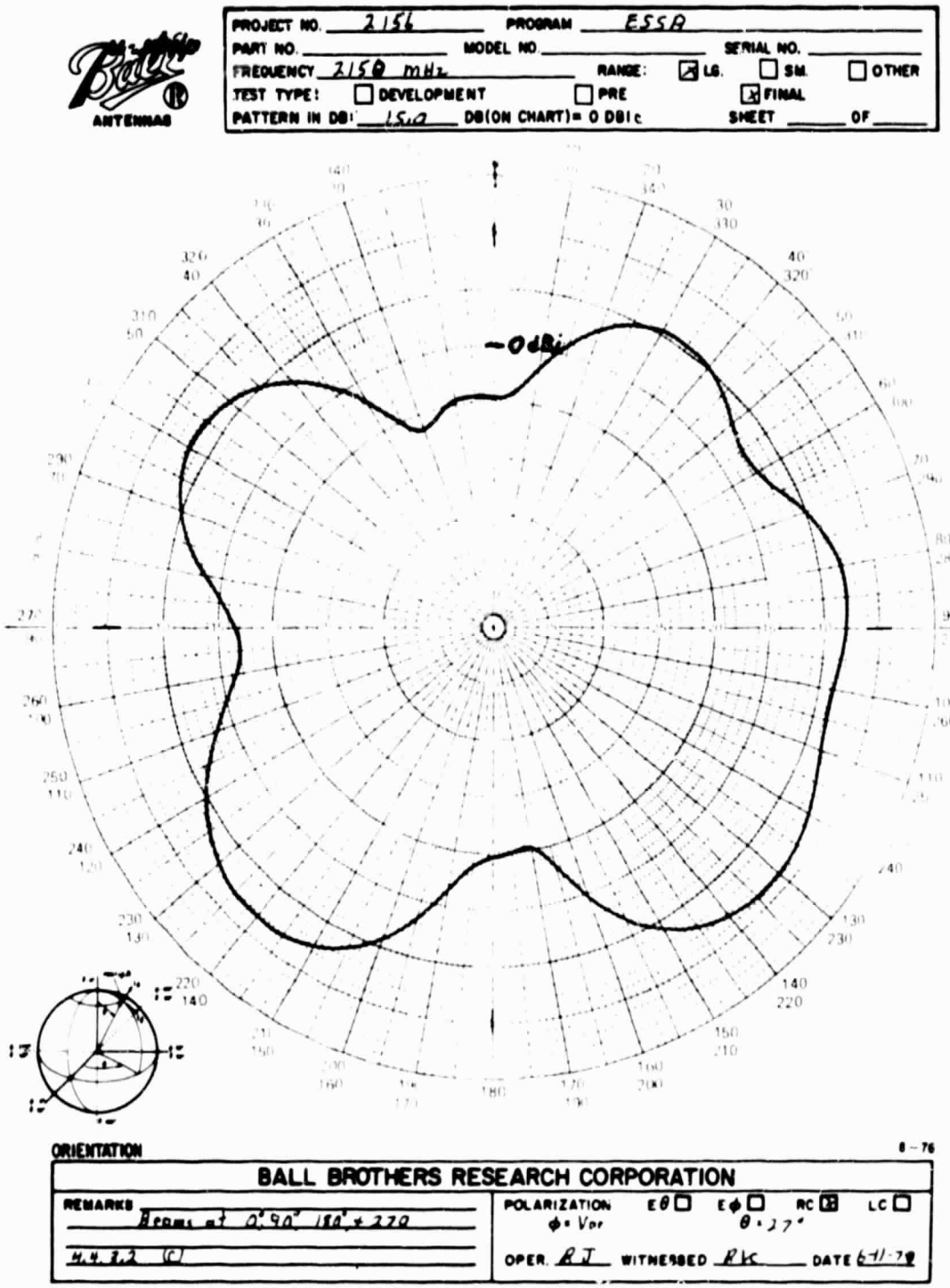

Figure 5-14 Four Beam Pattern - 0^{o}, 90^{o}, 180^{o} & 270^{o}

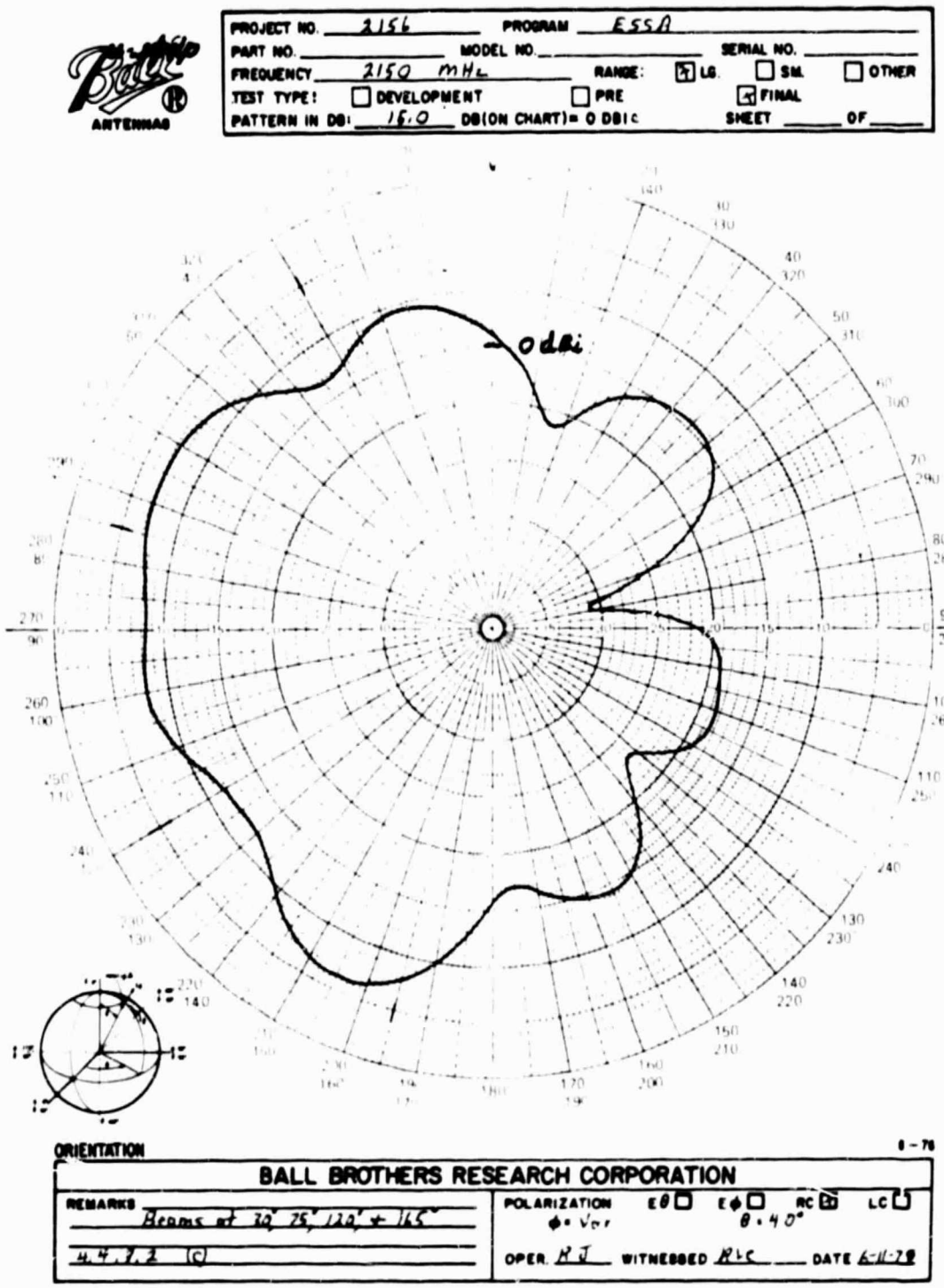

Figure 5-15 Four Beam Pattern - 30°, 75°, 120° & 165°

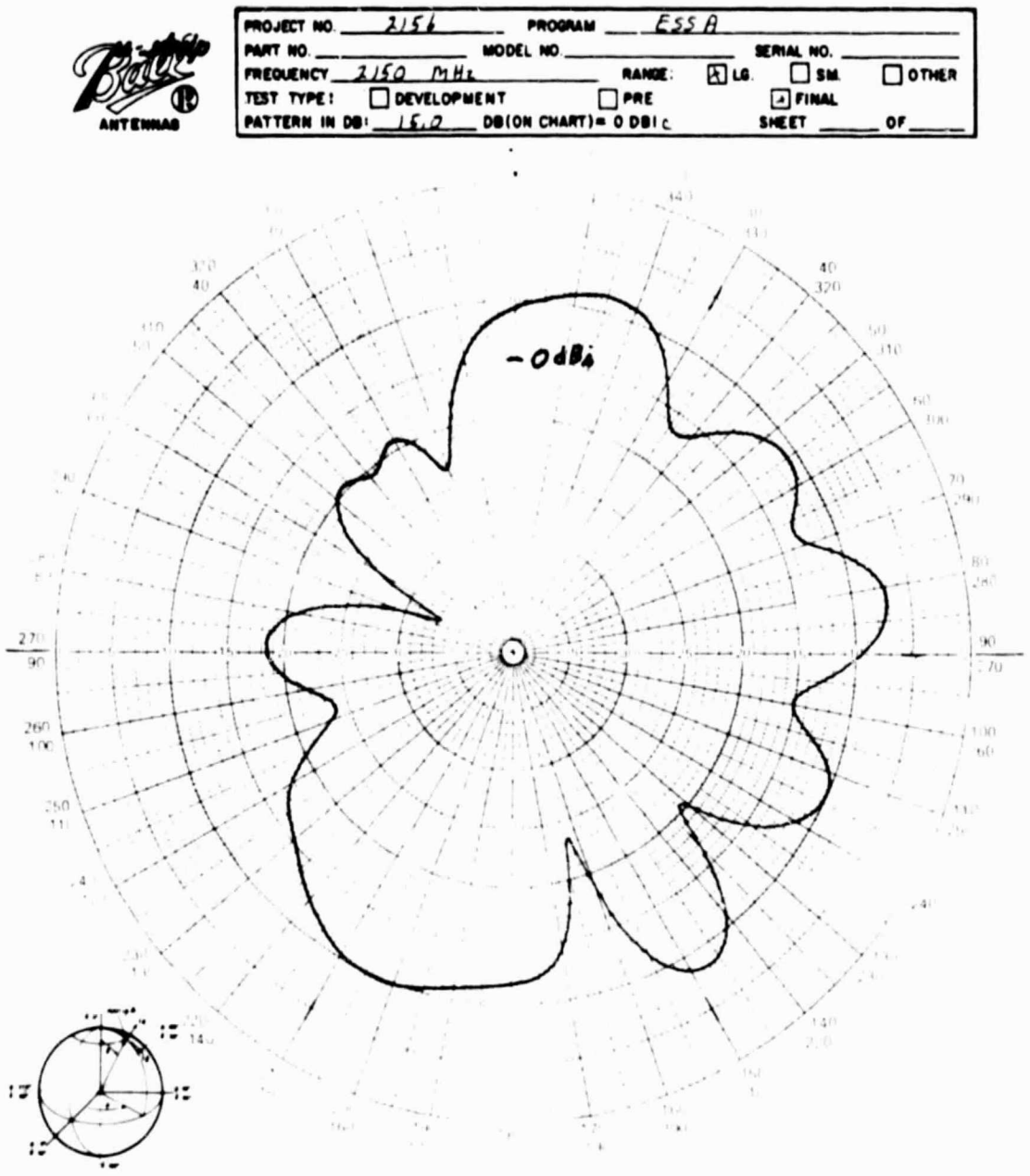

Figure 5-16 Four Beam Pattern - 150°, 210°, 270° & 330°

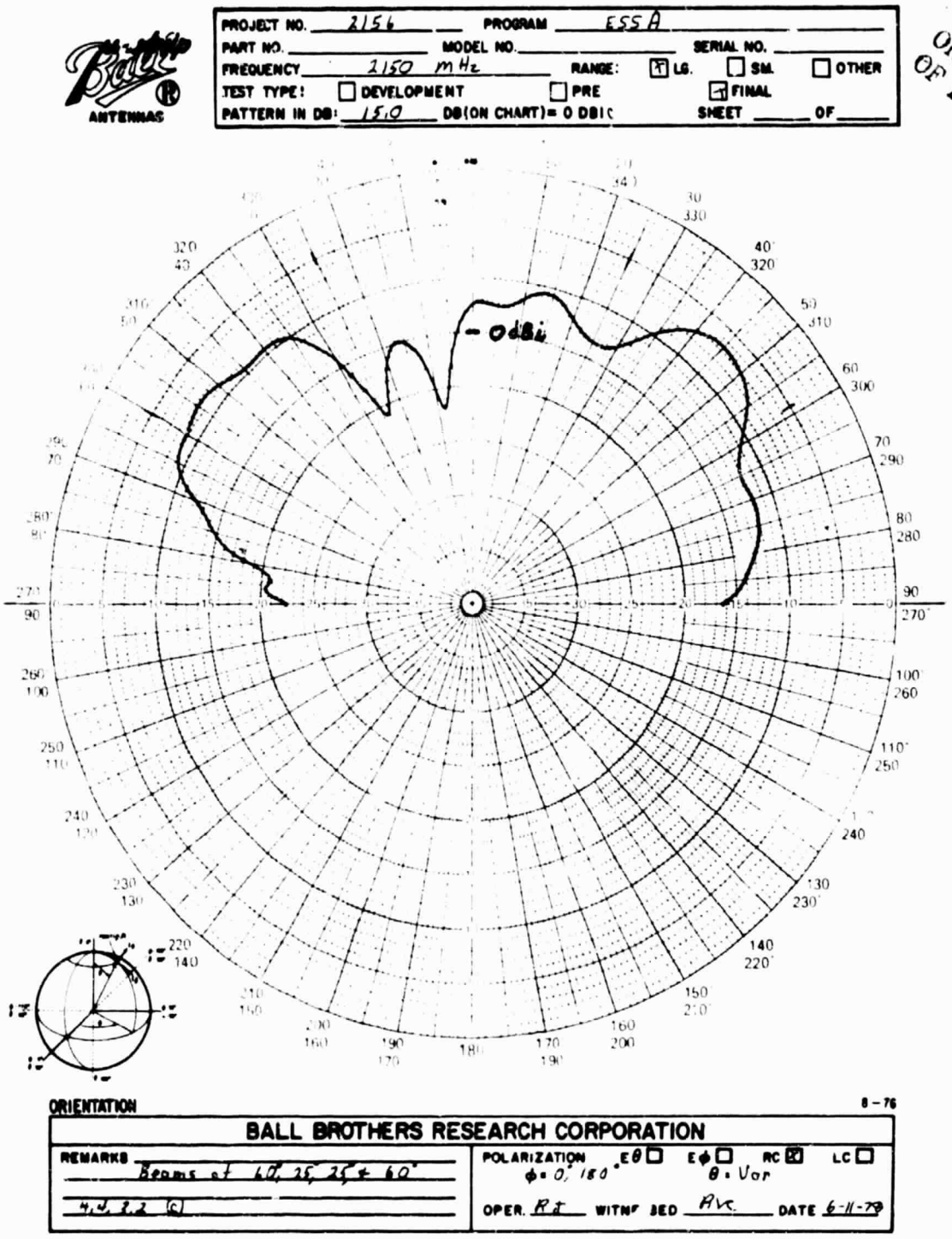

Figure 5-17 Four Beam Pattern - 25°, 60°, 300° & 335°

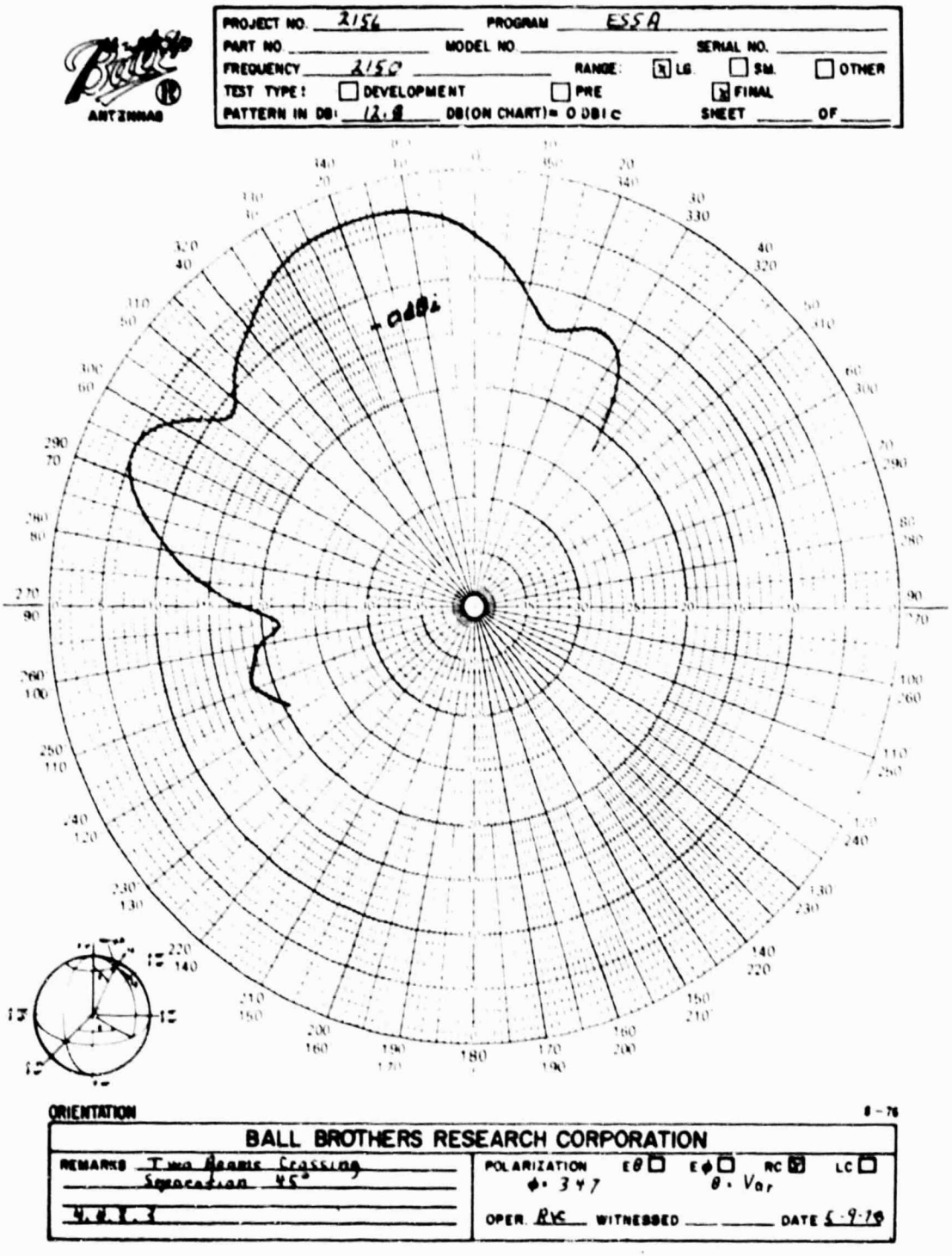

Figure 5-18 Crossing Beams - 45° Separation

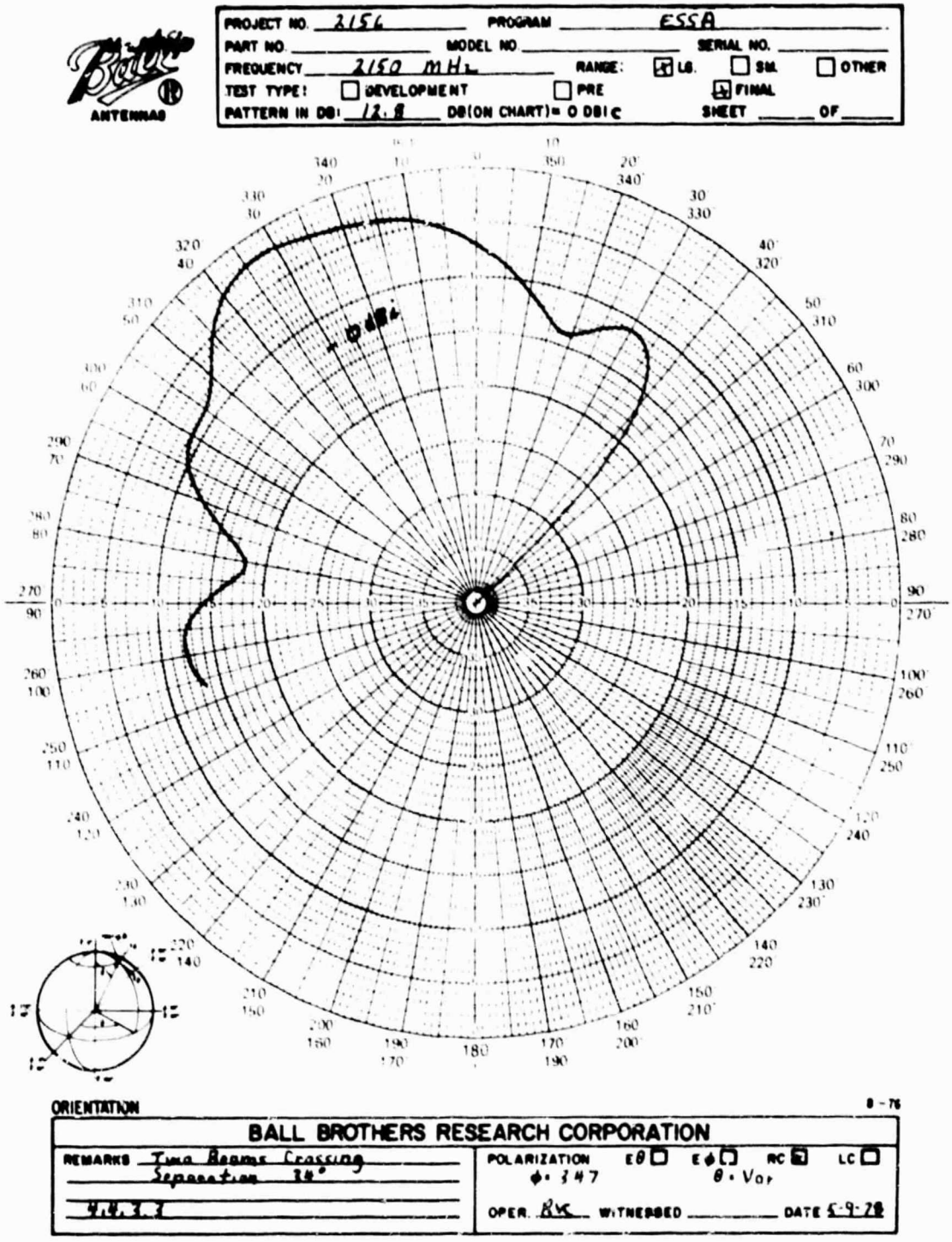

Figure 5-19 Crossing Beams - 34° Separation

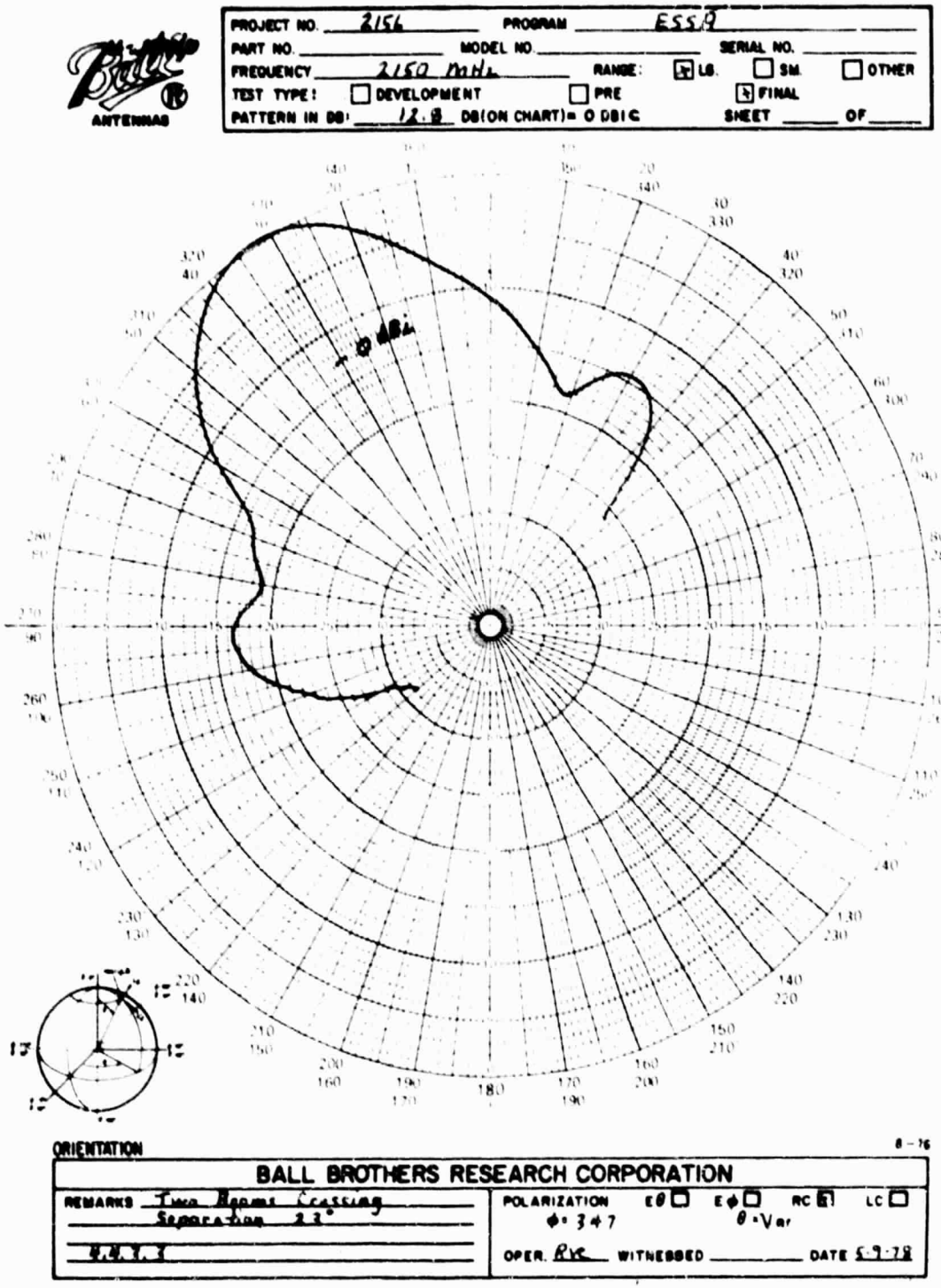

Figure 5-20 Crossing Beams - 23° Separation

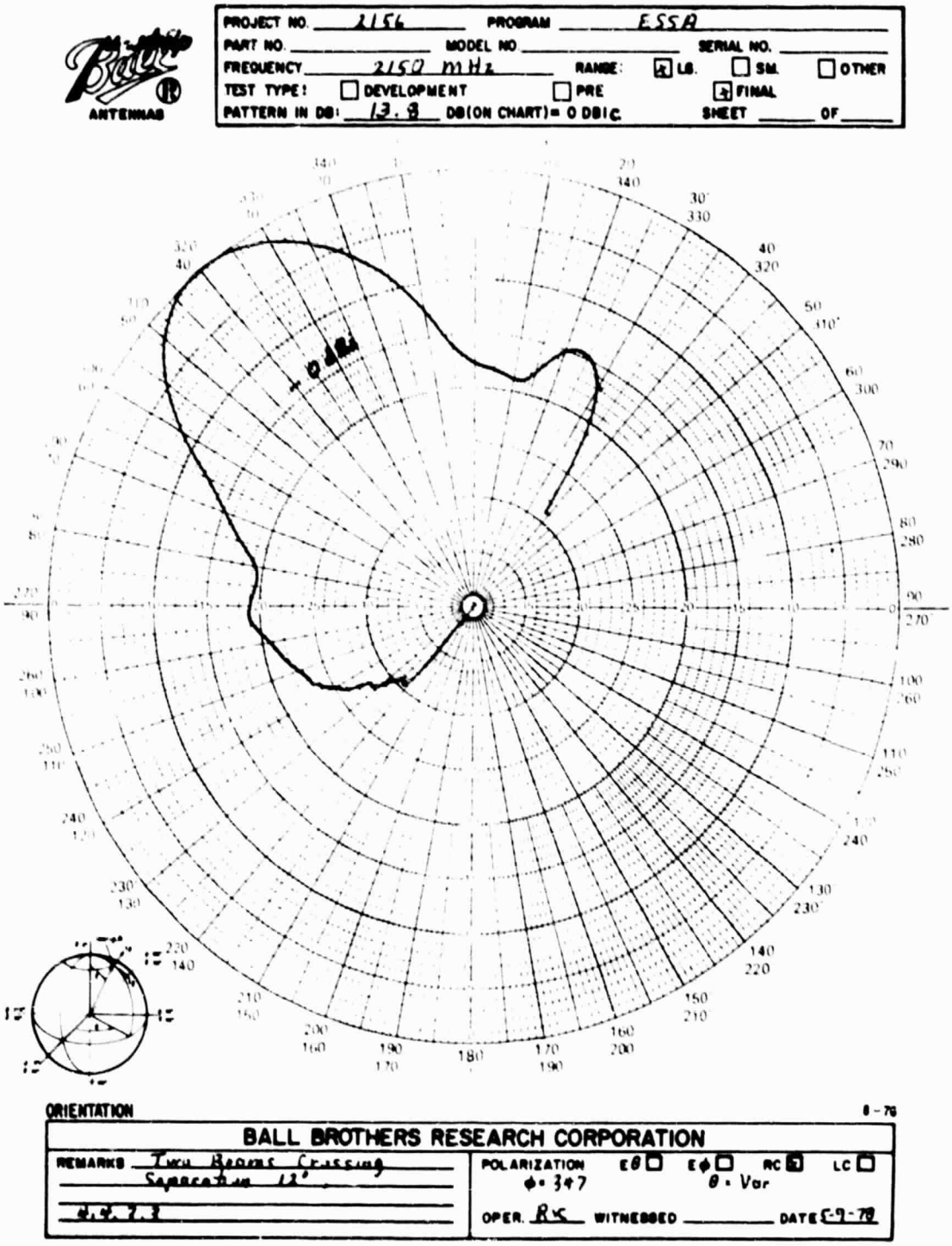

Figure 5-21 Crossing Beams - 12° Separation

5.4 Acquisition/Track Mode

Performance tests were conducted to evaluate the acquisition and track functions for both a 3-axis stabilized and spinning spacecrafts with emphasis on the former.

A simple two-way link was established in the antenna range and the basic test scenario proceeded as follows:

- A forward link was established for acquisition. The ESSA antenna received a 2106 MHz and determined the direction of arrival in real-time as described in Section 3.4. (The required duration of this link was less than 1 second for the 3-axis stabilized case. In the spinning tests the forward link transmission period was variable, corresponding to data collection for 3, 5 and 10 revolutions.

- Upon completion of the acquisition sequence a return link was established by transmitting a 2287 MHz signal from the ESSA antenna.

  - A gain measurement was taken.

  - Pointing error was determined.

Test results, special considerations and conclusions are presented for the stabilized and spinning cases respectively in Sections 5.4.1 and 5.4.2.

5.4.1 3-Axis Stabilized Spacecraft

Pointing errors were determined using the same test technique described for the directive mode. There are, however, three pointing direction terms available for determining the error sources. The first is the calculated or derived pointing direction. This is the final output of the acquisition phase algorithm sequence. The second is the beam pointing direction in which the

calculated value is rounded off to the nearest beam steering increment. Finally, there is the true or line of sight direction determined mechanically with the antenna range.

In general, we know from the directive mode tests that the pointing errors are comparable to the beam steering resolution. If the magnitude of the mean error increases, in this mode, the presumed source will be the ambiguity in the calculated direction.

The test data for the same 50 beams used and selected at random is presented in Table 5-8.

The mean pointing errors for the calculated direction and the beamed direction are nearly equal at 5.22^{o} and 5.16^{o} respectively. Since the mean pointing error for the directive mode alone was 3.6^{o}, additional error due to the acquisition phase was minimal. On the average the direction of arrival for the received signal was determined to within $\pm 1.6^{o}$. Acquisition accuracy is better than the $\pm 3^{o}$ beam steering ambiguity because it is calculated from a 4 beam weighted average.

The results of the acquisition and track mode for the 3-axis stabilized spacecraft are excellent. A 5.2^{o} mean pointing error results in a gain reduction of roughly 0.5 dB with respect to the peak gain. Since this is less than the 0.7 dB figure assumed for beam crossover loss the coverage gain is unaffected. This is also confirmed by the 13.1 dB mean gain level from Table 5-8. This figure is 0.3 dB higher than the coverage gain cited in reference (1).

In view of the test results it is unlikely that pointing errors can be reduced by modifying the acquisition algorithms. If more accurate pointing is desired it may be advantageous to sample adjacent beams in the vicinity of the acquisition beam and make a final determination based on a received signal amplitude comparison.

In addition phase measurements were taken to access the beam to beam phase variations for the directive beams of Phases II and III.

Table 5-8

3 AXIS STABILIZED ACQ/TRK PERFORMANCE

BEAM NO.	θ COMPONENT (DEG)			ϕ COMPONENT (DEG)			GAIN (dB)	SOLID ANGLE ERROR	
	TRUE	CALCULATED	BEAM	TRUE	CALCULATED	BEAM		CALCULATED	BEAM
1	0	5.2	4.0	0	326.4	0.0	14.2	5.2	4.0
2	1.5	5.2	4.0	45	326.4	115	14.2	5.1	2.5
3	3.0	.1	0.0	90	188.0	90	13.6	3.0	3.0
4	4.5	3.0	0.0	135	1.1	135	13.0	6.9	4.5
5	6.0	5.2	3.0	130	193.6	180.0	13.9	1.5	3.0
6	7 5	0.0	0.0	225	180.5	180	13.0	7.5	7.5
7	9.0	3.8	2.0	270	334.5	0.0	10.8	8.1	0.0
8	10.5	12.1	13.3	315	306.1	3.5	12.9	2.4	2.8
9	12.0	9.6	13.5	5	348.0	345	12.7	4.0	4.6
10	13.5	9.1	15.0	50	18.7	40.0	13.0	7.4	2.9
11	15.0	15.6	20.0	95	94.0	95.0	13.7	0.7	5.0
12	16.5	13.6	17.8	140	125.5	125.0	13.8	4.7	4.6
13	18.0	16.5	17.0	185	178.8	170.0	13.1	2.4	4.6
14	19.5	18.1	20.0	230	228.8	220	13.6	1.5	3.4
15	21.0	22.2	29.0	275	274.5	270	13.2	1.2	8.3
16	22.5	30.3	31.7	320	300.1	295	13.5	11.7	14.5
17	24.0	20.6	20.0	10	354.0	353.5	12.9	6.9	7.3
18	25.5	23.0	30	55	52.9	61	13.8	2.6	5.3
19	27.0	27.6	26.5	100	93.6	93.0	13.8	3.0	3.2
20	28.5	30.3	34.5	145	136.2	135	13.3	4.7	7.9
21	30.0	26.3	27.0	190	188.4	201.5	13.3	3.3	6.2
22	31.5	29.5	32.0	235	233.0	227.0	14.2	6.4	4.2
23	33.0	33.1	34.5	280	288.2	290	12.5	4.5	5.7
24	34.5	32.1	31.4	325	324.8	330	13.1	2.4	4.1
25	36.0	39.4	41.0	15	12.9	22	13.0	3.6	6.6

Table 5-8 (Cont'd)

3 AXIS STABILIZED ACQ/TRK PERFORMANCE

BEAM NO.	θ COMPONENT (DEG)			ϕ COMPONENT (DEG)			GAIN (dB)	SOLID ANGLE ERROR	
	TRUE	CALCULATED	BEAM	TRUE	CALCULATED	BEAM		CALCULATED	BEAM
26	37.5	33.1	34.0	60	57.1	68.0	13.6	4.7	5.8
27	39.0	30.4	31.5	105	108.0	111	12.9	8.8	8.3
28	40.5	40.5	46.0	150	144.0	150.0	13.3	3.9	5.5
29	42.0	39.0	41.0	195	189.5	192	14.1	4.7	2.2
30	43.5	43.6	46.0	240	233.0	242	14.1	4.8	2.9
31	45.0	40.0	46.0	285	281.7	284	12.8	5.5	1.2
32	46.5	42.8	42.0	330	330.4	340	11.7	3.7	8.3
33	48.0	50.7	52.0	20	3.7	17	12.5	9.0	4.6
34	49.5	44.5	42.0	65	63.8	64	12.0	5.1	7.5
35	51.0	46.1	47.5	110	104.2	107	13.4	6.5	4.2
36	52.5	46.5	49.0	155	149.5	152	13.2	7.3	4.2
37	54.0	53.7	53.0	200	189.1	193	12.5	8.8	5.7
38	55.5	56.3	59.0	245	232.4	242	13.3	10.5	4.3
39	57.0	58.5	61.0	290	286.6	293	13.8	3.2	4.8
40	58.5	56.3	56.0	335	333.5	344	10.9	2.5	8.0
41	60.0	59.1	55.0	25	20.8	25	13.3	3.7	5.0
42	61.5	62.3	67.0	70	66.3	69.5	12.1	3.4	5.5
43	63.0	59.0	57.0	115	109.8	115.0	13.8	6.1	6.0
44	64.5	57.0	58.0	160	163.1	164.5	13.7	8.0	7.6
45	66.0	82.5	64.0	205	202.5	207.5	13.7	4.2	3.0
46	67.5	65.1	67.5	250	240	248	13.6	9.5	1.8
47	69.0	76.7	73.0	295	294.6	299.5	12.8	7.7	5.8
48	70.5	65.4	70.0	340	340.5	346	12.2	5.1	5.7
49	72.0	71.3	71.5	30	22.3	26	11.6	7.3	3.8
50	73.5	70.7	77.0	75	69.5	75	12.0	5.9	3.5

Five directions were selected at random and tested one at a time. The ESSA antenna and range coordinates were synchronized and the line of sight direction for the random test case was established. The acquisition/track function was initiated and the final resolved beam was used as the 0^{o} phase reference. The phase of the seven directive beams used in the converging process, Phases II and III, were measured with respect to this reference. The results are given in Table 5-9 for the five test cases.

The maximum phase variation is less than the 20^{o} specification limit for all five cases. As a result the algorithm sequence is acceptable in terms of phase variation.

Table 5-9

Beam to Beam Phase Variations for Acquisition Sequence

LINE OF SIGHT DIRECTION (deg)		RELATIVE PHASE OF PHASE II BEAMS (deg)			RELATIVE PHASE OF PHASE III BEAMS (deg)				MAXIMUM PHASE VARIATION
θ	ϕ	1	2	3	1	2	3	4	(deg)
56	117.5	+2	-2.5	+1	-9.3	-6.5	+8.4	0	14.9
52	50	+4.7	+19	+0.5	-2.0	+1.5	0	+12	18.5
24	1.6	+5.5	+2.0	+4.5	+20	+6.5	-1.5	-1.8	15.5
75	213	-5.8	-14.5	-1.0	-16.5	-16.5	-2.5	0	15.5
64	288	0	+2.8	-6.2	+0.5	+13.5	0	+0.5	19.7

5.4.2 Spinning Spacecraft

Limited testing was carried out to evaluate the basic acquisition and track algorithms for a spinning spacecraft. Since these functions are so inter-dependent, the only meaningful performance parameter is tracking or electronic beam despinning accuracy as a function of acquisition time.

The test scenario proceeded as follows:

- A forward link was simulated at 2106 MHz by transmitting to the rotating ESSA antenna.
- The acquisition mode was initiated but the data collection period, Phase V, was varied.
- The true spin rate was determined by measuring the time interval between output pulses from an electro-optical revolutions counter.

The spin rate error is simply the difference between the calculated value (from the acquisition phase) and the true value determined mechanically. This rate error was converted into an angular pointing error after 100 revolutions or 36,000 degrees of rotation. Data from the 5 and 10 rpm test cases is shown in Figures 5-22 and 5-23 respectively. The average rate error is based on ten independent test cases.

Although it is difficult to draw conclusions from such limited test data, it appears that there are no fundamental flaws in either the control sequence logic or execution of the algorithms.

On the assumption that this is valid data, we can make quantitative conclusions regarding the tracking performance of the present system.

1) For a 5 rpm spin rate a data collection period or acquisition phase of roughly 108 seconds will be required to ensure a beam pointing error of less than 6^{o} after 200 revolutions or 40 minutes.

Beam pointing errors greater than 6^{o} are unacceptable because the gain roll-off will exceed 0.7 dB* causing the coverage gain to drop.

* 0.7 dB is significant because coverage gain calculations assume this as a maximum gain roll-off regardless of source; beam crossover or pointing error.

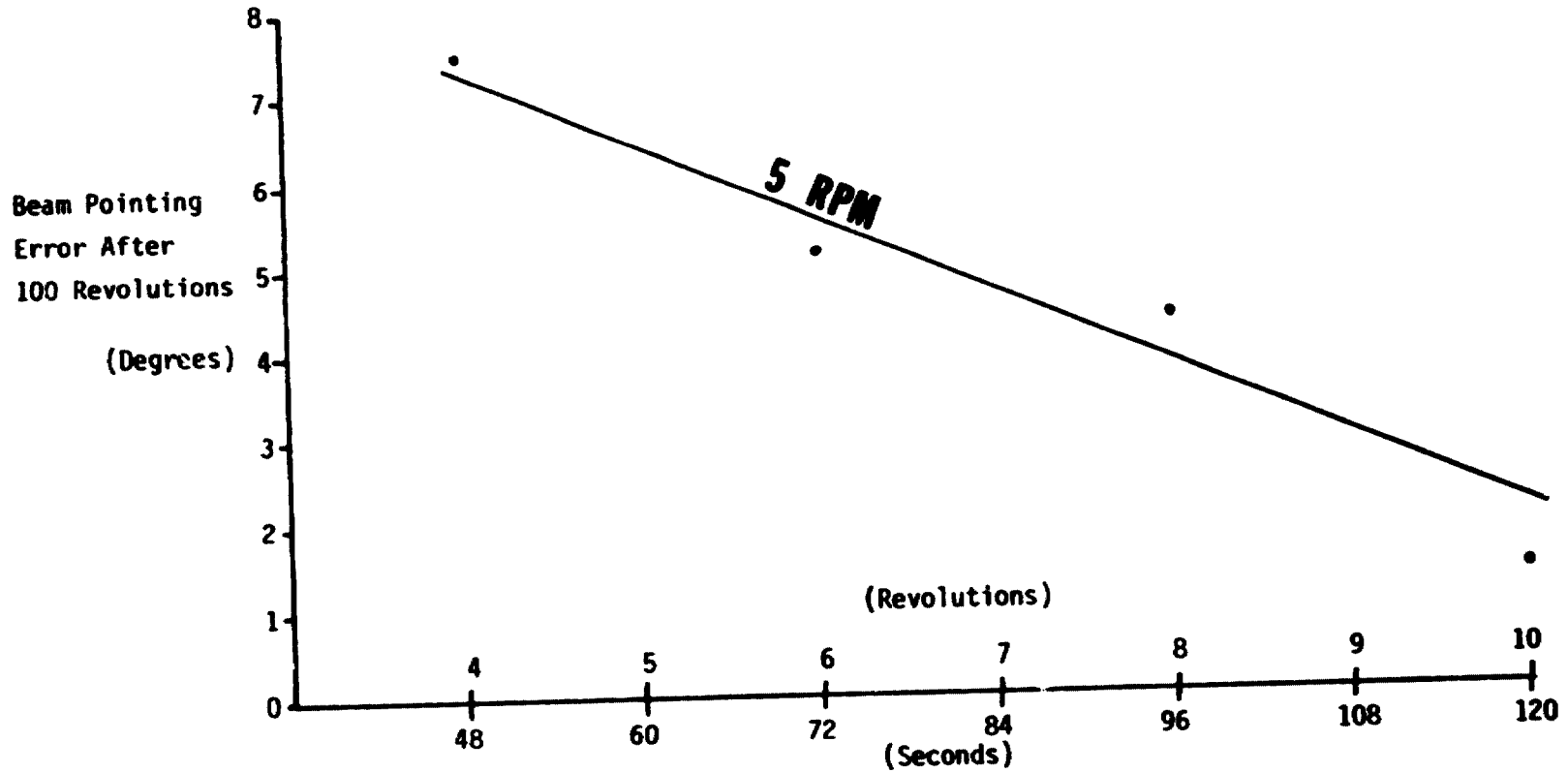

DATA Collection Period - PHASE V

Figure 5-22 Tracking Accuracy for 5 rpm Spinning Spacecraft

F79-08

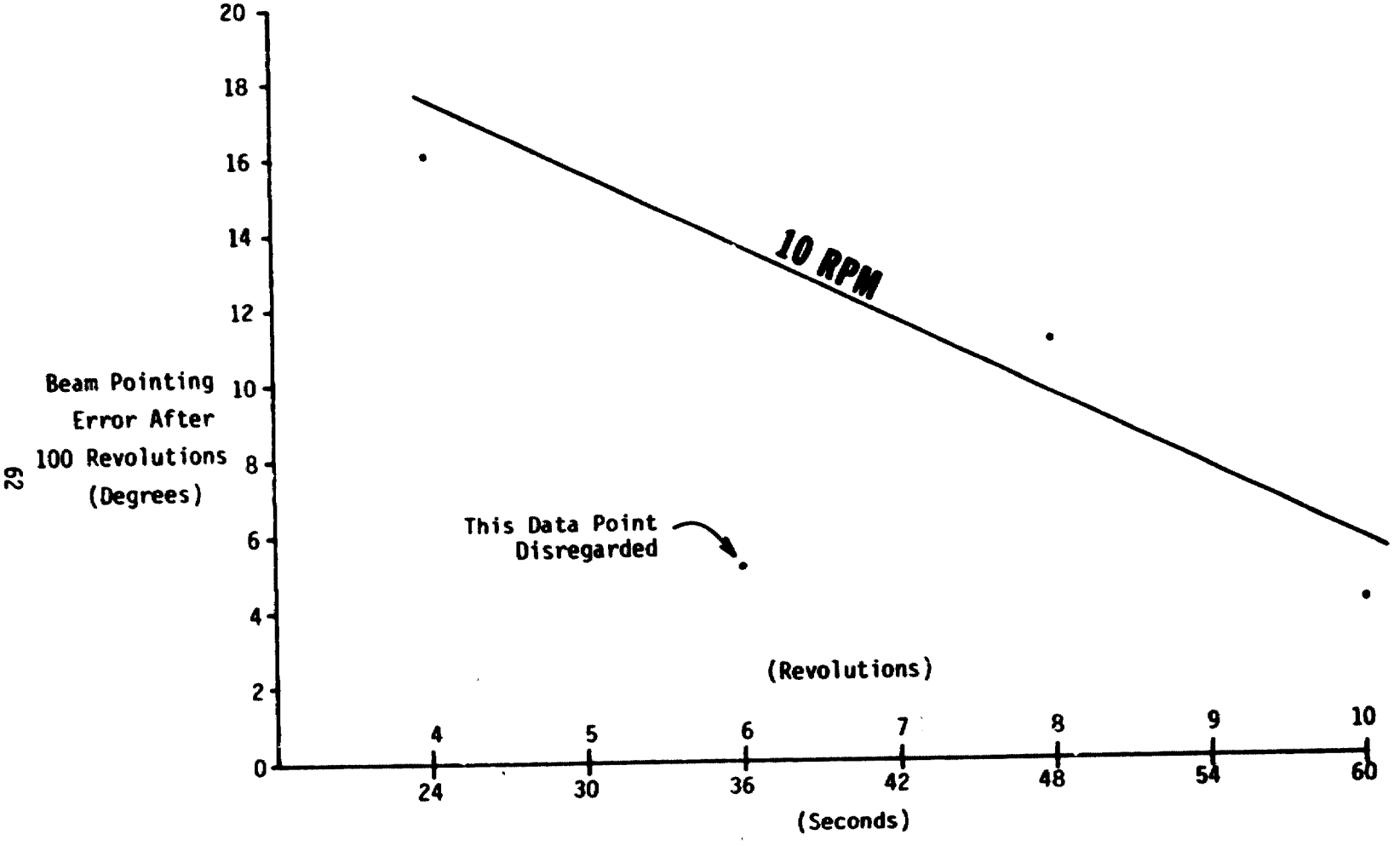

Figure 5-23 Tracking Accuracy for 10 rpm Spinning Spacecraft

F79-08

2) For a 10 rpm spin rate an acquisition phase of nearly 80 seconds will be required to ensure a beam pointing error of less than 6^0 after 400 revolutions or 40 minutes.

Initially it seems paradoxical that an acquisition period of 108 seconds is required at 5 rpm but only 80 seconds are needed for 10 rpm. This is reasonable however, since accuracy depends on the number of data points and not the collection time.

Another factor is that the Phase V timing increments were chosen to favor the higher rpm rates to satisfy the general case. Improved performance will result by optimizing the timing intervals for a specific spin rate.

Phase measurements were not taken for this mode. However, since adjacent beams are used in both the acquisition and track functions, beam to beam phase variations in excess of the previously determined value of 10^0 degrees maximum[5] are not expected. Measured phase data for electronic beam despinning will be required ultimately for complete performance characterization.

6.0 RELATED STUDY EFFORTS

During the course of the contract several related study efforts were conducted in special interest areas. Although this subject material is outside the scope of this report and therefore not included, this section is provided to acquaint the reader with these additional topics. A summary of the scope and conclusions are presented for each task in the sections that follow.

6.1 Low Gain ESSA Configurations for Scout Applications

The purpose of this study was to determine the RF radiation characteristics for three Scout compatible ESSA antenna configurations. The three configurations analyzed included an 8-inch diameter truncated sphere, a 15-inch diameter truncated sphere and a toroidal surface with a 25-inch major diameter and a 12-inch minor diameter.

The results of this effort include a performance comparison, Table 6-1, weight, size and power estimates, Table 6-2, and a plot of coverage gain versus ESSA antenna size, Figure 6-1.

A complete description of this work is contained in a study report entitled "Scout Compatible ESSA Antenna Systems for Spinning Spacecraft," dated 1 August 1978. A companion document containing a preliminary engineering proposal for the development of a first user flight model is entitled "Flight Model Development of an ESSA System on a Spinning Spacecraft," dated 1 September 1978.

6.2 Thermal Model Description and Analysis Results

Thermal models were developed for the Engineering Model ESSA antenna with three different internal electronics configurations as follows:

Model	Configuration	Nodes
I	Antenna Electronics and one TDRSS Transponder	62
II	Antenna Electronics and two TDRSS Transponders	69
III	Antenna Electronics, GPS electronics and two TDRSS Transponders	76

The models and subsequent analysis were developed to identify any major thermal problems due to heat dissipation from internal electronics systems. The results of this analysis are summarized in terms of predicted temperatures for each of the electronics packages. The data from the three models indicates that thermal control of the ESSA antenna and associated electronics can be accomplished with

Table 6-1

PERFORMANCE COMPARISON OF CANDIDATE ARRAYS

CHARACTERISTICS	8" Dia. ESSA	15" Dia. ESSA	Toroidal ESSA
COVERAGE GAIN	5.4 dBi	8.7 dBi	11.5 dBi
ELEVATION COVERAGE LIMITS	±180°	±130°	15 to 165°
SPHERICAL COVERAGE	100% *	88% *	96% *
BEAMWIDTH			
ELEVATION	60°	40°	62°
AZIMUTH	60°	40°	22°
NUMBER OF ELEMENTS	12	41	162
NUMBER OF BEAMS	21	109	182
ELEMENTS PER SUBARRAY	1 and 2	4	7
BEAM STEERING INCREMENTS			
ELEVATION	30°	18°	20°
AZIMUTH	30°	18°	10°
PHASE VARIATION - BEAM TO BEAM	35° Max 26° Typ	20° Max 15° Typ	22° Max 17° Typ

* Assuming No Spacecraft Blockage

Table 6-2

SIZE, WEIGHT AND POWER ESTIMATES

	SIZE	WEIGHT	POWER
8-INCH DIAMETER ESSA ANTENNA	--	0.4 Kg (0.9 lb)	--
ELECTRONICS	15 x 10 x 5 cm (5.9 x 3.9 x 2 in)	0.65 Kg (1.4 lb)	6.3 watts
15-INCH DIAMETER ESSA ANTENNA	--	2.3 Kg (5 lb)	--
ELECTRONICS	15 x 11 x 5 cm (5.9 x 4.3 x 2 in)	0.66 Kg (1.5 lb)	7.4 watts
25-INCH DIAMETER TOROIDAL ESSA ANTENNA	--	8.2 Kg (18 lb)	--
ELECTRONICS	18 x 11 x 5 cm (7.1 x 4.3 x 2 in)	0.8 Kg (1.8 lb)	11.5 watts

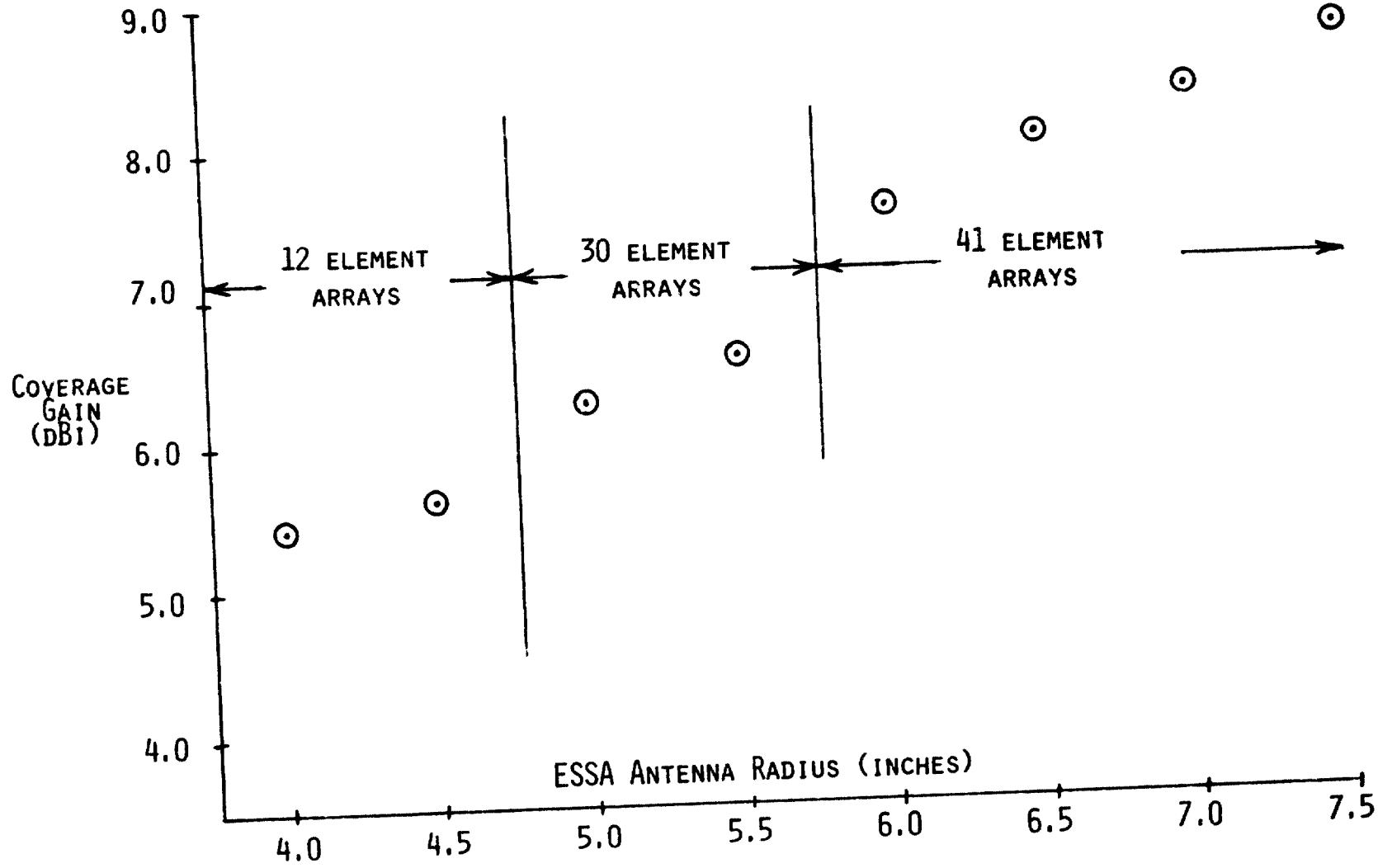

Figure 6-1 Coverage Gain -vs- ESSA Antenna Size

selective surface finishes; no active or semi-active thermal control devices are needed. The table below is a summary of the results for the various electronics packages:

ITEM	ALLOWABLE $T_{max}(^oC)$	ALLOWABLE $T_{min}(^oC)$	PREDICTED $T_{max}(^oC)$	PREDICTED $T_{min}(^oC)$
Antenna Elec.	40	0	26	2
GPS	50	-20	11	7
Transponder (1)	40	-10	40	25
Transponder (2)	40	-10	22	10

It should be noted that the above predicted temperature ranges could be reduced by allowing close thermal coupling between the various electronic boxes. Hand calculations indicate that the internal temperature range could be held to $20^oC \pm 10^oC$ using this technique. Also, the present design uses only radiative couplings for thermal control. Therefore, the operating range of warm instruments could be lowered by the use of custom design conductive interfaces with the internal support ring and/or the spherical shell.

In this effort, no attempt was made to find an "optimum" thermal design. Further refinement in the external finishes and the internal conductive interfaces should allow accommodation of a wide variety of internal electronics complements.

The situation would even be further improved if the antenna were in a spinning configuration. A spinning antenna would have much lower Ts across the shell and consequently a more even temperature distribution on the shell and antenna elements.

The details of this effort are documented in two reports entitled "Thermal Model Description" and "Thermal Analysis Results" both dated 25 August 1978.

6.3 ESSA II Analysis and Test Results

The purpose of this task was to assess the gain characteristics of ESSA type antennas employing phase corrected apertures. This type of antenna is referred to as ESSA-II. Following the analysis phase a 38 cm radius model was implemented to demonstrate the performance improvement.

Although the experimental model was only moderately successful, the projected performance for a 38 cm R ESSA-II is 15.85 dB which is 1.85 dB above the coverage gain of the same size ESSA-I.

Performance projections for ESSA-II type antennas between 38 cm and 102 cm in radius are given in Figure 6-2. ESSA-I and ESSA-II performance comparisons for the same size range are summarized in Figure 6-3.

This task is described in a separate report entitled "Gain Improvement Feasibility Study Report and Hardware Implementation Test Results," dated 10 May 1979.

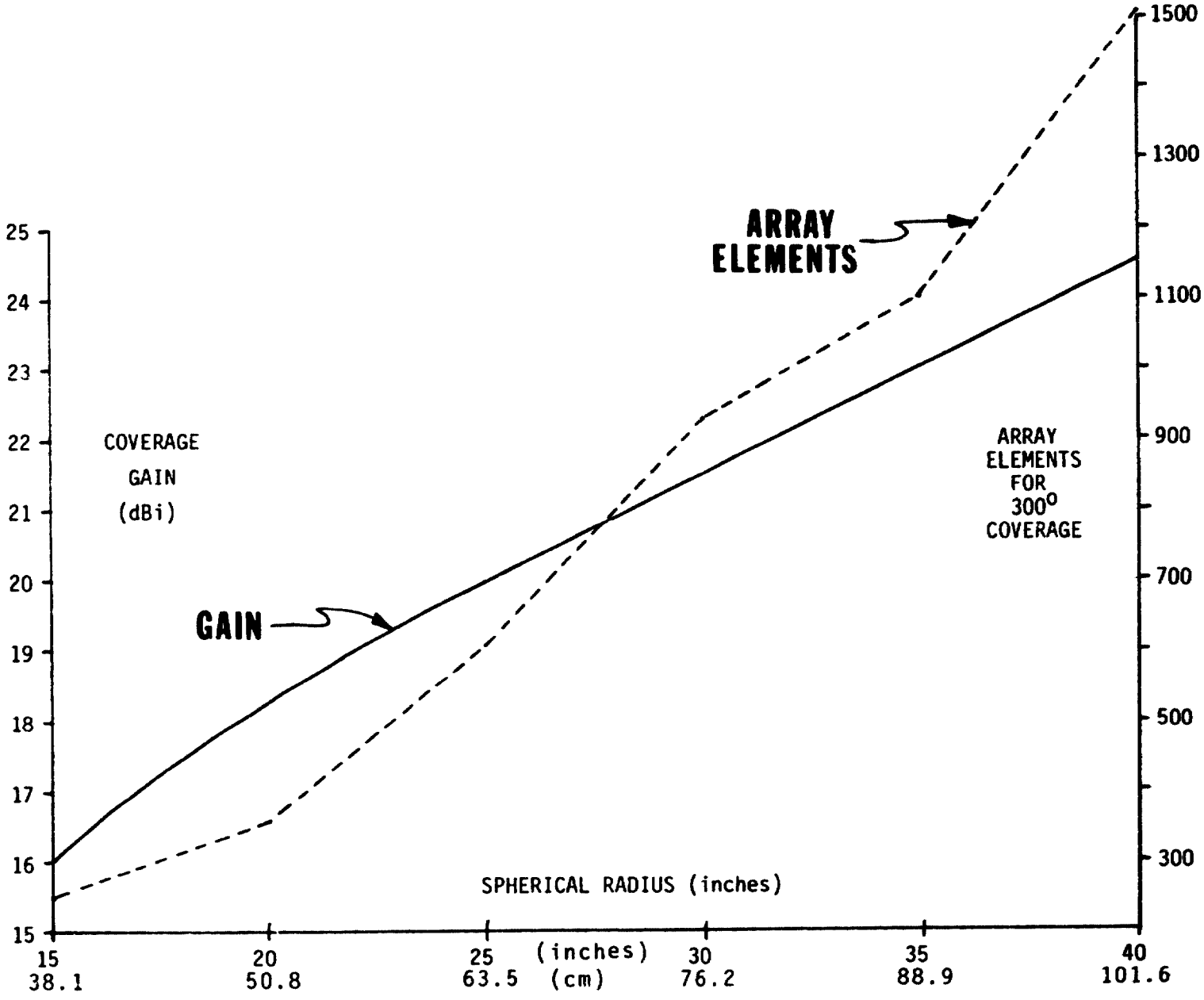

Figure 6-2 ESSA-II Performance Projections

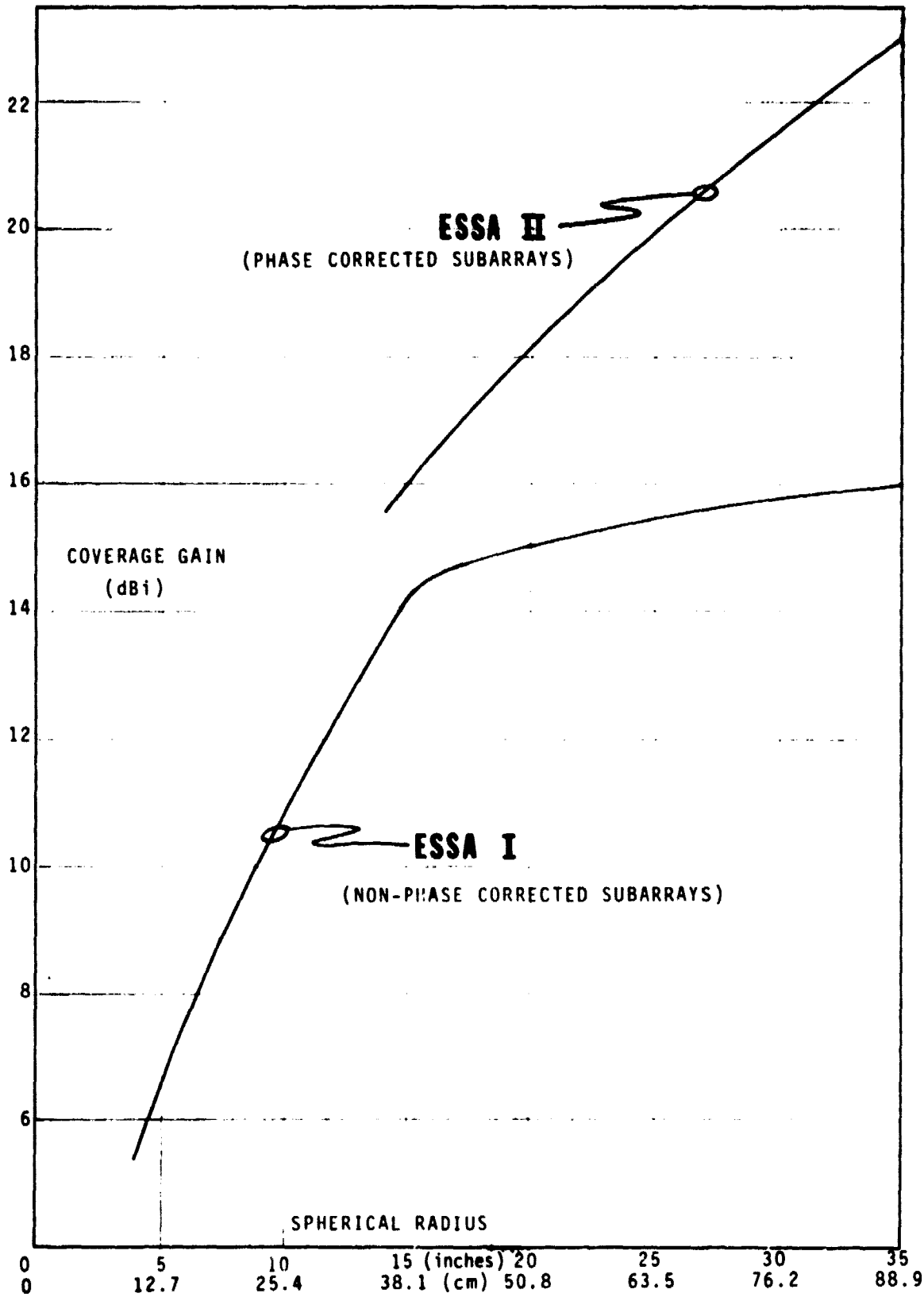

Figure 6-3 ESSA I and II Performance Comparison

7.0 REFERENCES

1) "Electronic Switching Spherical Array Antenna," Final Report NASA Contract NAS5-23518, NASA-CR-156757, April 1978.

2) Ref. 1, pp. 19-24.

3) "Electronic Switching Spherical Array," Study Report, NASA Contract NAS5-24268, pp. 11-16, 20 December 1977.

4) Ref. 1, Pg 7.

5) Ref. 1, Page 30

APPENDIX A
Software Flow Diagrams

BEAM-FORMING ALGORITHM

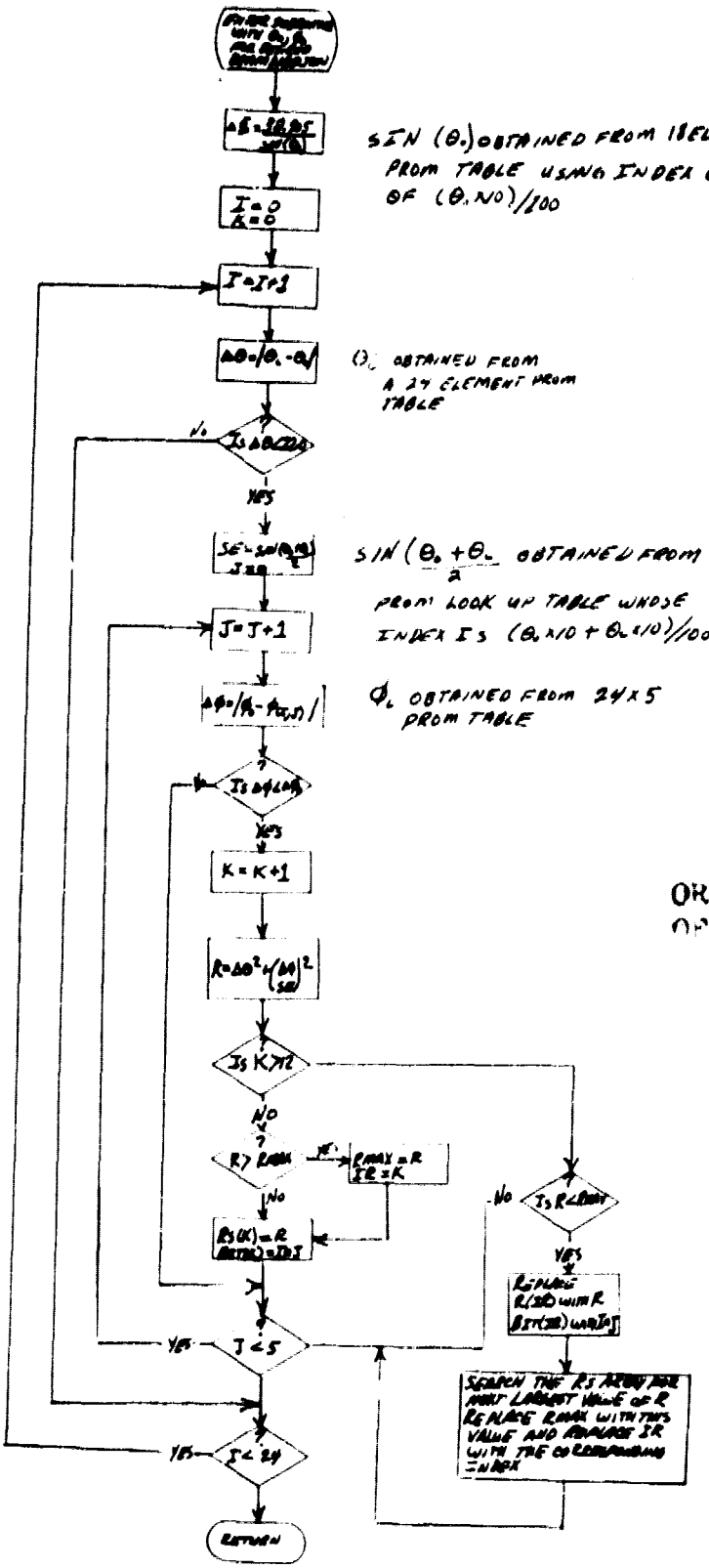

OBJECTIVE: FIND SINGLE ELEMENT (θ_i, ϕ_{ij}) WITH MAXIMUM RECEIVED SIGNAL

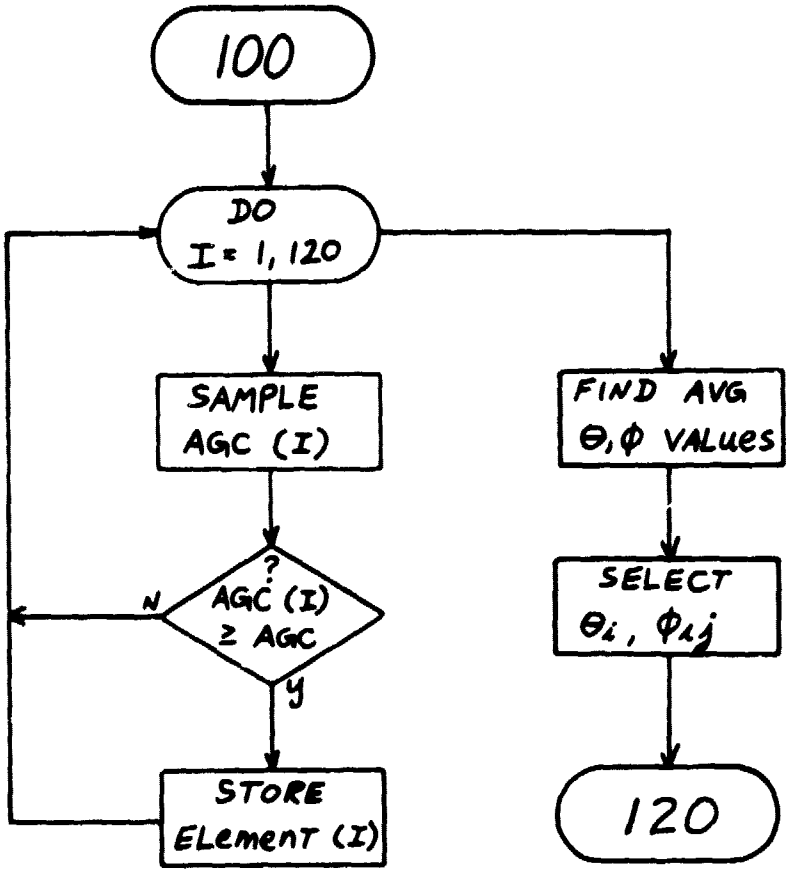

Acquisition Sequence - Phase I

OBJECTIVE: DETERMINE MOST PROBABLE DIRECTION FOR SEARCH

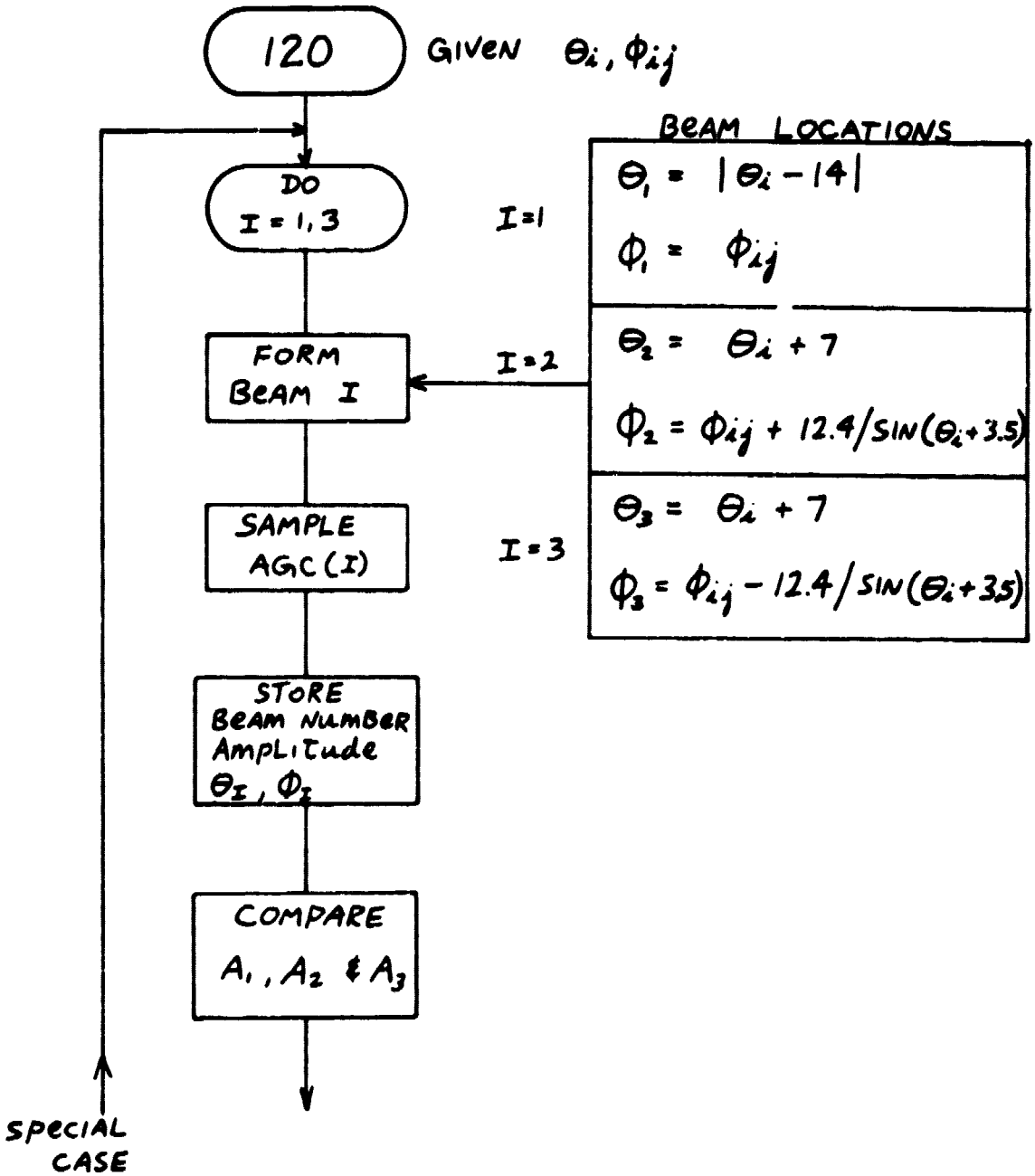

OBJECTIVE: FIND CONSTANT θ VALUE (θd) FOR DESPIN

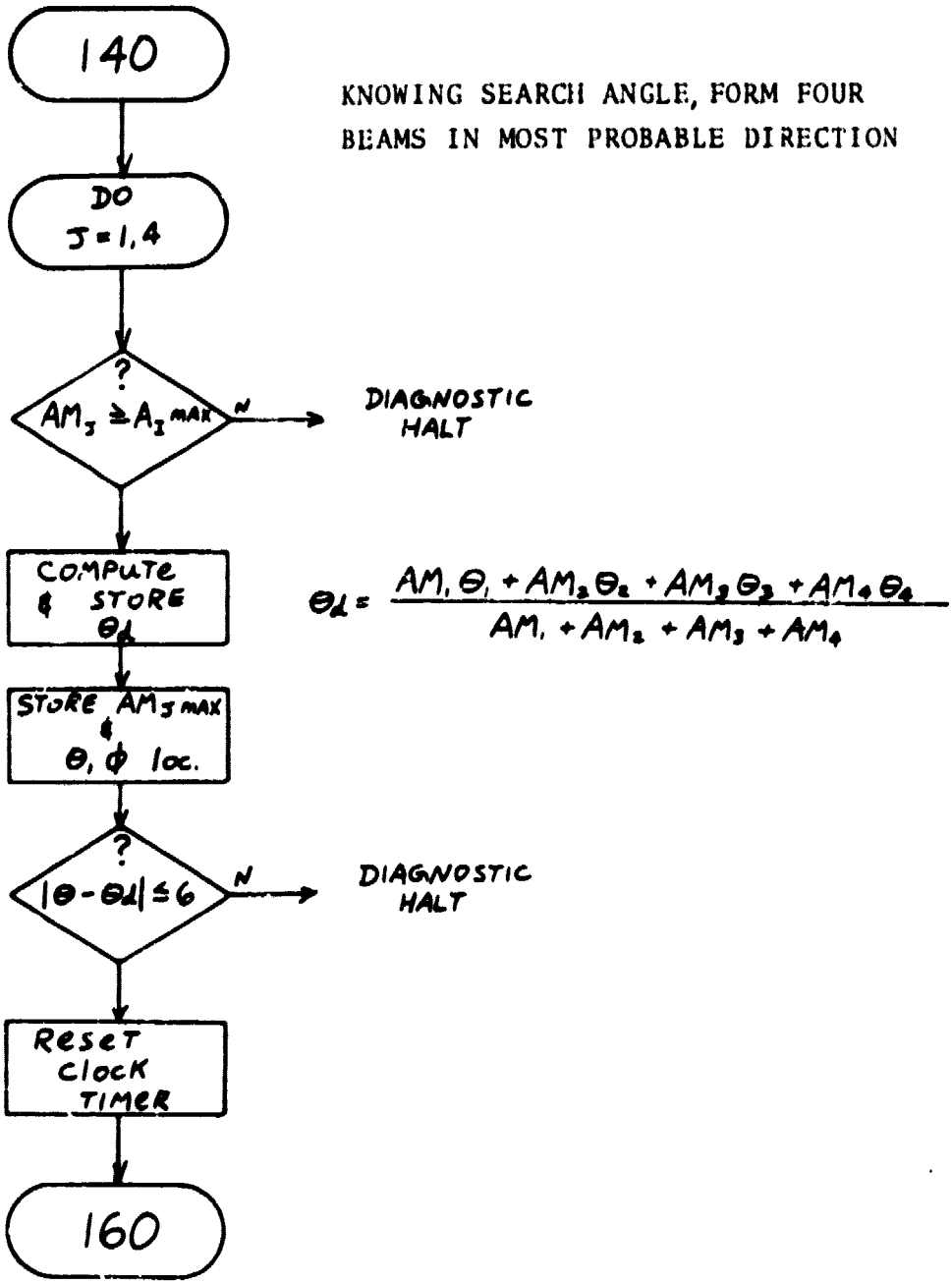

Acquisition Sequence - Phase III

OBJECTIVE: COLLECT DATA FOR ϕ_b (t) and $d\phi/dt$ COMPUTATIONS

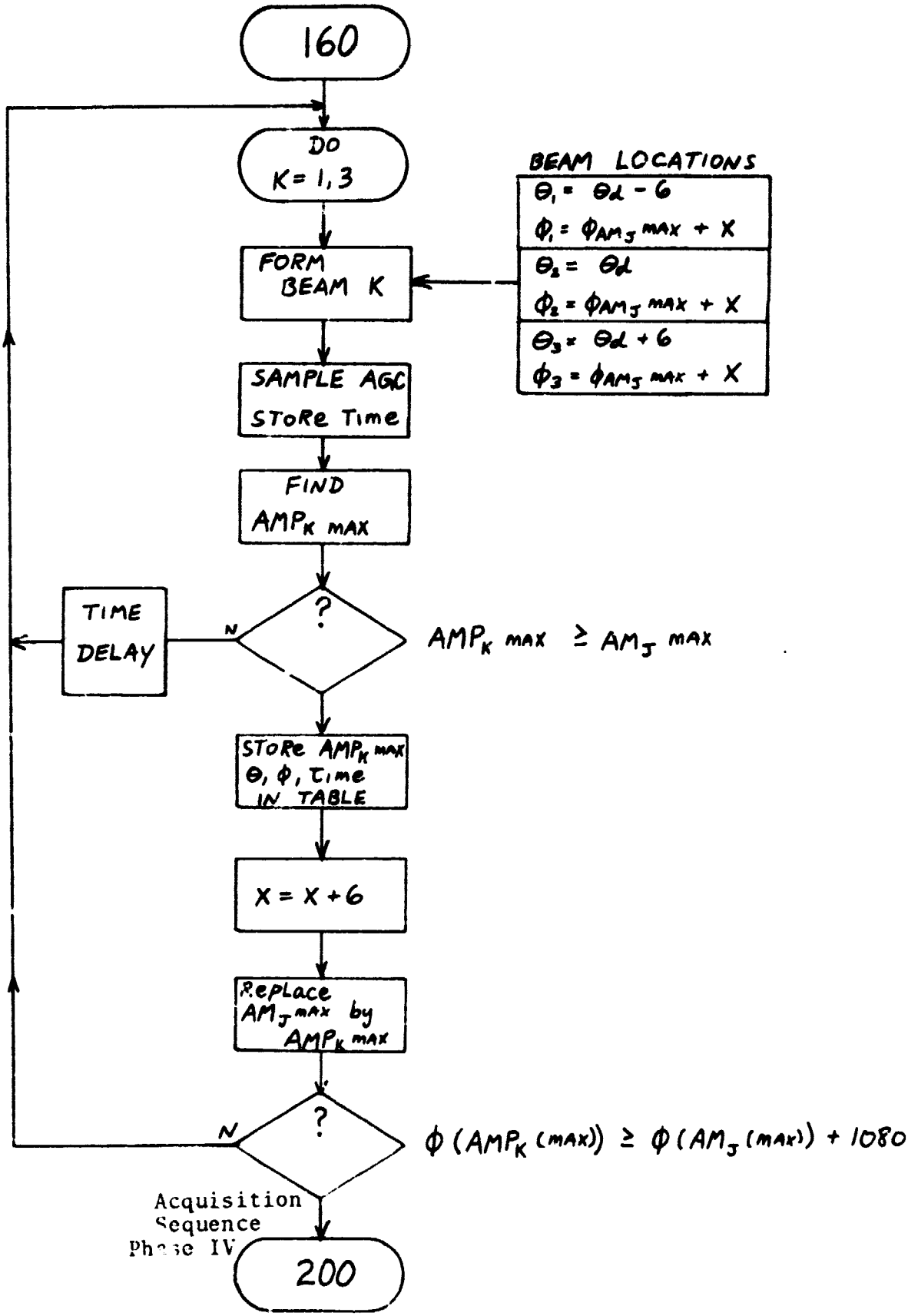

ALGORITHM FOR BEAM DESPINNING

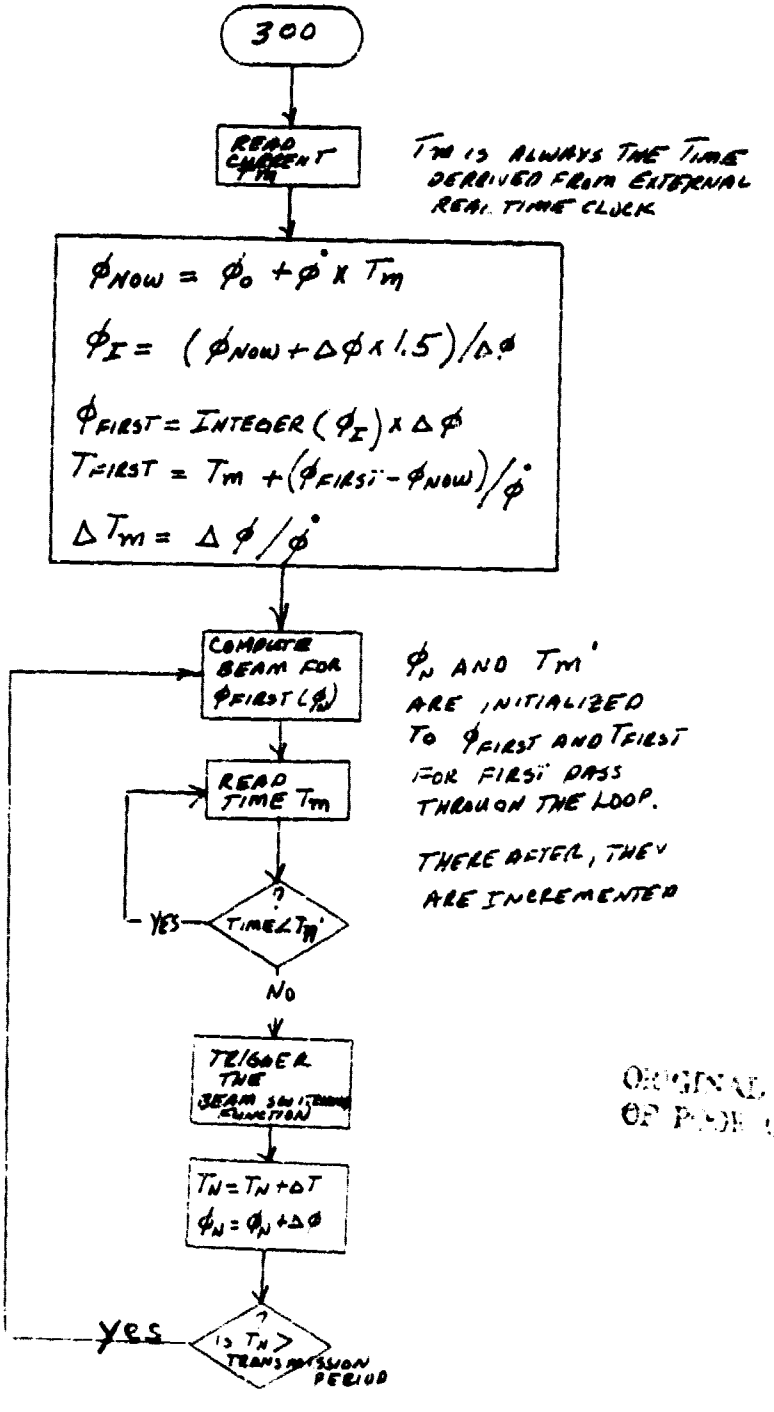

Flow Diagram for Track Mode

APPENDIX B
Microprocessor Controller Schematics

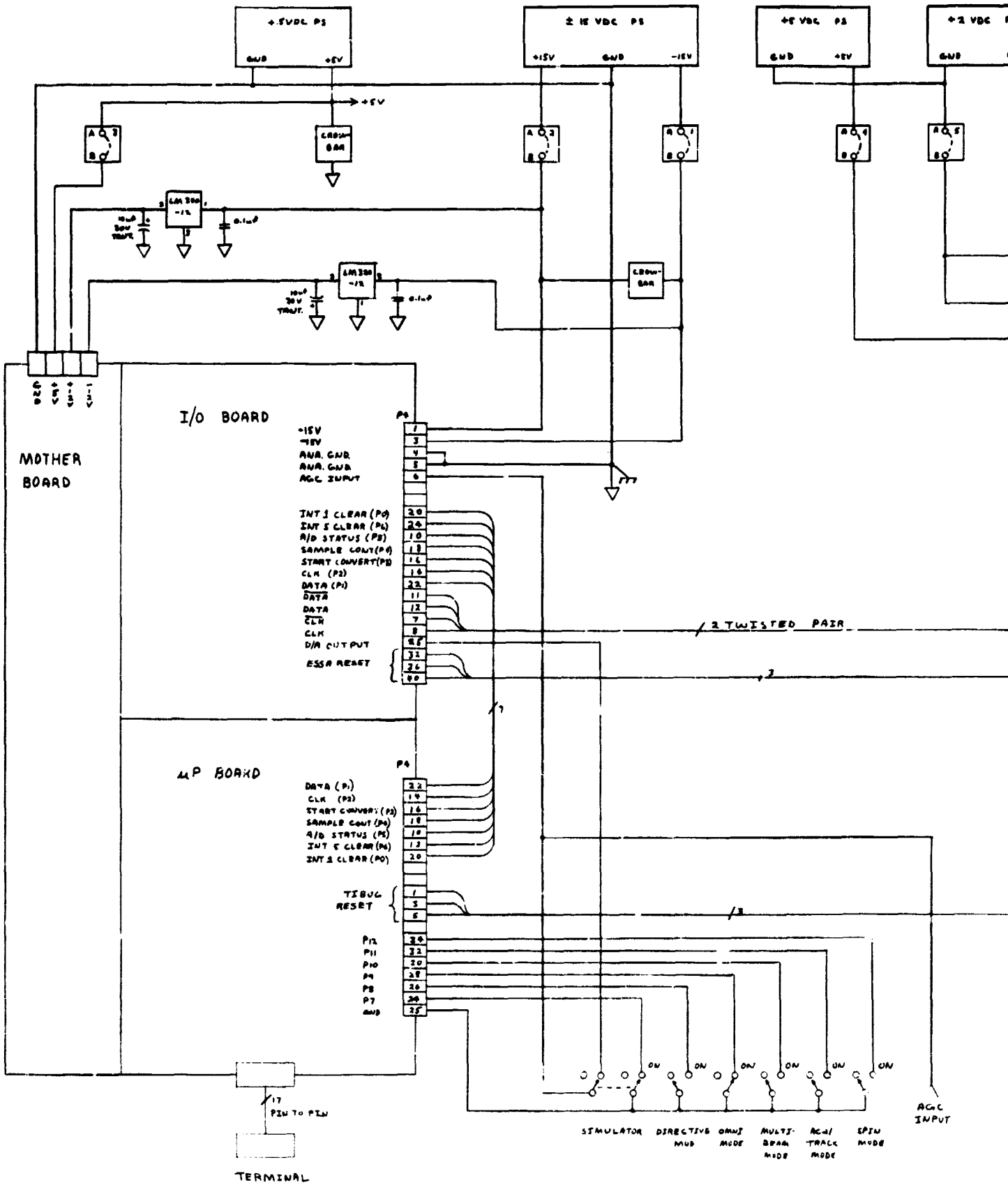

FOLDOUT FRAME 1

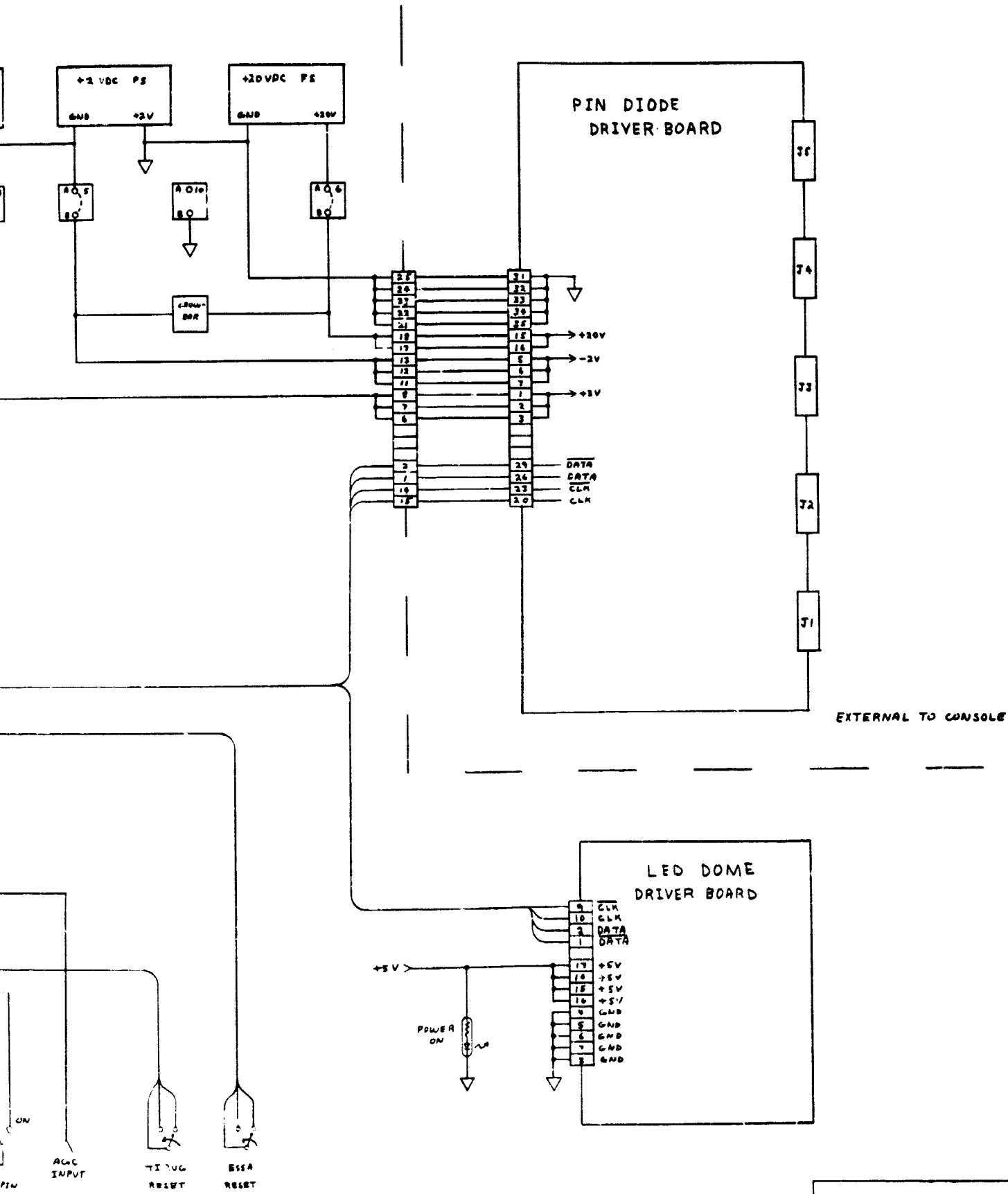

FOLDOUT FRAME 2

ESSA INTERCONNECTION DWG

R. TRUMBULL
3/24/78

B2

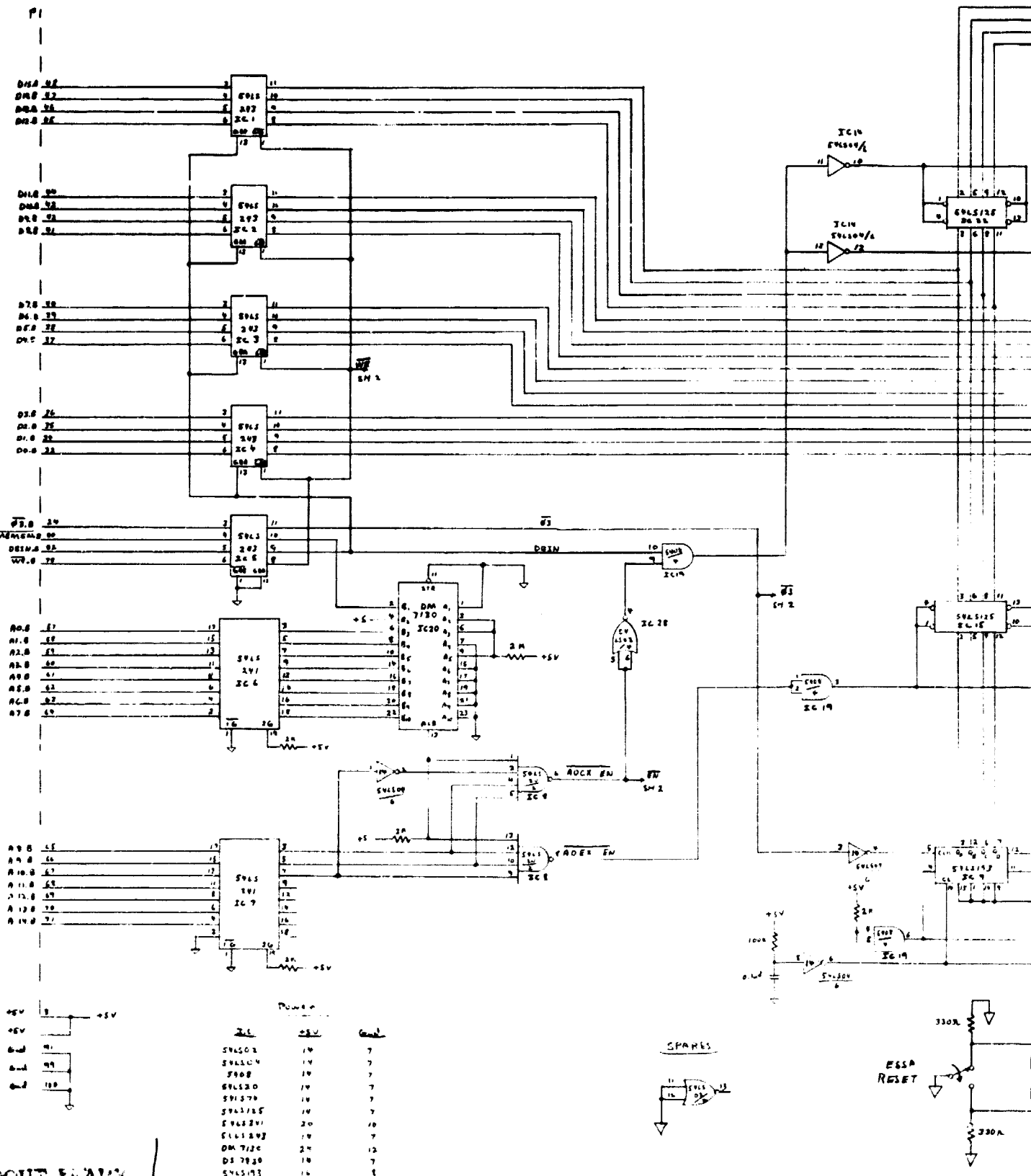

IC	+5V	Gnd
54LS02	14	7
54LS04	14	7
5908	14	7
54LS20	14	7
5913 74	16	7
54LS125	14	7
5965 3V1	20	10
54LS367	16	8
DM 7130	24	12
DS 7830	16	8
54LS193	16	8

FOLDOUT FRAME

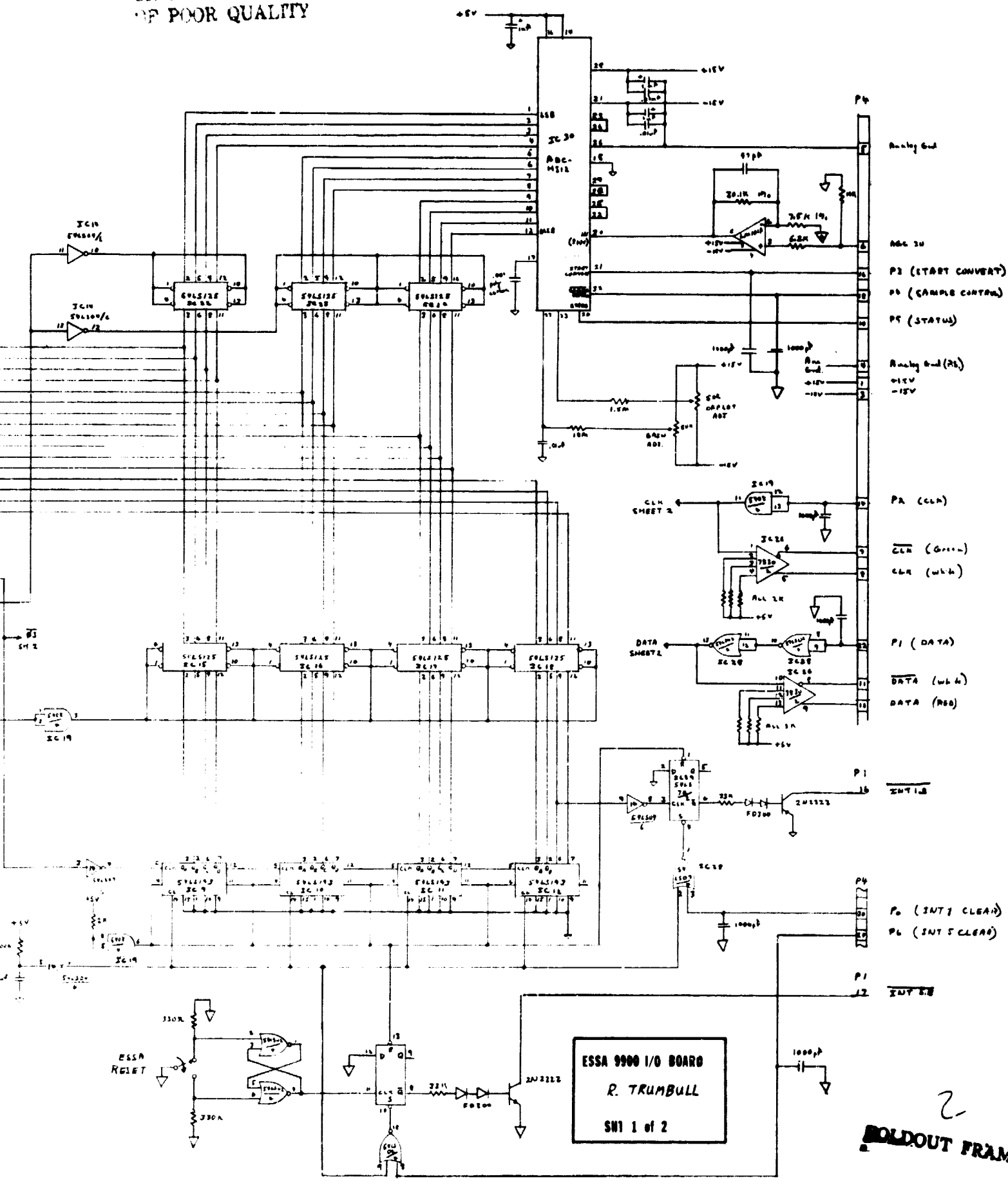

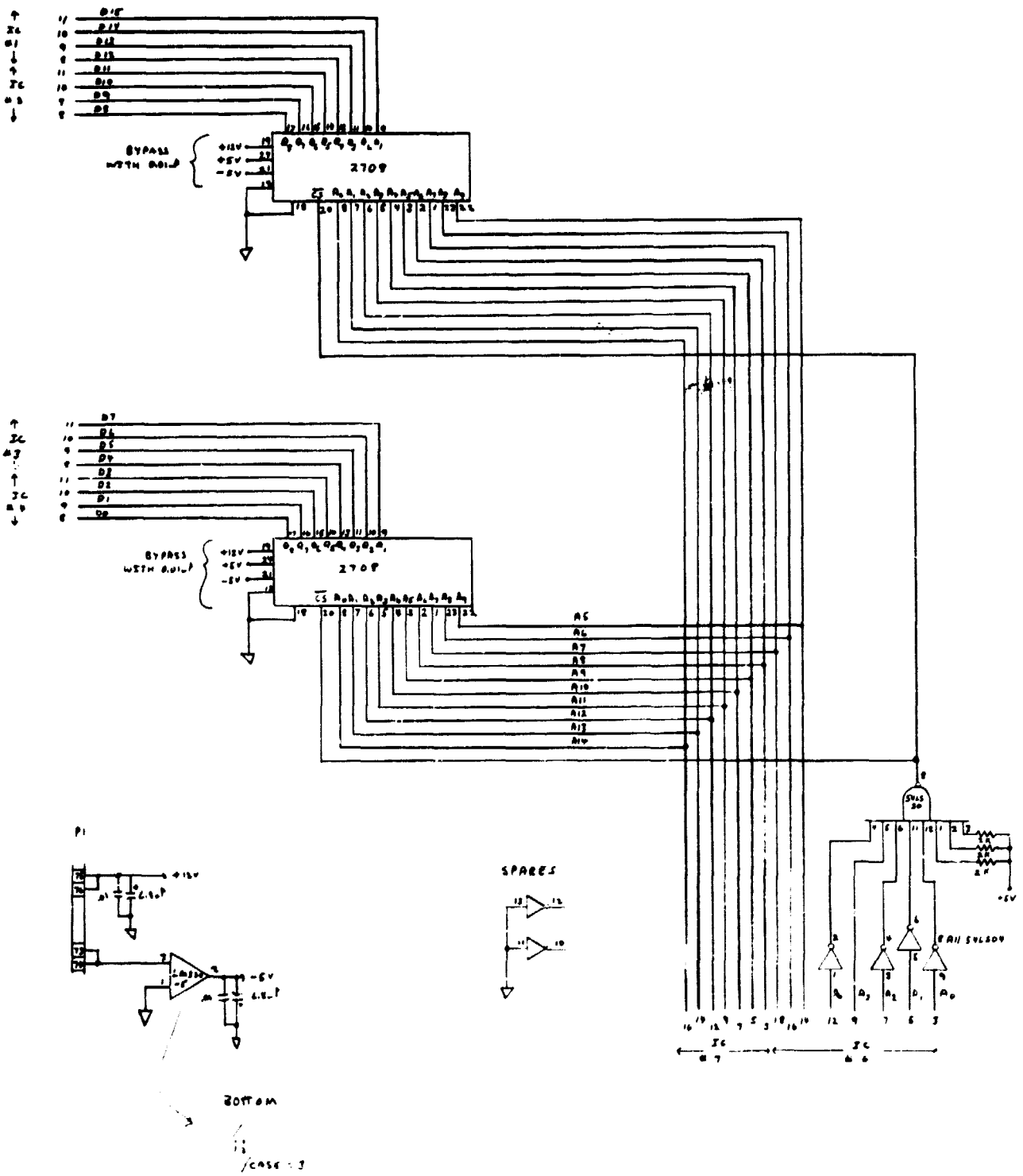

FOLDOUT FRAME

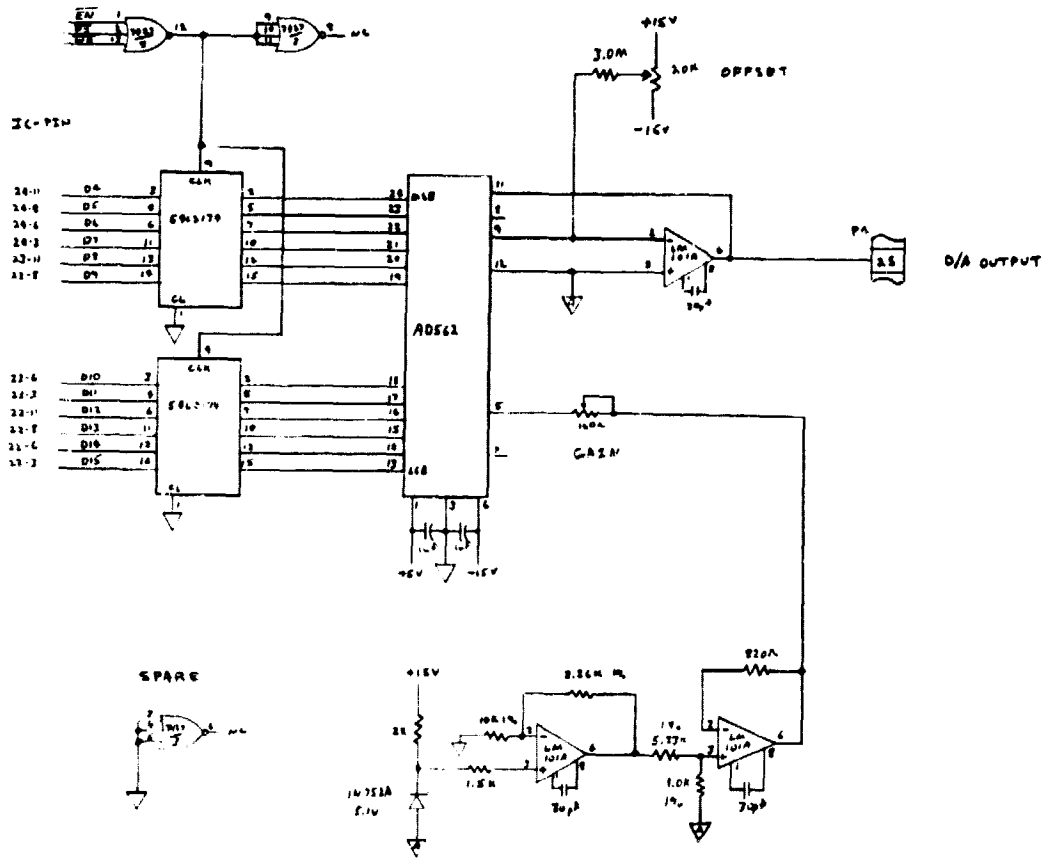

ESSA 9900 I/O BOARD
SHT 2 of 2
R TRUMBULL
3/21/75
B4

2

FOLDOUT FRAME

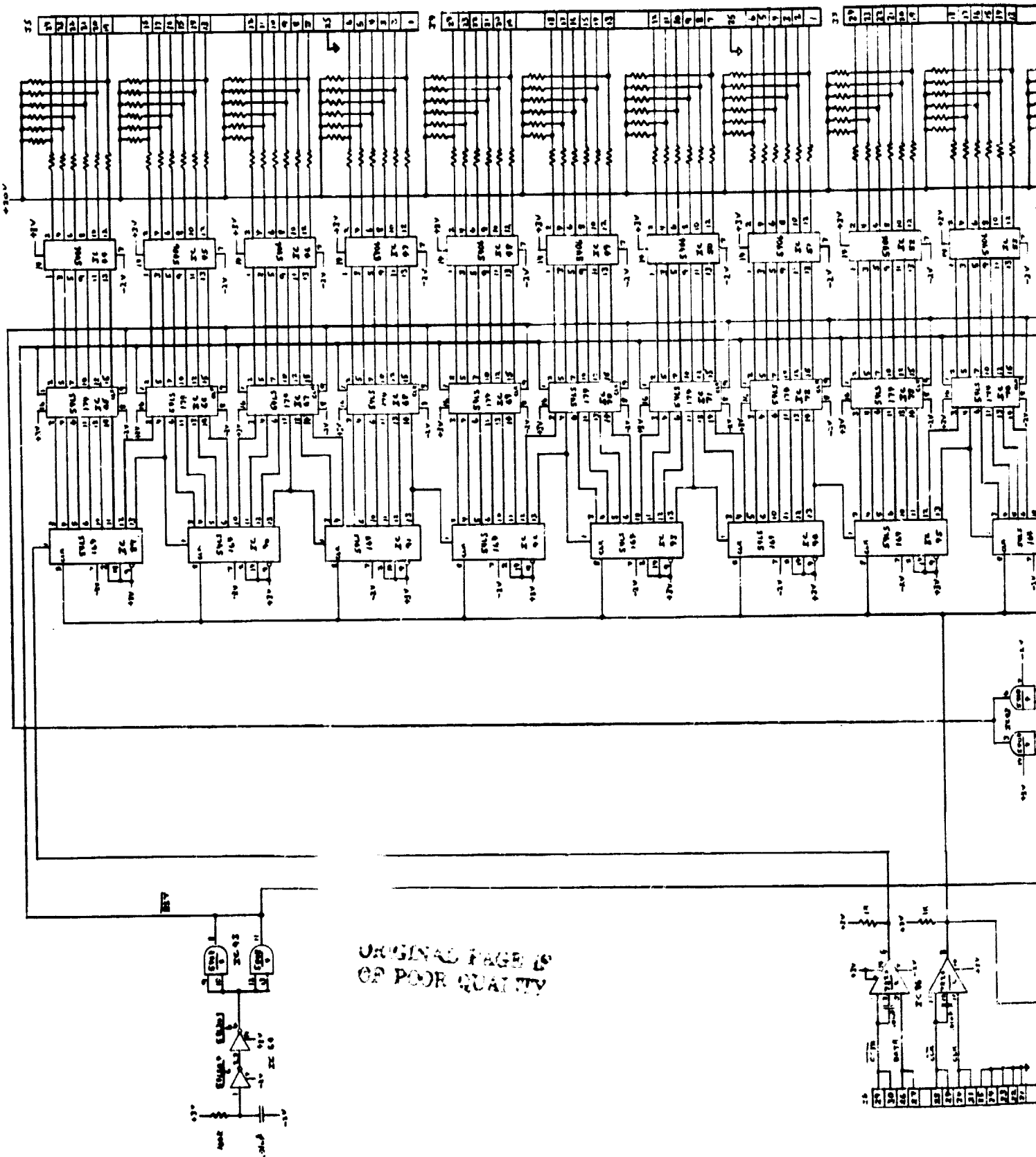

FOLDOUT FRAME

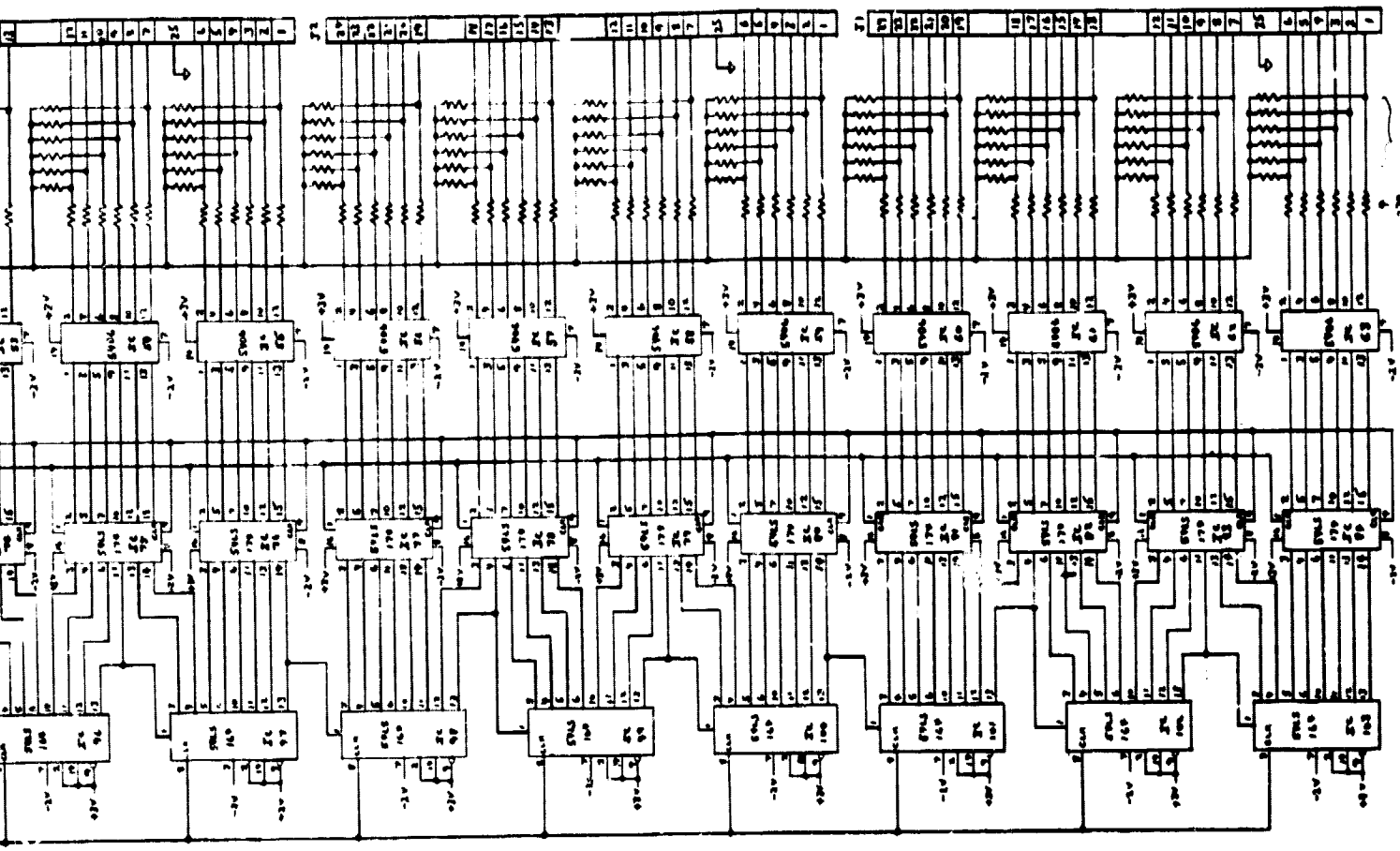

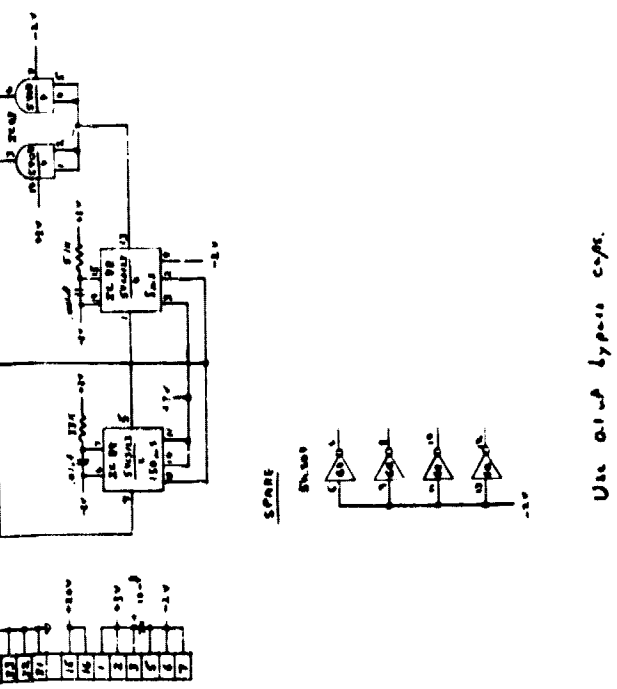

BOLDOUT FRAME

ESSA PIN DIODE DRIVER BOARD

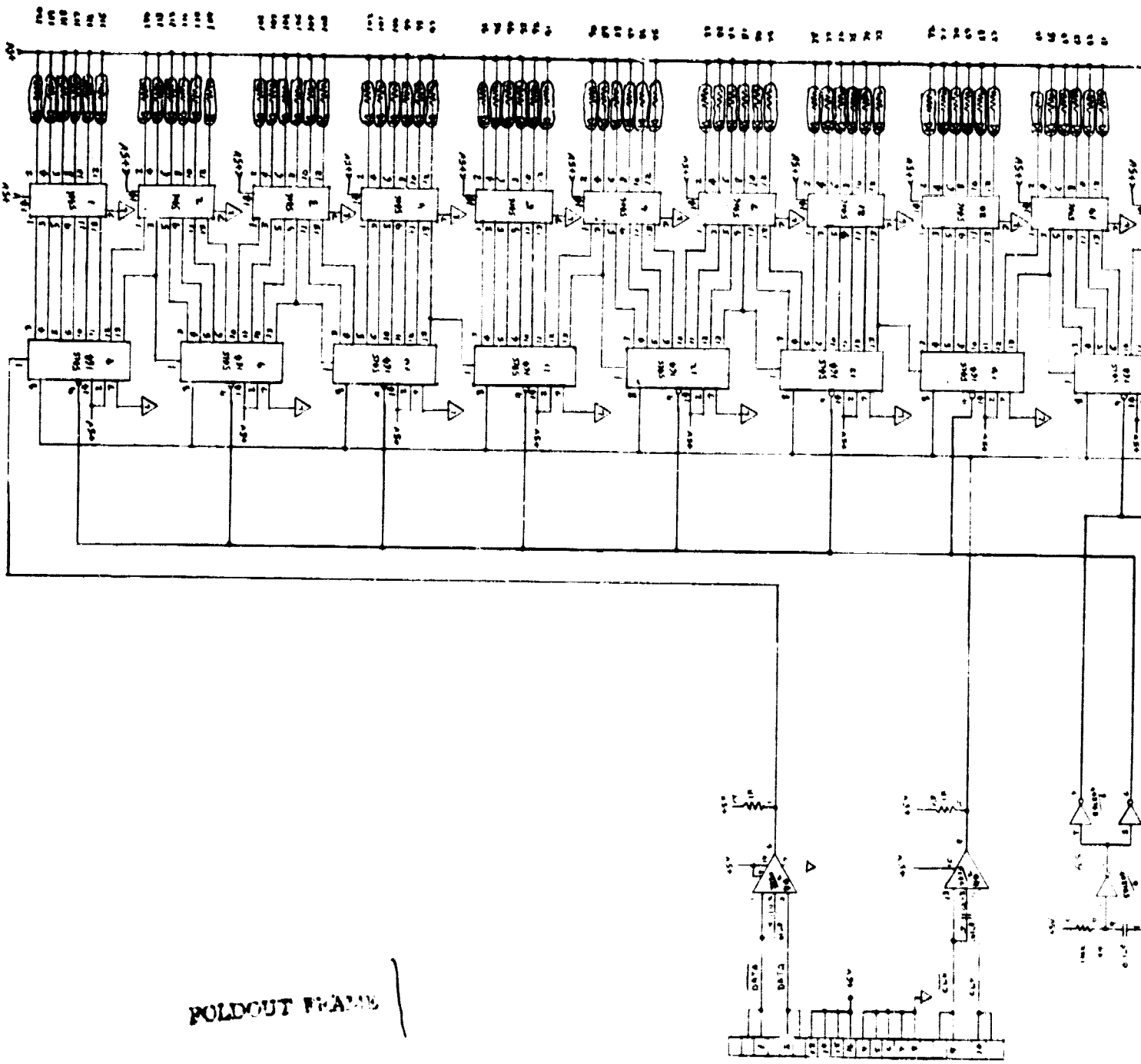

FOLDOUT FRAME

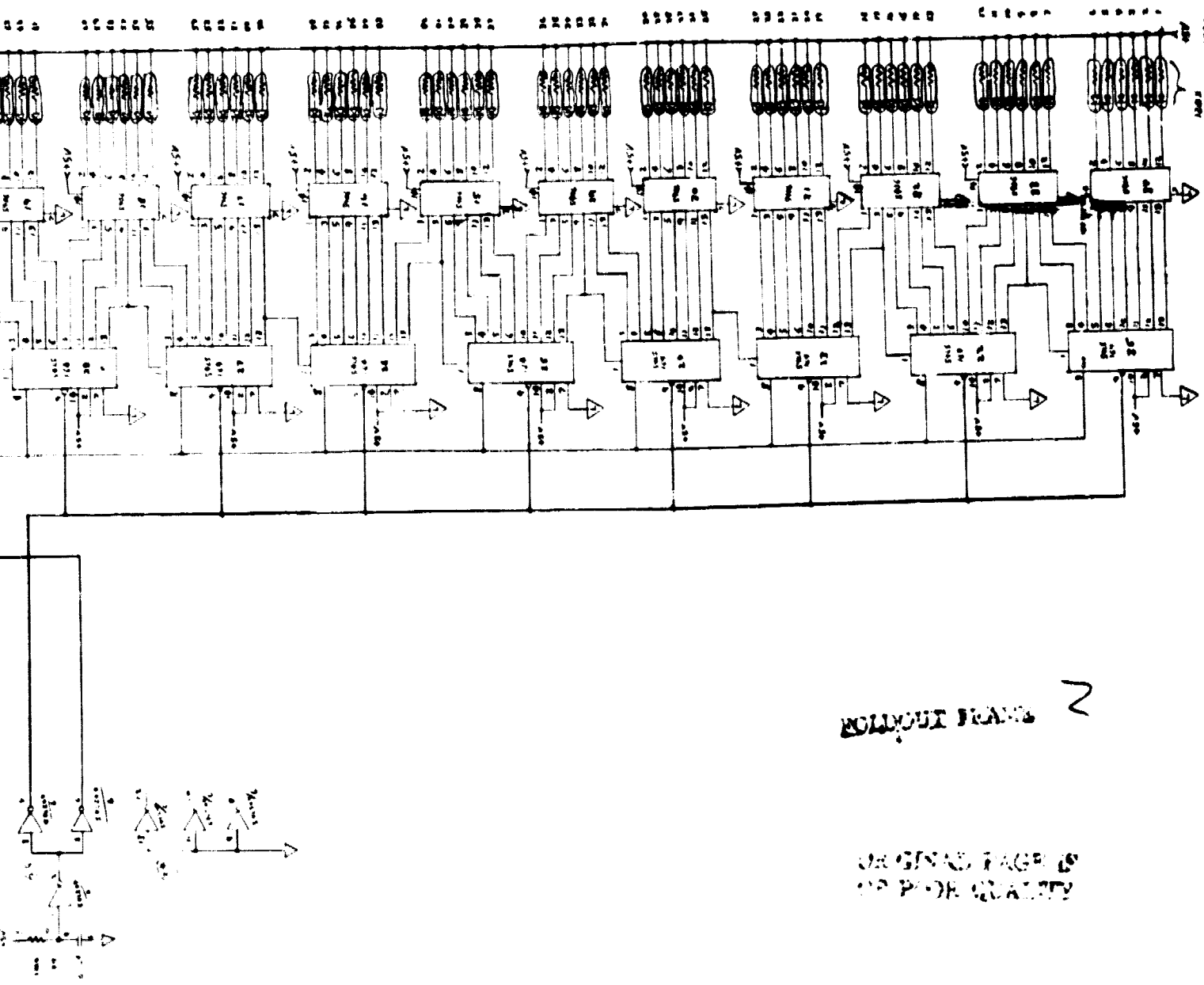

ROLLOUT BOARD 2

ORIGINAL PAGE IS
OF POOR QUALITY

LED DOME DRIVER BOARD

APPENDIX C
Microprocessor Controller Operating Instructions

1) GENERAL INFORMATION

The ESSA electronics consist of a control console and a hand-held terminal. The control box contains the TI-990 microprocessor and a BASD designed interface electronics board. This board primarily converts the digital computer commands into the analog signals which control the antenna and display dome.

Although, the display dome gives a visual representation of the active antenna elements, the theory of operation between the two is different. That is, the display dome functions in a serial mode, but the antenna drivers operate in a parallel mode. The active "1's" on the display dome actually march through each display LED until the entire 120 element display has been clocked in. This is evident by the flickering appearance of the LEDs when the pattern is being changed. In the antenna, however, the active "1's" are serially clocked into shift registers from which the entire 120 element pattern is transferred in parallel to the PIN diode drivers with a single clock pulse.

The ESSA control electronics also interface to a set of switches on the front panel. There are two reset switches. The TI-Bug RESET is used once each time power is turned on. The ESSA/RESET is used to regain control when the processor is occupied in an operational mode. It will not be needed for modes where return of control is automatic. These are modes: 1 - directive beam, 2 - omni, 3 - multibeam, and 4 - acquisition and track non-spinnings, 5 - spinning is with switches 4 and 5 both on.

2) INITIAL TURN ON

- Connect the TM990/301 microterminal to "TERMINAL" connector on the ESSA Control Console front panel.

- Turn off all mode select switches and turn the console PWR-ON switch to on.
- Depress the TI-BUG/RESET button on the consol.
- Depress [CLR]
- Enter 1030
- Depress [EPC]
- Depress [RUN]

The program will now execute the 'Reset' portion of the ESSA control program as shown in the flow chart in Figure 1. The default beam and target positions are copies from permanent memory (PROM) to volatile memory (RAM) for the default cases. Table 1 shows a summary of the most pertinent parameters. Section 4 provides a description of how to modify these parameters at run time.

Note that the program examines the Operational Mode Select switches as they appear left to right. If you attempt to run mode 4 and forget to turn the toggle switch for mode 1, 2 or 3 off, you will be disappointed.

3) HOW TO RUN ESSA IN AN OPERATIONAL MODE

- If ESSA is in active omni or ACQ/TRK - DESPIN depress ESSA/RESET
- Select the operational mode by setting one of the mode select switches on the control console to ON. Mode 4 has a spinning or stationary option. Mode

TABLE 1

SELECTED ESSA CONTROL PARAMETERS

Hexadecimal Address	Default Hex	Value Decimal	Program Label	Program Function	Mode Switch
'FE80'	'100'	25.6	IPH	Initial Beam Steering ϕ	Direction
'FE82'	'100'	25.6	ITH	Initial Beam Steering θ	Direction
'FE84'	'1F4'	50.0	KPH	Initial Target ϕ TDRS Location	ACQ/TRK
'FE86'	'208'	52.0	KTH	Initial Target θ	ACQ/TRK
'FE88'	'2'	2	NMB	Number of Multi-Beams Commands	Multi-Beam
'FE8A'	'170'	36.8	IP(1)	Initial Set of ϕ Steering Coordinates for Multi-Beam Operations	
'FE8C'	'6D0'	174.4	IP(2)		
'FE8E'	'440'	108.8	IP(3)		
'FE90'	'834'	210.0	IP(4)		
'FE92'	'230'	56.0	IT(1)	Initial Set of θ Steering Coordinates for Multi-Beam Operations	
'FE94'	'190'	40.0	IT(2)		
'FE96'	'230'	56.0	IT(3)		
'FE98'	'230'	56.0	IT(4)		
'FEE6'	'1F4'	500	FEE6	Input Simulator Spin Rate (RPMX100)	Spin
'FEE8'	0	0	DRTXX	Options--Not Valid for Hand Terminal	
'FE08'	4	4	REVS	Number of Revs to Monitor Spin Rate	
'FF0C'	0	0	BMDLY	Count to Delay After Forming Each Beam to Facilitate Display (Higher Count is Longer Delay)	

NOTE: Decimal points for all angular values are implied, e.g. 300 is assumed to be 30.0.

5 requires both ACQ/TRK and SPIN to be on. This is controlled by the toggle switch on the far right. The simulator ON/OFF switch on the far left should always be up unless you are operating with an external AGC input.

- o Depress [H/S] terminal button.
- o Depress [RUN]

NOTE: Be sure to first turn the mode select switch OFF before changing to a new mode or ESSA/RESET will cause the program to just re-enter the same active program.

4) HOW TO MODIFY THE CONTROL PARAMETERS AT RUN TIME

- o Restore default conditions (see Paragraph 5)
- o Mode Switch OFF
- o Depress [H/S] on terminal
- o Depress TI-BUG/RESET on console
- o Depress [CLR] on terminal
  → (See Below for decimal to hexadecimal conversions)
- o Depress the hexadecimal number keys on the terminal to enter the parameter's hex address (see Table 1)
- o Depress [EMA] The current value is displayed
- o Modify the value by depressing the hex button on the terminal.

- Enter the new value by depressing EMD; or depress EMDI if you wish to examine or modify a set of values which are sequential in memory.

- Select mode switch

- Depress [RUN]

If you wish to use the microterminal's built-in hexadecimal to decimal conversion capability, insert the following steps at the point denoted by the arrow above. Remember that all angles are entered in degrees x 10 as whole numbers.

- Depress [D→H]

- Enter the data via hex data key depressions. The decimal data in the five right-hand digits on the terminal are converted (i.e. 270^{o} is 2700 HEX = 0ABC).

- Depress [D→H] The results of the conversion are displayed in the four right hand digits of the display.

- Repeat above H→D for hexadecimal to decimal

5) TO RESTORE DEFAULT CONDITIONS

- Set all mode switches OFF

- Depress [H/S]

- Depress [RUN]

- Refer to Section 3 for mode selection

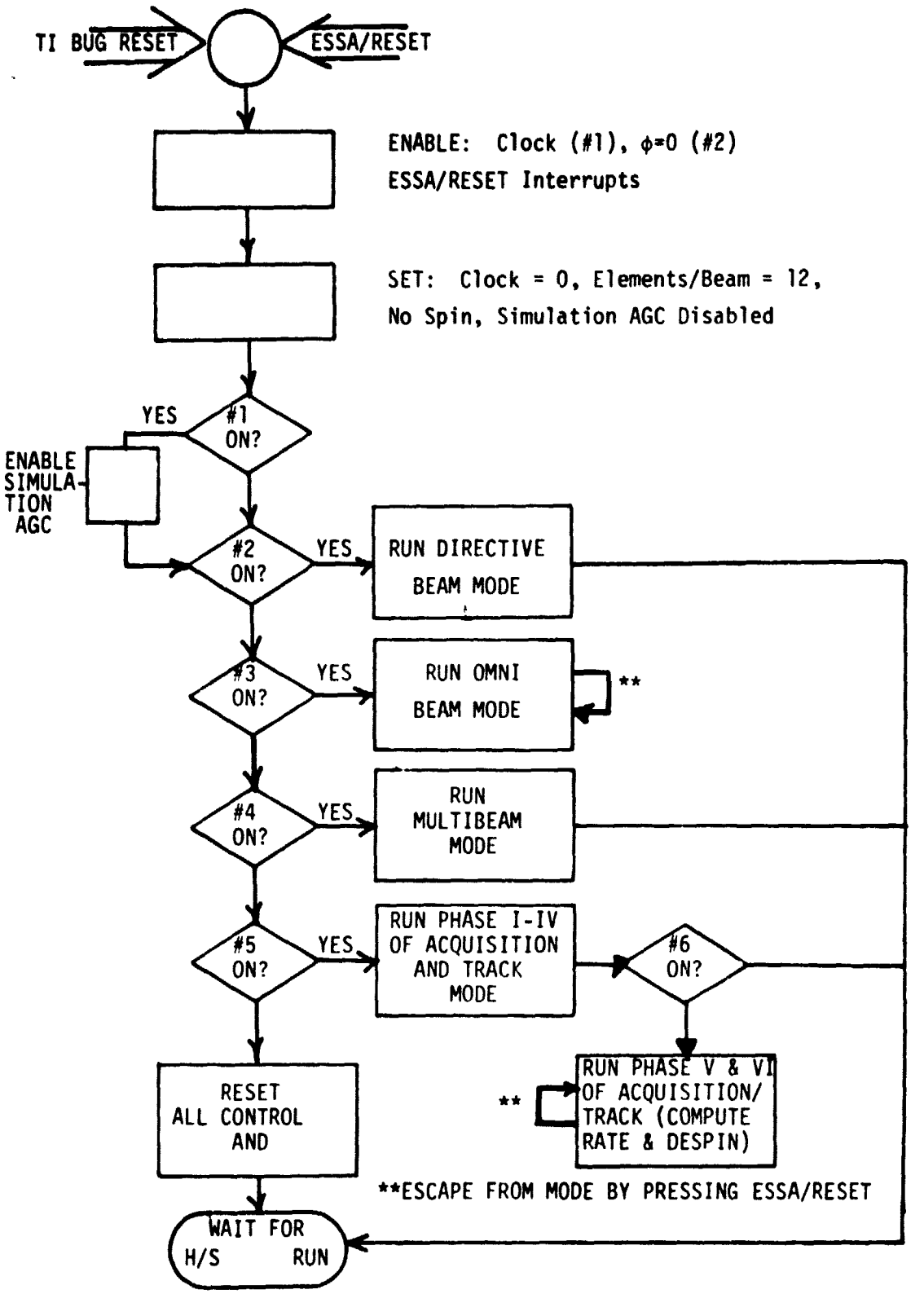
TI BUG RESET
ESSA/RESET
ENABLE: Clock (#1), ϕ=0 (#2)
ESSA/RESET Interrupts
SET: Clock = 0, Elements/Beam = 12,
No Spin, Simulation AGC Disabled
#1 ON?
YES
ENABLE SIMULATION AGC
#2 ON?
YES
RUN DIRECTIVE BEAM MODE
#3 ON?
YES
RUN OMNI BEAM MODE
**
#4 ON?
YES
RUN MULTIBEAM MODE
#5 ON?
YES
RUN PHASE I-IV OF ACQUISITION AND TRACK MODE
#6 ON?
RUN PHASE V & VI OF ACQUISITION/ TRACK (COMPUTE RATE & DESPIN)
**
RESET ALL CONTROL AND
**ESCAPE FROM MODE BY PRESSING ESSA/RESET
WAIT FOR H/S RUN

Figure 1